Charles University in Prague

Faculty of Science

Department of Biochemistry

Study programme: Biochemistry

Ing. Bc. Tomáš Ovad

Phosphorylation of eukaryotic initiation factor 2α by alternative phosphate sources catalyzed by heme-regulated kinase: kinetic analysis

Fosforylace eukaryotického iniciačního faktoru 2α alternativními zdroji fosfátu katalyzovaná kinasou regulovanou hemem: kinetická analýza

MASTER THESIS

Supervisor: doc. RNDr. Markéta Martínková, Ph.D.

Prague 2023

Prohlašuji, že jsem závěrečnou práci zpracoval samostatně a že jsem uvedl všechny použité informační zdroje a literaturu. Tato práce ani její podstatná část nebyla předložena k získání jiného nebo stejného akademického titulu.

V Praze, 15. srpna 2023 Ing. Bc. Tomáš Ovad

Acknowledgement

I would like to express my heartfelt gratitude to doc. RNDr. Markéta Martínková, Ph.D., for her unwavering guidance and support throughout my studies, as well as for inspiring my interest in biochemistry. Words cannot convey my thanks to RNDr. Jakub Vávra, for his patient mentorship and assistance with technical challenges during my research. My sincere thanks extend to the other members of our research group, especially doc. RNDr. Václav Martínek, Ph.D., Mgr. Artur Sergunin and Bc. Lukrécie Sophie Vojáčková. I am deeply thankful to my parents and grandparents, for their relentless support through every phase of my life's journey. Next, my sincere thanks belong to my partner Tomáš, whose presence transformed my academic pursuits into the most gratifying years of my life. Lastly, a profound acknowledgment belongs to my lifelong friend, Lenka, for devotedly standing by me through thick and thin.

Abstract

This master thesis focuses on the phosphorylation of the eukaryotic initiation factor 2α (eIF2α) by the heme-regulated inhibitor (HRI), a key reaction in the regulation of eukaryotic protein synthesis. Kinetic parameters of this reaction in the presence of ATP as the phosphate donor were determined previously. However, there are no reports on the potential of alternative NTPs (GTP, UTP, CTP) to serve as the sources of phosphate for this reaction. In this thesis, the wild-type HRI enzyme was produced by heterologous expression in *E. coli* and its kinase activity was assayed in the presence of ATP, GTP, UTP, and CTP. Kinetic parameters and heme half-maximal inhibitory concentrations for the HRI kinase reaction with the use of each NTP as a phosphate donor were determined. To validate these kinetic experiments, contaminations by ATP in the solutions of GTP, UTP, and CTP were excluded with the aid of ion-pair reversed-phase high-performance liquid chromatography. It has been shown that ATP is the most efficient phosphate donor for the HRI kinase reaction, although the remaining NTPs (GTP, UTP, CTP) may be utilized as the sources of phosphate for this reaction as well. This broadened specificity of the HRI enzyme may hold physiological significance in conditions which disrupt the normal concentrations of NTPs, such as tumor growth. Additionally, the effect of cytochrome *c* on the kinase activity and absorption spectra of HRI was studied. While the HRI kinase activity was unaffected by the presence of cytochrome *c*, the spectral analyses hinted at a potential protein–protein interaction between cytochrome *c* and the HRI holoform.

Keywords: heme-regulated inhibitor, eukaroytic initiation factor 2, nucleoside triphosphate, phosphate donor, cytochrome *c*

Abstrakt

Tato diplomová práce je zaměřena na fosforylaci eukaryotického iniciačního faktoru 2α (eIF2α) inhibitorem regulovaným hemem (HRI), která je klíčovou reakcí v regulaci eukaroytické proteosyntézy. V předešlých studiích byly stanoveny kinetické parametry této reakce v přítomnosti ATP jako donoru fosfátu. Nebyla však studována možnost využití alternativních NTP (GTP, UTP, CTP) jako zdrojů fosfátu pro tuto reakci. V této diplomové práci byl heterologní expresí v *E. coli* získán *wild-type* enzym HRI a byla studována jeho kinasová aktivita v přítomnosti ATP, GTP, UTP a CTP. Byly určeny kinetické parametry a střední inhibiční koncentrace hemu pro reakci katalyzovanou HRI v přítomnosti jednotlivých NTP jako zdrojů fosfátu. Pro validaci těchto kinetických experimentů byly vyloučeny kontaminace ATP v roztocích GTP, UTP a CTP pomocí iontově párové chromatografie. Ukázalo se, že ačkoli ATP je nejefektivnějším zdrojem fosfátu pro kinasovou aktivitu HRI, i zbývající NTP (GTP, UTP, CTP) mohou být v dané reakci využity jako donory fosfátu. Tato rozšířená specifita enzymu HRI může být fyziologicky relevantní za podmínek, které narušují normální hodnoty koncentrací NTP (např. rozvoj nádoru). Dále byl studován vliv přítomnosti cytochromu *c* na kinasovou aktivitu a absorpční spektra proteinu HRI. Zatímco kinasová aktivita HRI nebyla přítomností cytochromu *c* ovlivněna, spektrální analýza naznačila možnost protein–proteinové interakce mezi cytochromem *c* a holoformou proteinu HRI.

Klíčová slova: inhibitor regulovaný hemem, eukaryotický iniciační faktor 2, nukleosidtrifosfát, zdroj fosfátu, cytochrom *c* [IN ENGLISH]

Contents

List of abbreviations and symbols

ADP	adenosine 5′-diphosphate
APS	ammonium persulfate
ATF	activating transcription factor
ATP	adenosine 5′-triphosphate
Bcl2	B-cell lymphoma 2
BH	Bcl-2 homology
Cdc37	cell division cycle 37
CHOP	CCAAT-enhancer-binding protein homologous protein
CK	casein kinase
CReP	constitutive repressor of eIF2α phosphorylation
CTP	cytidine 5′-triphosphate
DMSO	dimethyl sulfoxide
DHA	dihydroartemisinin
EDTA	ethylenediaminetetraacetic acid
eIF2	eukaryotic initiation factor 2
eIF2α	α subunit of the eukaryotic initiation factor 2
eIF2α–P	phosphorylated α subunit of the eukaryotic initiation factor 2
ER	endoplasmic reticulum
Fe(II)–HRI	HRI holoform with heme in the Fe(II) state
Fe(III)–HRI	HRI holoform with heme in the Fe(III) state
Fe(II)–CO	HRI holoform with the heme Fe(II) ion coordinated by CO
Fe(II)–NO	HRI holoform with the heme Fe(II) ion coordinated by NO
GADD34	growth arrest and DNA damage-inducible protein 34
GCN2	general control nonderepressible 2
GDP	guanosine 5′-diphosphate
GPC	gel permeation chromatography
GTP	guanosine 5′-triphosphate
HPLC	high-performance liquid chromatography
HRI	heme-regulated inhibitor
Hsc70	heat shock cognate 70
Hsp90	heat shock protein 90

IPTG	isopropyl β-D-1-thiogalactopyrasonide
LB	Luria-Bertani
mRNA	messenger RNA
MARK2	microtubule affinity-regulating kinase 2
MCL-1	myeloid leukemia cell differentiation 1
Met–tRNA$_i^{Met}$	methionine-binding initiator transfer RNA
NTP	nucleoside 5′-triphosphate
ORF	open reading frame
PERK	PKR-like ER kinase
PKR	RNA-dependent protein kinase
PMSF	phenylmethylsulfonyl fluoride
PP1	protein phosphatase 1
SDS	sodium dodecyl sulfate
SDS–PAGE	sodium dodecyl sulfate–polyacrylamide gel electrophoresis
TEMED	*N,N,N′,N′*-tetramethylethylenediamine
Tris-HCl	tris(hydroxymethyl)aminomethane hydrochloride
tRNA	transfer RNA
uORF	upstream open reading frame
UTP	uridine 5′-triphosphate
A	absorbance
$K_{0.5}^{\mathrm{NTP}}$	apparent half-saturation constant
$K_{\mathrm{M}}^{\mathrm{NTP}}$	apparent Michaelis–Menten constant
K	binding constant
$k_{\mathrm{cat}}^{\mathrm{NTP}}$	catalytic constant
η^{NTP}	catalytic efficiency
[eIF2α–P]	concentration of eIF2α
[heme]	concentration of heme
[NTP]	concentration of NTP
V	elution volume
$\mathrm{IC}_{50}^{\mathrm{NTP}}$	half-maximal inhibitory concentration
h^{NTP}	Hill coefficient
v_0	initial velocity
$v_{\mathrm{lim}}^{\mathrm{NTP}}$	limiting velocity
$[\mathrm{eIF2}\alpha]_0$	maximal kinase activity
ε	molar absorption coefficient
M	molecular weight
A_{N}	normalized area

OD_{600}	optical density at 600 nm
k_d	rate constant of dissociation
Δt	reaction time
a_{rel}	relative kinase activity
λ	wavelength

Introduction

The addition of one or more phosphate groups to a protein can induce significant changes in its stability, activity, and/or subcellular localization, making phosphorylation a pivotal player among the diverse array of protein posttranslational modifications. An illustrative example of its importance lies in the integrated stress response, a highly conserved eukaryotic signaling cascade, where phosphorylation of the eukaryotic initiation factor 2 (eIF2) at its α subunit (eIF2α) is the central event. This crucial reaction is mediated by five distinct protein kinases, each responsive to various stress factors via their regulatory domains.[1–6]

The heme-regulated inhibitor (HRI) was the first member of the eIF2α kinase family to be discovered.[7] While HRI was initially recognized as the key regulator of hemoglobin synthesis in reticulocytes, subsequent investigations have revealed its expression in a wide range of tissues.[8,9] Moreover, pathways activated by HRI were shown to play critical roles in the growth and development of cancer cells, although many molecular details of these pathways remain elusive.[10–12] Recently, HRI-dependent signaling was reported to contribute to the acquisition of a persister phenotype in lung cancer cells treated with pro-apoptotic agents, with direct activation of HRI by cytochrome *c* being proposed as a key step in this process.[13]

In this master thesis, the HRI–catalyzed phosphorylation of eIF2α was investigated from two distinct perspectives. The first goal was to explore the potential of non-canonical nucleoside 5′-triphosphates (NTPs) to act as phosphate donors in this reaction. To achieve this, the kinetic parameters and the inhibitory effects of heme on these reactions were analyzed using *in vitro* kinase assays. Secondly, the thesis aimed to provide further insights into the effect of cytochrome *c* on HRI kinase activity and absorption spectra.

The thesis begins with a literature review, which is organized as follows. Firstly, the eukaryotic protein kinases superfamily is introduced, with the focus put on their essential structural components and the potential utilization of alternative phosphate donors. The section concludes with a brief discussion of the experimental procedures employed to evaluate the enzyme activity of protein kinases. Subsequently, an overview of the integrated stress response and the roles of the five eIF2α kinases. A separate section is then dedicated to the structural details and regulation mechanisms of HRI. The review concludes with a summary of studies investigating the roles of HRI in cancer development.

1 Literature review

1.1 Protein kinases

Since the groundbreaking discovery of phosphorylase kinase in the 1950s by Fischer and Krebs, reversible protein phosphorylation has been recognized as one of the most vital biological regulatory mechanisms.[14] Today, it is difficult to envision a cellular process that is not influenced by protein phosphorylation, governed by the balanced activities of protein kinases and phosphatases. This delicate equilibrium plays a pivotal role in maintaining cellular homeostasis. Accordingly, impairments to this balance are implicated in many pathologies, including oncological, neurological, metabolic, and immunological disorders.[15–17] For their exceptional contribution to modern biology and our understanding of cellular signaling, Fischer and Krebs were jointly awarded a Nobel Prize in Physiology or Medicine in 1992.[18,19]

The overall reaction catalyzed by protein kinases is deceptively simple (Fig. 1.1 on p. 8). It involves the transfer of the γ phosphoryl group from an NTP to a hydroxyl group of the protein substrate, resulting in the formation of a phosphoester bond and the release of a proton (H^+). The presence of divalent ions (typically Mg^{2+}) is required for the reaction.[20] Usually, adenosine 5′-triphosphate (ATP) is assumed to be the exclusive NTP serving as the phosphate donor for protein kinase reactions.[21] However, it would be short-sighted to disregard the presence of other NTPs in the cytosol, i.e. guanosine 5′-triphosphate (GTP), uridine 5′-triphosphate (UTP), and cytidine 5′-triphosphate (CTP). The potential of these NTPs to serve as alternative phosphate donors will be further discussed in Section 1.1.2 (p. 12).

The scheme in Fig. 1.1 (p. 8) illustrates that the phosphoryl group is normally transferred to a hydroxyl group, which is typical for eukaryotic organisms, where the protein kinases superfamily branches into three main categories.[22] Protein-Ser/Thr kinases phosphorylate aliphatic hydroxyl groups in Ser and Thr, while the aromatic hydroxyl group in Tyr is targeted by protein-Tyr kinases. Additionally, a minor group of eukaryotic kinases exhibits dual specificity, i.e. the capability of phosphorylating both Ser/Thr and Tyr residues.[23] Among the 538 kinases constituting nearly 2% of the human genome, only 90 are protein-Tyr kinases, with 58 being receptor tyrosine kinases.[22]

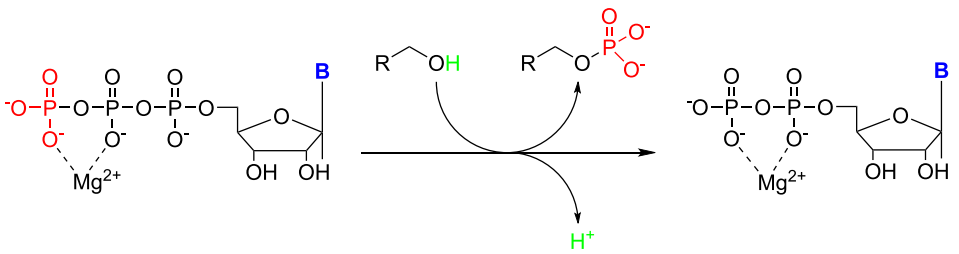

Figure 1.1: General net reaction catalyzed by protein kinases. The phosphoryl group (red) is transferred to a hydroxyl group on the protein substrate (R–OH), releasing a proton (green). The phosphoryl group is donated by an NTP, usually ATP (B denotes a general purine or pyrimidine base).

However, the chemistry of protein–phosphate bonds extends beyond the formation of phosphoesters at Ser, Thr, and Tyr residues. Phosphorylation at other residues yields phosphoramidates (His, Lys, Arg), acylphosphates (Asp, Glu), or thiophosphates (Cys).[24] Notably, phosphorylation at His and Asp plays crucial roles in two- and multi-component signaling systems in bacteria, fungi, and plants.[25] While such systems are absent in higher eukaryotes, the significance of His phosphorylation is increasingly recognized as a vital signaling element even in mammalian cells.[26] Nonetheless, the following discussion will primarily focus on the prototypical eukaryotic protein-Ser/Thr and Tyr kinases.

From a kinetic perspective, the protein kinase reaction (Fig. 1.1) can be classified as a bisubstrate reaction.[27] Substantial evidence confirms that these reactions predominantly follow sequential mechanisms,[28,29] although some exceptions, involving the ping pong mechanisms, have been reported.[30] The order of substrate binding is usually random, but in cases of an ordered mechanism, the NTP typically binds as the first substrate.[28,29] The reaction rate is generally limited by either the chemical step or the adenosine 5′-diphosphate (ADP) release. However, the nature of the rate-limiting step may be altered by additional regulation mechanisms, such as phosphorylation or ligand binding.[29]

The central question in studying sequential mechanisms is understanding the nature of the ternary complex.[27] Since the catalytic domain is largely conserved among the protein kinase superfamily, it has been expected that they share a common catalytic mechanism. Substantial research supports this notion and indicates that the general mechanism relies on a direct phosphoryl transfer with a dissociative transition state.[31,32] In this state, the phosphoryl group is largely separated from the donor before forming a significant bond with the acceptor. This stands in contrast to analogous nonenzymatic reactions of phosphate triesters, which typically follow associative mechanisms.[29]

1.1.1 Structure and catalytic mechanism

Considering the immense range of potential protein substrates, specific regulatory mechanisms are needed for the individual protein kinases. Structurally, these differences are mainly reflected in the regulatory domains and the substrate recognition elements. On the other hand, the catalytic site is located in the kinase domain, which remains highly conserved among the eukaryotic protein kinases superfamily.[16,17,33,34] A crucial breakthrough in understanding the catalytic mechanism arose from studying the X-ray structure of a complex between protein kinase A and a substrate-mimicking inhibitor.[35,36] Recent reports indicate that all protein-Ser/Thr and protein-Tyr kinases share the key catalytic residues and fundamental protein folding characteristics, originally established for protein kinase A.[37,38] This structural similarity primarily applies to the active conformation of the kinases. In the inactive states, larger structural variations are observed, corresponding to the diversity of mechanisms regulating the activities of different kinases.[16,17,33,34]

All eukaryotic protein kinase domains comprise two lobes: a small *N*-terminal lobe and a larger *C*-terminal lobe, connected by a flexible hinge region.[16,17,33,34] The ATP-binding site resides within a cleft between these lobes. The *N*-lobe contains a five-stranded β sheet and an α helix known as the αC helix, while the *C*-lobe is predominantly α-helical. In terms of substrate binding and catalysis, key conserved sequences in the *N*-lobe include the glycine-rich phosphate-binding loop (G-rich loop), the AXK motif, and a conserved Glu91 residue (in the αC helix). As for the *C*-lobe, the most important elements are the catalytic loop (containing the Y/HRD-motif and a key Lys168 residue), and the DFG- and APE-motifs, which mark the beginning and end of the activation loop (A-loop).[16,17,33,34]

The binding of ATP by protein kinases and its positioning for a successful phosphoryl transfer relies on interactions with multiple elements of the kinase domain.[39,40] First, the adenine ring is sandwiched by hydrophobic interactions with many residues of the *N*-lobe and a single residue of the *C*-lobe. The anchoring of the adenine ring is further supported by the formation of hydrogen bonds with the residues in the hinge region. Additionally, the ribose hydroxyl groups form hydrogen bonds with residues in the *C*-lobe. Next, the phosphate groups interact with the G-rich loop, with the Lys72 of the AXK-motif and the Lys168 of the catalytic loop. The Lys72 residue forms a crucial salt bridge with Glu91 of the αC helix. The presence of this salt bridge is required to further stabilize the interaction of Lys72 with the phosphates. Finally, the Asp184 of the DFG-motif

recognizes the Mg^{2+} ions bound to ATP, which assures proper positioning of the β and γ phosphates.[39,40]

On the contrary, the binding of the protein substrate relies solely on the interactions with the *C*-lobe. Specifically, recognition of the protein substrate is mediated by the backbone residues in a region *C*-terminal to the A-loop, forming the 'P + 1' loop.[41,42] This name originates from the hydrophobic interaction with the P + 1 residue of the substrate (P being the site targeted by the kinase). However, interactions with other residues in the substrate are also necessary for correct substrate recognition. Typically, a minimum of four residues on either side of the P site interact with the P + 1 loop of the kinase.[43] The importance of neighboring residues around the phosphorylated site is further exemplified by the fact that free amino acids are seldom phosphorylated by protein kinases.[44] Note that protein-Tyr kinases contain a conserved Pro residue, which interacts with the phenolic group of the target Tyr, thus positioning it for catalysis.[45]

In terms of the reaction mechanism of protein kinases, the catalytic loop's Y/HRD-motif, specifically the Asp166 residue, plays a pivotal role.[46,47] Functioning as a catalytic base, Asp166 accepts a proton from the substrate's hydroxyl group. This deprotonation enhances the nucleophilicity of the substrate's oxygen atom, facilitating its attack on the electron-deficient phosphorus atom in ATP's γ phosphate. The presence of Mg^{2+} ions coordinated by the Asp184 residue further aids this process by reducing electrostatic repulsion among the phosphate groups, which would otherwise hinder the nucleophilic attack. Moreover, the salt-bridge interaction between Lys72 and Glu91 is critical for the transfer process. When this interaction is intact, the αC helix adopts an inward conformation, corresponding to the active state of the kinase. Conversely, disruption of the bridge between Lys72 and Glu91 leads to an outward conformation of the αC helix, typically resulting in kinase inactivation. Given the importance of these four residues (Lys72, Glu91, Asp166, and Asp184) for catalysis, they are often referred to as the K/E/D/D-signature motif of eukaryotic protein kinases.[16,17,33,34]

While the inward conformation of the αC helix is essential for protein kinase activation, it may not be sufficient on its own. The A-loop, located in the *C*-lobe, harbors multiple phosphorylation sites, and in many instances, their phosphorylation is also necessary for achieving kinase activity.[38] For example, in protein kinase A, phosphorylation at Thr197 is a prerequisite for its kinase activity.[36] The phosphorylation of the A-loop facilitates transitions between the 'open' active state and various 'closed' conformations, wherein the A-loop physically obstructs the binding of the protein substrate to the active site. Phosphorylation of the A-loop

may rely either on autophosphorylation (*cis*- or *trans*-), or on heterophosphorylation by another kinase.[38] Moreover, the active state of the A-loop may be further stabilized by association with regulatory proteins. This stabilization contributes to fine-tuning the enzyme's activity and responsiveness to cellular signals.[38,48,49]

In fact, phosphorylation-based signaling extensively relies on the kinases' remarkable ability to dynamically reorganize their conformations in a tightly regulated manner.[34] Besides the interactions discussed above, this adaptive switching is facilitated by another element of the kinase architecture. Two hydrophobic 'spines' emerge as a result of interactions in two groups of residues scattered within both the small and large lobes.[50,51] The spines are anchored to the F helix of the *C*-lobe. The F helix, which is highly hydrophobic and extends through the entire *C*-lobe, acts as a robust scaffold for the entire kinase core.[50,51] Anchoring the two spines to the F helix establishes a dynamic linkage between the lobes for optimal kinase activity. First, the regulatory spine comprises two residues from the *N*-lobe and two from the *C*-lobe.[50] Second, the catalytic spine is similar to the first one, but its assembly is not completed until ATP binds.[51]

Apart from the Mg^{2+} ion bound by the Asp184 of the DFG-motif and by the β and γ phosphates, a second Mg^{2+} ion is bound by the Asn171 residue of the catalytic loop and by the α and γ phosphates.[52] The roles of these two divalent ions have been the subject of extensive debate, as some kinases have been reported to be stimulated,[53,54] while others to be inhibited by Mg^{2+} ions.[55] However, the dichotomy was resolved by identifying two distinct roles of Mg^{2+} ions, exerting opposing effects on the reaction rate.[20] Firstly, both Mg^{2+} ions stabilize the transition state, thereby facilitating the phosphoryl transfer reaction. Once the transfer is complete, one of the Mg^{2+} ions is released along with the ADP product. Nevertheless, the second Mg^{2+} ion remains bound at the second site and, attracted by the ADP product, may hinder its release, which may thus become a rate-limiting step. The subsequent release of the second Mg^{2+} ion likely induces a conformational change that stimulates the release of the Mg–ADP product.[20]

In summary, Mg^{2+} ions play essential roles in ATP binding at the active site of protein kinases, reducing the electrostatic barrier during phosphoryl transfer, and facilitating efficient product release. Experiments with other divalent metal ions highlighted the unique ability of Mg^{2+} to fulfill all these tasks.[56] This explains why Mn^{2+} ions were reported to enhance phosphorylation for certain substrates, while an inhibitory effect was observed for others.[57] Moreover, considering the substantially higher concentration of Mg^{2+} compared to Mn^{2+}, Mg^{2+} salt of ATP is expected to be the more prevalent cosubstrate in protein kinase reactions.[57]

1.1.2 GTP, UTP, CTP: Outsiders or game changers?

When discussing protein kinase reactions, ATP is often implicitly assumed to serve as the source of the phosphate group. This exclusive role of ATP can be supported by two main arguments.[21] Firstly, the hydrolysis of the β,γ-phosphoanhydride bond in ATP is associated with a largely negative change in standard Gibbs energy, making the overall reaction (as depicted in Fig. 1.1 on p. 8) thermodynamically favorable. Secondly, intracellular ATP concentrations are considerably higher when compared to other NTPs (GTP, UTP, CTP), or other potential phosphate donors like inorganic pyrophosphate. The abundance of ATP apparently increases the likelihood of it being preferentially utilized.[21]

However, the first argument can be challenged relatively easily, as the large gain in Gibbs energy could theoretically be achieved from the hydrolysis of any other NTP. The discussion of the second argument is somewhat more complex. Traut comprehensively analyzed reports on concentrations of various purine and pyrimidine nucleotides in mammalian cells.[58] Figures 1.2a and 1.2b depict the average values of NTP concentrations in normal and tumor cells, respectively.

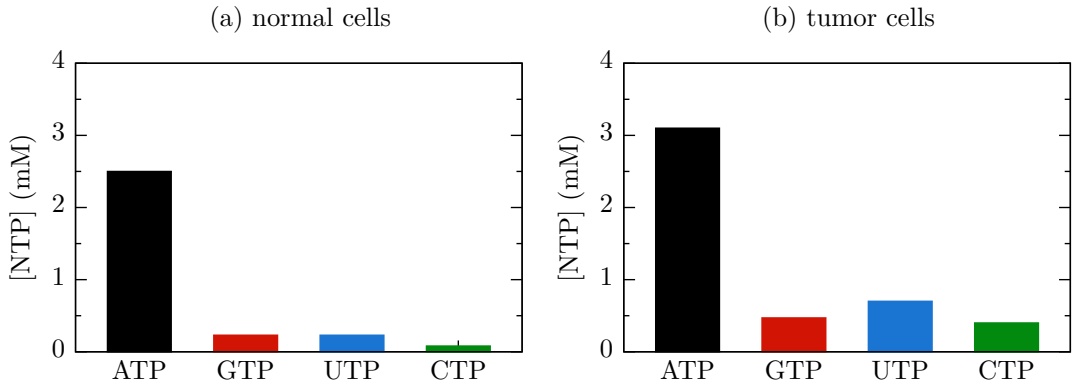

Figure 1.2: Average concentrations of various NTPs (ATP, GTP, UTP, and CTP) in mammalian cells: a) normal cells, b) tumor cells. Plots were created based on data from Ref.[58]

The data confirm that the intracellular pool of NTPs is indeed dominated by ATP. Furthermore, cancer development seems to be associated with a general increase in cellular NTP concentrations, presumably due to the increased rates of the cell cycle.[58] However, the concentration ratios of the various NTPs are also altered during this process. For instance, while the ATP/CTP ratio in normal cells is ≈30, this value decreases to ≈8 in tumor cells. Additionally, it is noteworthy that reports on the concentration of a given NTP in the same cell line or tissue can

vary by 5–50 fold.[58] This suggests that deviations in both absolute and relative NTP concentrations may be linked to specific developmental stages of cells or their attainment of unique functions.

Research on the utilization of non-canonical NTPs (GTP, UTP, CTP) by protein kinases has been relatively scarce. However, one remarkable exception is casein kinase 2 (CK2), which exhibits efficient utilization of GTP alongside ATP for both its autokinase and kinase activities.[59] Several analogous instances have been reported, including the calcium/calmodulin-dependent protein kinase II,[60,61] the mst-3 kinase,[62] and the epidermal growth factor receptor kinase.[63] Additionally, protein kinase Cδ was found to preferentially employ GTP as the phosphate donor for autophosphorylation, and intriguingly, with certain autophosphorylation sites specific to GTP only.[64] In a comprehensive screening of 200 mammalian kinases, a noticeable affinity for GTP was observed in only a small subset of kinases.[65] Apart from CK2, these included the mitogen-activated protein kinase kinase and the B-raf kinase. Nevertheless, subsequent kinase assays revealed that only CK2 effectively utilized GTP as the phosphate donor.[65]

The prototypical structure of kinase domains in the active state (see Section 1.1.1, p. 9) suggests that binding noncanonical NTPs is very unlikely.[39,40] Besides other interactions, ATP forms three crucial hydrogen bonds with highly conserved residues in the kinase domain, firmly fixing its adenine ring in the proper position.[66] However, the same hydrogen bond pattern cannot be applied to GTP, as its N1-atom acts as a hydrogen bond donor and the carbonyl oxygen as an acceptor, in contrast to the equivalent atoms in ATP (see Fig. 1.3).[67] As a result, GTP cannot establish hydrogen bonds with the same residues as observed for ATP.

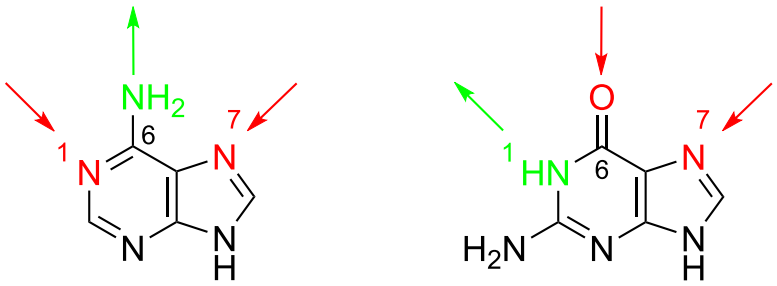

a) b)

Figure 1.3: a) Hydrogen bond pattern of adenine, ensuring its stable positioning within the conserved active site of protein kinases. Red (green) arrows indicate the hydrogen bond accepting (donating) atoms. b) Hydrogen bond pattern of the equivalent atoms in guanine. Adapted from Ref.[67]

Clues for explaining the ability of CK2 to utilize both ATP and GTP were first provided by site-directed mutagenesis.[68,69] Full elucidation of the mechanism was achieved by investigating the crystal structure of CK2 and its complexes with ATP and GTP analogs.[70,71] It has been shown that while ATP binds to CK2 in the usual manner, the guanine ring undergoes a displacement, deviating from the position usually assumed by adenine. This displacement allows the guanine O6-atom to form the hydrogen bond that is normally established by the adenine N1-atom. An extra hydrogen bond is formed with Val116, which simultaneously engages in a hydrogen bond with Asn118, a residue previously identified as crucial for GTP utilization.[69] However, due to the displacement of GTP, a gap emerges at the site usually occupied by the adenine N6-atom. Interestingly, this void is filled by a water molecule. In this way, water molecules play a role in assisting the guanine ring in mimicking the canonical hydrogen bond pattern of adenine in order to bind to CK2.[71] Finally, this model of GTP binding by CK2 was suggested to be valid for the other kinases capable of utilizing GTP, which *"is perhaps not as rare among protein kinases as typically assumed"*.[71]

1.1.3 Quantification of protein kinase activity

The determination of protein kinase activity typically involves quantifying the phosphorylated product. This section provides a brief overview of the techniques used for this purpose, especially when the protein substrate and its phosphorylation sites have already been described. However, the mapping of potential phosphorylation sites, identification, and subcellular localization of phosphorylated proteins are considerably more complex tasks, constituting a distinct research field known as phosphoproteomics.[72] While delving into these aspects is beyond the scope of this text, it is worth noting that significant progress has been made in this area, thanks to advancements in mass spectrometry and applications of fluorescent biosensors.[73,74]

A traditional method for kinase activity quantification is the direct isotope labeling of the phosphate donor. In this method, a kinase assay is performed with a [γ-^{32}P]-labeled NTP. The phosphorylated protein product is subsequently detected by autoradiography.[75] Moreover, this approach allows for *in vivo* applications, as endogenous ATP can be labeled by the [γ-^{32}P]-labeled orthophosphate in intact cells.[72] Obvious drawbacks of isotope labeling are the safety hazards associated with working with radioactive isotopes. Although alternative labels were designed to avoid the use of radioactive isotopes (such as biotinylation or

fluorescent tags), these approaches are generally much less sensitive.[72,76,77]

Another traditional approach for quantifying protein phosphorylation involves utilizing antibodies specific to particular phosphorylated sites in protein targets. The detection of the phosphorylated product is typically carried out using Western blotting.[72,76,77] Moreover, antibodies have been successfully applied to study kinase activity by other methods, such as flow cytometry,[78] immunohistochemistry,[79] or enzyme-linked immunosorbent assay.[80] Nevertheless, rigorous optimizations of the experiments are necessary, due to the potential lack of specificity of antibodies to the particular sites of interest, a general problem to be expected when working with antibodies.[72,76,77]

Furthermore, the standard sodium dodecyl sulfate–polyacrylamide gel electrophoresis (SDS–PAGE) can be partially effective in separating the unphosphorylated and phosphorylated forms of the same protein. The phosphorylated proteins exhibit a slight decrease in electrophoretic mobility compared to their unphosphorylated counterparts.[81] This mobility shift cannot be solely attributed to differences in molar masses, as the addition of even a few phosphate groups cannot be resolved on standard gels. However, it is hypothesized that SDS is repelled by the phosphate anions present in phosphorylated proteins, leading to a decrease in charge density on the protein surface. This change manifests as an apparent shift in molecular weight.[72] Despite its usefulness in certain cases, this approach is not universally applicable, as only specific proteins exhibit such distinctive behavior between their unphosphorylated and phosphorylated forms.[81]

An elegant solution to overcome the limitations of standard SDS–PAGE in detecting protein phosphorylation is to couple it with a phosphate-labeling reagent. Kinoshita et al. proposed the use of a synthetic phosphate-binding ligand (Phos-tag), a 1,3-bis[bis(pyridin-2-ylmethyl)amino]propan-2-olato zinc(II) complex.[82] The Phos-tag-based kinase assays follow the same procedure as the standard SDS–PAGE, with the main distinction lying in the preparation of the resolving gel. In this method, acrylamide-pendant Phos-tag is added to the gel mixture and subsequently copolymerizes, resulting in a Phos-tag acrylamide gel. During the separation, phosphorylated forms bind to Phos-tag, leading to a reduction in their electrophoretic mobility with respect to unphosphorylated forms.[83] Several optimizations of the original method have been reported, with either manganese(II) or zinc(II) ions being chelated by the anion in Phos-tag.[84–87]

Phos-tag SDS–PAGE enables highly accurate and sensitive quantification of phosphorylated proteins, with distinct bands formed by proteins phosphorylated to different extents. However, it is essential to note that lower mobility does not

necessarily indicate a higher degree of phosphorylation.[72] An intriguing finding is that separate bands are produced by protein forms with the same number of phosphorylated sites if these sites differ between each form.[83] This suggests that the interaction of Phos-tag with the phosphorylated site is influenced by nearby amino acids. Although the precise mechanism remains unclear, it may be concluded that the mobility of different protein forms primarily depends on their affinity to Phos-tag. Consequently, the positions of the bands may not correlate with molecular weights, as observed in standard SDS–PAGE.[84–87]

1.2 Integrated stress response

Regulation of gene expression is a fundamental mechanism of how cells maintain and restore homeostasis during stress.[27] Eukaryotic cells are able to reprogram the last step of gene expression, the synthesis of proteins, in response to a variety of intrinsic and extrinsic factors. The response is mediated by five protein kinases, each regulated by different stress signals (heme or amino acids deficiency, heat shock, oxidative or mitochondrial stress, viral infection, etc.). When activated, these kinases phosphorylate eIF2. As a result, general protein synthesis is impaired and preferential translation of a subset of specialized messenger RNAs (mRNAs) is stimulated. Since various stress inputs converge on this universal output, this highly conserved signaling pathway is termed the *integrated* stress response.[1–6] The new translational program allows the cell to save energy and amino acid stores, and to simultaneously activate recovery mechanisms. However, the integrated stress response eventually activates the apoptotic machinery if the stress factor is excessive in duration and/or intensity. Dysregulation of the integrated stress response has significant pathological consequences, which renders the five kinases pivotal pharmacological targets.[1–6]

1.2.1 Basic mechanisms

In the initiation phase of mRNA translation, the key event is the recognition of the (5′)AUG start codon, which signals the beginning of the open reading frame (ORF). While bacterial ribosomes are guided by the Shine–Dalgarno sequence, eukaryotic translation relies on scanning mRNA from the 5′ end until the first AUG sequence is encountered.[88] The association of the eukaryotic ribosome to mRNA is supported by numerous proteins (the initiation factors), out of which eIF2 plays a pivotal role in the dynamics of the scanning process.

eIF2 is a heterotrimeric GTPase, consisting of the α, β and γ subunits. The α subunit (eIF2α) is regulatory, as it contains a key Ser51 residue targeted by the five stress-response kinases.[89] The *N*-terminal domain of the γ subunit contains a binding site for GTP or guanosine 5′-diphosphate (GDP).[90] As common for signaling GTPases, the hydrolysis of GTP drives the transition of the protein to an inactive state. In the case of eIF2, the deactivation induces a loss of affinity to the methionine-binding initiator transfer RNA (Met–$\mathrm{tRNA_i^{Met}}$).[91] Since the non-catalyzed exchange of GDP for GTP would be too slow otherwise, the reactivation of eIF2 is assisted by a dedicated guanine nucleotide exchange factor,

eIF2B.[92] However, eIF2B is noncompetitively inhibited by phosphorylated eIF2 (eIF2α–P).[93]

Let us now explain further details of the eIF2 role in mRNA translation initiation. When charged with GTP, eIF2 binds Met–$tRNA_i^{Met}$ to form a ternary complex. With the aid of additional initiation factors, the ternary complex is recruited by the small ribosomal subunit to form the preinitiation complex, which binds mRNA at its 5′ 7-methylguanosine cap.[88] This assembly then starts scanning along the mRNA, until the start codon is recognized. The interaction of the mRNA start codon and the Met–$tRNA_i^{Met}$ anticodon induces the hydrolysis of eIF2–bound GTP, catalyzed by eIF5, a dedicated GTPase-activating protein.[94] The resulting eIF2–GDP complex is not bound by the Met–$tRNA_i^{Met}$, and it dissociates from the translational assembly.[88,91] This allows the ribosomal subunits to reassemble at the beginning of the ORF, and to commence the elongation phase.

The released eIF2–GDP complex may bind new Met–$tRNA_i^{Met}$ and participate in the next rounds of translation initiation, but it first needs to be 'recharged' with GTP by the nucleotide exchange factor eIF2B. eIF2B is a heterodecamer, with two ε subunits at the opposing ends of the protein serving as the binding site for the eIF2 substrate.[95] However, the conformation of eIF2 is dramatically altered by the phosphorylation at the α subunit. In particular, a hydrophobic patch is formed on the surface of eIF2 which enforces its binding to a different site of eIF2B. Since the proper positioning of eIF2 into the catalytic domain of eIF2B is no longer possible, eIF2α–P acts a noncompetitive inhibitor of eIF2B.[96,97]

The immediate outcome of the eIF2B inhibition by eIF2α–P is the reduction of the availability of ternary complexes. Evidently, this results in a severe decline in global protein synthesis. However, many eukaryotic mRNAs do not follow the simple "first AUG rule" described above, because the 5′ untranslated region contains multiple upstream ORF (uORF), which normally repress the translation of the main ORF. Paradoxically, the translation of such mRNAs is enhanced as a result of the eIF2α phosphorylation. These preferentially expressed proteins then become critical actors in the subsequent stages of the integrated stress response.[98,99]

A prominent example of such proteins is the activating transcription factor 4 (ATF4). In the 5′ untranslated region of the ATF4 mRNA, there are two uORF, and the second of them (uORF2) overlaps with the main ORF for ATF4. Under normal conditions, uORF1 is translated and re-initiation then occurs at the uORF2, which blocks the translation of the main ORF. To start translation at

the main ORF, the ribosome would have to bypass ORF2 being uncharged by the ternary complex, which is very unlikely because the ternary complexes are readily available. However, if ternary complexes are scarce, the likelihood of this bypass rapidly increases.[100,101] ATF4 levels are thus elevated under stress conditions. Many downstream signaling cascades are affected by ATF4 homodimers, or by heterodimers of ATF4 with other transcription factors. The regulation of ATF4 is the best characterized one, yet there are other examples of preferentially expressed proteins, such as ATF5, growth arrest and DNA damage-inducible protein 34 (GADD34),[102] or the CCAAT-enhancer-binding protein homologous protein (CHOP).[103]

To restore the normal translational program after the stress response is complete, the Ser51 residue at eIF2α needs to be dephosphorylated. Two phosphatase complexes perform this task, both of which use protein phosphatase 1 (PP1) as the catalytic core, but differ in the regulatory subunit.[104] The first complex uses the constitutive repressor of eIF2α phosphorylation (CReP) as the regulatory subunit, while the second uses GADD34. While the expression of CReP is independent of eIF2α–P concentration,[105] the expression of GADD34 is regulated both at the transcriptional (by ATF4) and translational (similarly as ATF4) levels.[106] The GADD34–PP1 complex thus provides a feedback mechanism for attenuating the integrated stress response. The key processes of the integrated stress response are summarized in Fig. 1.4 on p. 20.

1.2.2 eIF2α phosphorylating kinases

At the core of the integrated stress response lie the five kinases responsible for catalyzing the phosphorylation of eIF2α. These protein-Ser/Thr kinases share extensive homologies in their catalytic domains, yet their regulatory domains differ vastly. Thanks to this diversity, each kinase is able to respond to different types of stressors. However, certain conditions activate multiple kinases at the same time (such as oxidative stress).[4] While numerous aspects of the activation mechanisms remain to be fully elucidated, it is widely hypothesized that dimerization and autophosphorylation play pivotal roles in activating all of the kinases.[1–6]

The first kinase identified to phosphorylate eIF2α was the HRI, initially discovered as a regulator of hemoglobin synthesis in reticulocytes and red blood cells.[7] Since unbound heme and globin chains are both potentially toxic to the cell, it is necessary to maintain their concentrations at the stoichiometric ratio. Under normal conditions, the binding of heme to the regulatory domain of HRI

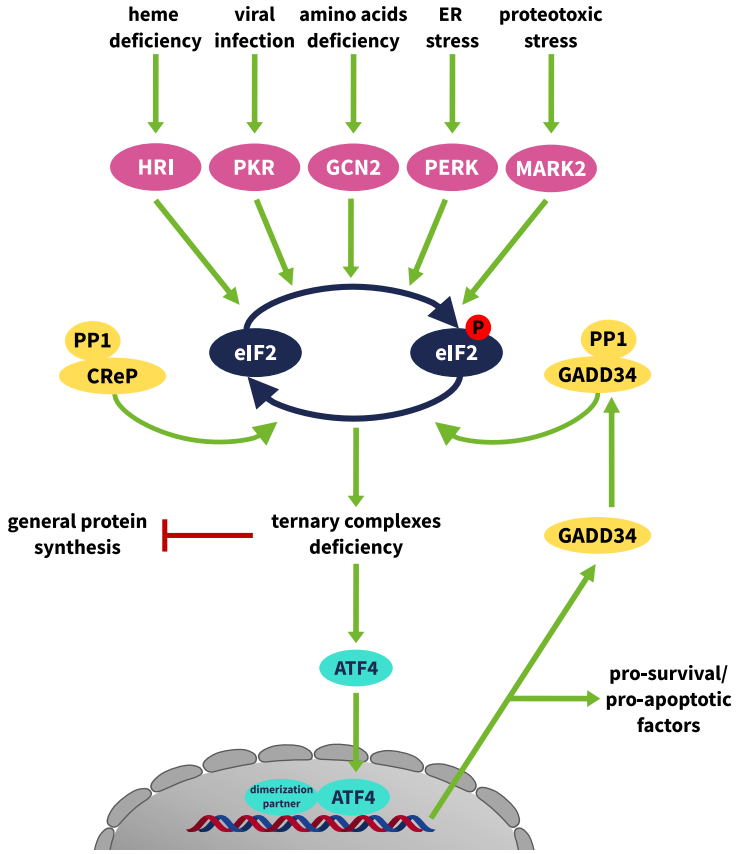

Figure 1.4: Key processes in the integrated stress response. Five kinases (HRI, PKR, GCN2, PERK, MARK2) phosphorylate eIF2α at the Ser51 residue, leading to a decrease in the ternary complex concentration. This decrease inhibits general protein synthesis while promoting selective synthesis of specific proteins, such as ATF4. ATF4 functions as a transcription factor, either as a homodimer or heterodimer, enhancing the transcription of pro-survival or pro-apoptotic genes, which are normally repressed. The activation of the integrated stress response is antagonized by two phosphatase complexes, CReP–PP1 and GADD34–PP1, with GADD34 expression being positively regulated by ATF4. The scheme was adapted from Ref.[4]

inhibits the eIF2α–kinase activity of HRI. However, when heme levels decrease, the HRI–heme complex dissociates, allowing eIF2α phosphorylation to occur. The subsequent attenuation of protein synthesis prevents the accumulation of unfolded globin chains, enabling the cell to survive until heme availability is restored.[107,108]

Although early studies utilized HRI purified from reticulocyte lysate, subsequent investigations confirmed the expression of HRI in various cell types and organs, including the liver, spleen, lungs, heart, brain, pancreas, kidneys, ovaries, and testes.[8,9] Several stress factors, such as heat shock, oxidative and osmotic stress, as well as proteasomal inhibition, have been shown to induce eIF2α phosphorylation by HRI.[109–111] These findings indicate that the functions of HRI ex-

tend well beyond its role in regulating hemoglobin synthesis. For a more comprehensive discussion of studies on HRI, see Section 1.3 (p. 23).

Later on, the double-stranded RNA-dependent protein kinase (PKR) was discovered. The primary function of this kinase is participation in the response to viral infection. By recognizing viral double-stranded RNAs, PKR phosphorylates eIF2α to inhibit the synthesis of both viral and host proteins.[112] The significance of PKR is underlined by the fact that many viruses acquired mechanisms to evade the PKR-induced response.[113] Additionally, PKR was shown to be upregulated by endogenous non-coding RNAs (such as microRNAs),[114,115] as well as by several RNA-independent signals (oxidative stress, stress of endoplasmic reticulum (ER), growth factor deprivation, bacterial infection, heparin).[116,117]

Nutritious stress is sensed by the general control nonderepressible 2 (GCN2) kinase, which was discovered next. GCN2 is activated in response to uncharged transfer RNA (tRNAs), which accumulate when there is an insufficient intake of essential amino acids and/or disruption in non-essential amino acid synthesis.[118] It has also been suggested that GCN2 can be activated by glucose deprivation in tumor cells. However, this activation was attributed to the increased consumption of amino acids as alternative energy sources when glucose levels are low.[119] Furthermore, there are additional reports indicating the activation of GCN2 in response to ultraviolet irradiation and viral infections.[120,121]

Unlike the previous three kinases, which were soluble cytosolic proteins, the subsequently discovered PKR-like ER kinase (PERK) spans the membrane of the ER. The *N*-terminus of PERK resides within the ER lumen, while its *C*-terminus containing the kinase domain is exposed to the cytosol.[122] This structural arrangement aligns with the role of PERK in the unfolded protein response. PERK becomes activated in response to the accumulation of unfolded proteins in the ER lumen and by attenuating global protein synthesis, it reduces the influx of nascent proteins into the ER.[123] This process allows the ER to refold the unfolded proteins and restore its homeostasis. However, emerging evidence suggests that PERK serves as a broader regulator of ER functions, including calcium homeostasis and redox status.[124] Moreover, PERK has been reported to be activated by ATP depletion resulting from glucose deprivation in neuronal and pancreatic β cells.[125,126]

Until recently, a consensus prevailed that the phosphorylation of eIF2α solely relied on the four kinases mentioned. Employing a gene-knockout strategy, Taniuchi et al. demonstrated that no additional kinases should be needed for the integrated stress response, at least in vertebrates.[5] Nevertheless, a novel study

unveiled the capability of the microtubule affinity-regulating kinase 2 (MARK2) to phosphorylate eIF2α in response to proteotoxic stress in mammalian cells.[127] Previously, MARK2 was recognized for its role in the regulation of microtubule dynamics, by phosphorylating the microtubule-associated proteins.[128]

1.3 Heme-regulated inhibitor

Building upon the varied roles of the eIF2α kinases outlined in the preceding section, this section will delve into more comprehensive details concerning the structure and regulation of HRI. As a heme sensor protein, HRI possesses a regulatory domain associated with its kinase domain, capable of sensing heme concentrations. Specifically, the structure of the HRI enzyme is divided into five domains.[13] The kinase domain contains a kinase-insert region, separating the kinase I and II domains. The *N*- and *C*-terminal domains surround the kinase domains from both sides (see Fig. 1.5).[13]

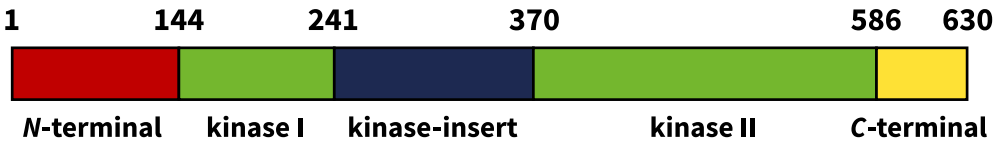

Figure 1.5: Five domains of the full-length HRI enzyme. Adapted from Ref.[13]

1.3.1 Heme coordination sites

The process of heme sensing and coupling it with the kinase activity of HRI remains a continuing research challenge. Early studies suggested that there were two distinct binding sites for heme in the structure of HRI.[129,130] In this model, heme binds strongly to the first binding site located in the *N*-terminal domain, while the second site in the kinase-insert domain allows for dynamic and reversible heme coordination. It was proposed that two heme molecules were bound per one HRI monomer.[131] The coordination into the *N*-terminal domain occurs cotranslationally and it is a prerequisite for proper folding and proteolytical stability of the HRI enzyme.[132] On the contrary, coordination into the second binding site is dictated by local heme concentration and it regulates the kinase activity of the holoenzyme. It was also hypothesized that two His residues were the axial ligands of the heme iron coordinated in the *N*-terminal domain.[133]

However, later studies have indicated that the stoichiometry of the HRI–heme complex is 1:1.[134,135] Spectroscopic studies have shown that the single iron(III) ion per HRI monomer forms a hexa-coordinate low-spin complex with a His and a Cys residue as the axial ligands.[134,136] The particular residues were later identified using site-directed mutagenesis.[137] Located in the *N*-terminal domain, His119 or His120 is the first axial ligand (with ligand switching between them). The second axial ligand (*trans* to the His residues in the *N*-terminal domain) is Cys409 in

the kinase II domain. This Cys residue is supposed to be a part of a heme-regulatory Cys–Pro motif since a mutation at the Pro410 resulted in the loss of the enzyme's affinity to heme.[137] However, HRI is generally flexible with respect to ligand switching, thus a mixture of species is expected in equilibrium, including hexa-coordinate Cys–Fe(III)–His, Cys–Fe(III)–H_2O/OH^-, and penta-coordinate Cys–Fe(III).

The coordination of heme by a Cys thiolate is a characteristic feature of heme-sensing proteins.[138] In this respect, it is suitable to mention that the sensing function of heme sensor proteins essentially relies both on thermodynamics and kinetics. Thermodynamically, the binding constant K of the heme–apoprotein complex must not be too large, and kinetically, the rate constant k_d of heme dissociation from the apoprotein must not be too low. In the case of HRI, for instance, the coordination of iron(III) by the Cys residue is weak enough, thus HRI can serve as a heme sensor ($k_d = 1.5{\cdot}10^{-3}$ s^{-1}, $K = 7.1{\cdot}10^9$ with the standard state of unit molarity).[134] On the contrary, the relatively stronger coordination of heme by His in myoglobin ($k_d = 8.4 \cdot 10^{-7}$ s^{-1}, $K = 8.3 \cdot 10^{13}$ with the standard state of unit molarity) is in line with its much different biological role.[139] These arguments may also explain the differences in the rigidity of heme coordination by the N-terminal and the kinase II domains of HRI.

Due to weaker electrostatic attraction, the coordination of a Fe(II) ion by a Cys thiolate is even weaker than that of Fe(III). For this reason, the reduction of heme Fe(III) to Fe(II) often causes the Cys thiolate to dissociate, if an additional stabilization of the Fe(II)–Cys complex is not provided (e.g. by networks of hydrogen bonds, as is the case of cytochrome P450 or nitric oxide synthase).[138] In the case of HRI, Fe(II) was shown to form a hexa-coordinate low-spin complex with His and neutral Cys thiol as the axial ligands.[136] However, the Cys residue rapidly dissociates and is replaced by unknown amino acids.[135,137] It thus seems that Fe(II) heme binds to HRI in a nonspecific manner, and does not function as a regulatory signal.[137]

The redox state of heme coordinated by HRI was also explored by kinetic assays of its kinase activity.[134,136] However, inconsistent results were reported by these studies. The Fe(II) HRI holoform was reported to have a 2.4fold higher activity than the Fe(III) holoform.[136] On the contrary, when the reactions were assayed at different concentrations of heme, the Fe(II) holoform was generally less active than the Fe(III) holoform. Both inhibition curves were sigmoidal and the half-maximal inhibitory concentrations (IC_{50}) values of Fe(III) and Fe(II) forms were 9.5 µM and 4.1 µM, respectively.[134]

1.3.2 Regulation: heme sensing and autophosphorylation

Along with the coordination of heme, the degree of phosphorylation is the second key regulatory mechanism of the HRI kinase activity. Even the earliest reports stated that there were multiple autophosphorylation sites in the structure of HRI and that the kinase activity with respect to eIF2α increases with the degree of autophosphorylation.[140] It was hypothesized that heme-deficient conditions induced such a conformational change in HRI which facilitated its autophosphorylation. It was concluded that HRI functioned as a dimer and the authors speculated that the autophosphorylation may occur either on each subunit independently, or by a transphosphorylation mechanism.

The successive research has preserved the consensus that the activation in HRI occurs in multiple stages, which include the gradual HRI autophosphorylation and the dissociation of heme. However, the details of the process have been long debated, especially the oligomerization states of the intermediates and the roles of individual HRI domains. It was first reported that HRI purified as an elongated homodimer with heme stably bound in the *N*-terminal domains of both subunits.[130] It has been suggested that reversible binding of heme into the kinase-insert domain converts the HRI dimer into an inactive form by inducing the formation of intersubunit disulfide bonds.[129,141] In the active HRI homodimer, conversely, the subunits are attached by noncovalent interactions only.

Bauer et al. have suggested that HRI dimerizes soon after its *de novo* synthesis and that the subsequent autophosphorylation occurs in two stages.[131] Later, the group identified Thr485 as the critical autophosphorylation site for attaining the eIF2α–kinase activity.[141] The updated model of HRI activation was proposed as follows (see Fig. 1.6 on p. 26): the HRI subunits bind heme stably into their *N*-terminal domains during translation. The dimers are then rapidly formed and undergo the first stage of autophosphorylation. The partially autophosphorylated dimers are protected against aggregation, yet their eIF2α–kinase activity is still low. The second stage of autophosphorylation yields stable elongated homodimers, which can reversibly bind heme molecules into the kinase domains (while still binding heme in the *N*-terminal domains). In the presence of heme, the kinase-domain binding sites are occupied and the kinase activity is suppressed, presumably by the formation of intersubunit disulfide bonds. On the contrary, heme-deficient conditions favor the last stage of autophosphorylation, which involves the key Thr485 residue. Then, the dimeric HRI enzyme attains full eIF2α–kinase activity.

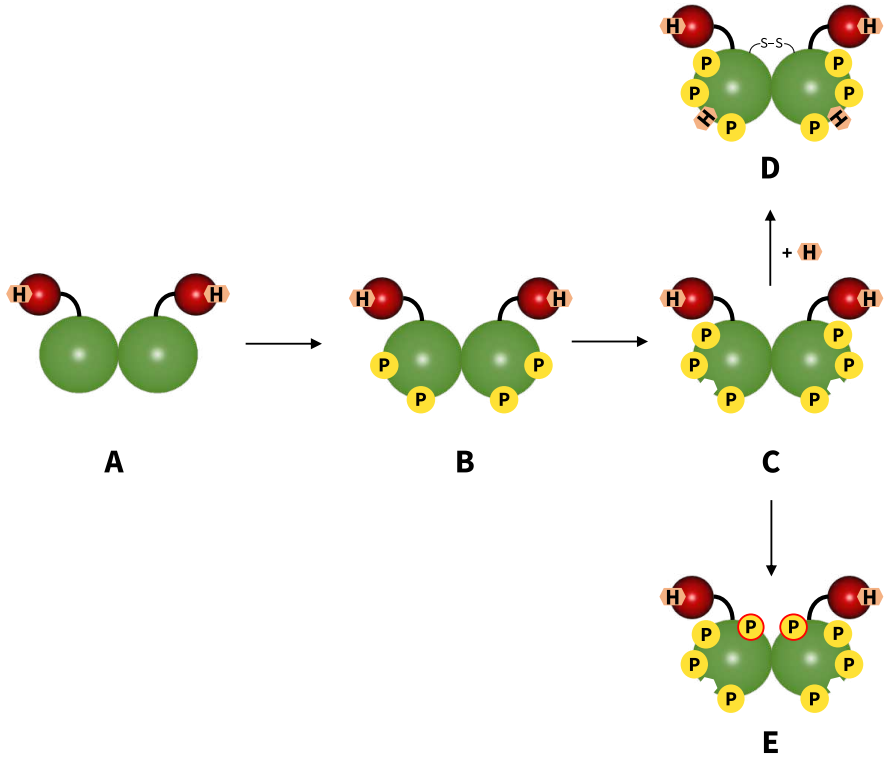

Figure 1.6: Early model of HRI activation. The nascent HRI (red – *N*-terminal domain, green – *C*-terminal domain) dimerizes into an inactive dimer **A**, which is protected against aggregation by autophosphorylation at several sites, yielding species **B**. After additional autophosphorylations, the HRI dimer is able to bind heme reversibly into the kinase domain (**C**). The binding of heme converts HRI into an inactive form **D**. In heme deficiency, HRI attains full eIF2α–kinase activity upon undergoing the final stage of autophosphorylation (**E**). This includes the phosphorylation at the key Thr485 residue (red circle). The scheme was adapted from Refs.[131,141]

The autophosphorylation sites in mouse HRI were later identified with the aid of mass spectrometry.[142] While the *N*-terminal domain contains 5 sites only, 16 and 12 were localized in the kinase-insert and the kinase domains, respectively. Using site-directed mutagenesis, it was shown that out of the total 33 autophosphorylation sites, Tyr193, Thr485, and Thr490 were essential for the eIF2α–kinase activity. It has thus been proposed that the first stage of autophosphorylation involves these three key residues, while the remaining sites are autophosphorylated in the second stage (this is inconsistent with the model shown in Fig. 1.6, according to which the Thr485 residue is phosphorylated in the last stage of activation). Moreover, a pulldown assay performed in this study revealed an additional function of autophosphorylation: it suppresses the interaction between the *N*-terminal domain and the kinase domains.[142] The critical role of interdomain interactions in regulating HRI kinase activity has also been reported.[143]

The model of HRI activation described above (Fig. 1.6 on p. 26) was later challenged by several findings. First, various oligomerization states of HRI in solutions were reported, including dimers, trimers, hexamers, or even larger aggregates.[134,144] Next, the 1:1 stoichiometry of the heme complex with a HRI monomer was postulated.[134,135] Biophysical studies also provided deeper insights into the structural changes induced by heme binding to HRI.[13,145,146] The results suggest that under normal physiological conditions, the nascent HRI subunits bind heme and form inactive structures in ranging oligomerization states.[144] The *N*-terminal domain supports the formation of such oligomers.[134] However, the conversion of HRI into an active form requires the formation of stable dimers. The latest report indicates that the *C*-terminal coiled-coil domain is responsible for this activatory dimerization.[13] Since the formation of dimers was shown to facilitate efficient autophosphorylation, it is assumed that the subunits of the dimer phosphorylate each other. This *trans* autophosphorylation mechanism was shown to be dominant since the *cis* mechanism (i.e. each subunit autophosphorylating itself) is much slower.

Nevertheless, the precise role of heme binding in the activation process of HRI remains unclear. It seems that the sensing of heme by HRI is mediated through interdomain interactions and changes in the tertiary structure, rather than by mere interactions of heme with the protein surface.[13,131,137] Igarashi et al. have presumed that the dissociation of heme weakens the interaction between the *N*-terminal domain and kinase domains, which allows the activatory autophosphorylation to occur.[142] Autophosphorylation then further weakens the interdomain interactions, enhancing the eIF2α–kinase activity.[142] The latest report points out that heme inhibition occurs through a heme-binding site located in the kinase domain outside the kinase-insert region, although the kinase-insert region accounts for efficient both autokinase and eIF2α–kinase activities of HRI.[13]

1.3.3 Regulation: additional mechanisms

As outlined in the previous sections, the regulation of HRI kinase activity involves two crucial mechanisms: heme sensing and autophosphorylation. However, the signaling cascades converging on the regulation of HRI seem to be much more complex, given the wide array of stress factors responded to by HRI (heat shock, exposure to heavy metals, oxidative stress, etc.). In many cases, it remains unclear whether the stressors are able to activate *directly*, or whether additional proteins are needed to mediate the response.[107,108]

After HRI was shown to form a complex with the heat shock protein 90 (Hsp90) in rabbit reticulocyte lysates,[147,148] it has been proposed that an inactive HRI–Hsp90 dimer is formed in the presence of heme, while under heme-deficient conditions, the dimer dissociates and HRI acquires the eIF2α–kinase activity.[149] Later experiments have indicated that Hsp90 stabilizes HRI and assists newly synthesized HRI molecules in acquiring a proper conformation, which can later be activated by phosphorylation.[150] Although this function is consistent with the prominent role of Hsp90 as a cytoplasmic chaperone, further studies have confirmed that Hsp90 enhances the eIF2α–kinase activity of HRI during heat stress, so as to inhibit global protein synthesis.[151,152] Together, it seems that the association of HRI and Hsp90 serves both functions. Under physiological conditions, Hsp90 acts as a chaperone, while the heat shock conditions modulate the HRI–Hsp90 interaction in such a manner that activates the HRI kinase activity.

The molecular details of HRI activation from the inactive HRI–Hsp90 remain to be fully elucidated. On one hand, it has been suggested that the HRI–Hsp90 interaction is mediated by a co-chaperone, such as cell division cycle 37 (Cdc37), which also assists the folding of other protein kinases.[153] A study of mutant Cdc37 protein showed that the *N*-terminal domain of Cdc37 interacted with immature HRI, while the *C*-terminal domain interacted with Hsp90. On the other hand, Mukai et al. observed that Hsp90 enhanced the eIF2α–kinase activity of HRI via a direct protein–protein interaction (i.e. without the co-chaperone) if HRI was phosphorylated and heme was deficient.[154] Autophosphorylation of HRI was thus identified as the prerequisite for the interaction with Hsp90, while Hsp90 was not able to enhance the autokinase activity of HRI.

A co-immunoprecipitation study recently supported the hypothesis that direct protein–protein interaction may be critical to the association of HRI and Hsp90.[144] It was shown that the association was dominantly mediated by the kinase I domain of HRI. However, the other domains aided to stabilize and modulate this interaction, since the isolated kinase I domain was not able to bind alone to Hsp90. Presumably, the association of HRI and Hsp90 *per se* does not require the assistance of other factors, while the transition of HRI into the active state may be driven by additional proteins, such as Cdc37, heat shock cognate 70 (Hsc70), or p23.[151] For instance, Hsc70 was shown to attenuate the autokinase activity of HRI, thereby suppressing the subsequent activation.[155,156] The participation of different proteins in the regulation of HRI kinase activity probably assures a dynamic response to various stresses.

Although the role of autophosphorylation in the activation of HRI is unquestionable, it cannot be excluded that other protein kinases may also phosphorylate HRI under physiological conditions. The possibility of heterophosphorylation was mentioned even in the earliest studies, which concluded that while 3′,5′-cyclic-adenosine-monophosphate-dependent kinase had no effect on the activity of HRI,[157,158] the opposite may be true for 3′,5′-cyclic-adenosine-monophosphate-independent kinases.[140] An extensive study of phosphorylation sites at cellular proteins has shown that HRI contains motifs recognized by CK1 and CK2, and by glycogen synthase kinase 3.[134,159] These findings support a previous report of HRI activation by CK2.[160] Much as the participation of HRI in protein kinases cascades needs to be further elucidated, it may be an important facet of the full picture of the integrated stress response.

Apart from proteins, many chemical agents were reported to modulate the activity of HRI. For instance, metal ions were originally reported to activate HRI, and thus inhibit protein synthesis.[161,162] Nevertheless, experiments with purified HRI implied the opposite–Hg^{2+} ion was the most potent inhibitor with IC_{50} = 0.6 µM, followed by a set of cations with IC_{50} of 2–9 µM (Cu^{2+}, Cd^{2+}, Zn^{2+}, Pb^{2+}).[163] Moreover, although arsenite ions were shown to regulate HRI activity by both *in vitro*[109] and *in vivo*[164] studies, the kinase assays with the purified enzyme did not reveal any significant change in HRI activity in the presence of these ions.[163]

Notably, nitric oxide and carbon monoxide were shown to regulate the activity of HRI by binding to the heme iron in its structure.[165] Compared to the Fe(III)–HRI holoform, the eIF2α–kinase activity of the Fe(II)–NO complex was 5fold higher, while that of the Fe(II)–CO complex was 1.2fold lower.[136] Based on a spectroscopical study of the heme axial ligands under various conditions, it was suggested that the binding of NO causes both exogenous ligands (His and Cys) to dissociate.[136] The binding of NO in a penta-coordinate manner by HRI then induces such conformational changes in the apoprotein which enhance its eIF2α–kinase activity. On the contrary, CO forms a hexa-coordinate complex within the Fe(II)–HRI holoform, in which the coordination of heme iron by the His residue is retained, preventing the activatory structural changes to occur (only a weak interaction of CO with amino acids close to the binding site was reported).[166] Note that NO was also shown to reverse the inhibition of HRI induced by Hg^{2+} ions.[163] In summary, it seems that eIF2α phosphorylation by HRI may contribute to the diverse stress responses mediated by NO and CO.[167,168]

1.3.4 Catalysis

While considerable efforts have been put into the elucidation of heme sensing by HRI, the literature concerning its kinase domains remains relatively scarce. Although the residues presumably adopt the highly conserved architecture in the active state, unambiguous evidence for this assumption is missing. This is primarily caused by the absence of information on the secondary or tertiary structure of HRI.

Nonetheless, the canonical catalytic residues appear to be preserved in the structure of HRI. Site-directed mutagenesis studies targeting Lys196 have shown that altering this residue leads to an inactive,[141] and in some cases, an insoluble species.[134] It is believed that this Lys196 residue is analogous to Lys168 in protein kinase A, a residue known to play a critical role in ATP phosphate binding and positioning (see Section 1.1.1, p. 9).[16,17,33,34] Furthermore, HRI is unequivocally activated by autophosphorylation, a characteristic shared by many members of the eukaryotic protein kinase superfamily.[141,142] Studies have suggested that the Thr485 and Thr490 autophosphorylation sites are located in the HRI's putative A-loop. As autophosphorylation of these residues is essential for catalysis, it appears that their function is comparable to that of the residues in the A-loop of protein kinase A. That is, phosphorylation likely induces a conformational change that alleviates the physical hindrance of the active site by the A-loop.[141,142]

Valuable insights into the process of ATP and eIF2α substrates binding were provided by kinetic studies. Importantly, the phosphorylation of eIF2α constitutes a bisubstrate reaction (Eq. 1.1). Consequently, it is necessary to conduct kinetic analyses separately for each substrate. The obtained results are then interpreted as apparent kinetic parameters.

$$\text{eIF2}\alpha + \text{ATP} \longrightarrow \text{eIF2}\alpha\text{–P} + \text{ADP}. \tag{1.1}$$

The initial kinetic analyses demonstrated that the rate of eIF2α phosphorylation by HRI followed the Michaelis-Menten equation with respect to ATP concentration, while a sigmoidal dependence was observed for the concentration of eIF2α.[134] Comparing the Hill coefficient between the full-length HRI enzyme and a *N*-terminus truncated mutant, it has been proposed that the *N*-terminal domain enhances the positive cooperativity of HRI subunits with respect to the eIF2α substrate. In a more recent biophysical study of the isolated kinase domain, no rearrangements at the secondary structure level were found, further supporting the notion that the cooperativity of subunits is reliant on the *N*-terminal domain.[146]

While the *N*-terminal domain may not be considered critical for the catalytic mechanism of HRI itself, studies have shown that the interaction between the *N*-terminal and kinase domains does reduce the catalytic efficiency of HRI.[130,134] This observation aligns with the significance of interdomain interactions highlighted in Section 1.3.2 (p. 25).[142,143] Subsequent investigations have confirmed that the *N*-terminal domain does not directly participate in either eIF2α–kinase activity or HRI enzyme autophosphorylation.[13] Present findings suggest that the *N*-terminal domain stabilizes the inactive conformation of HRI in the presence of heme, likely through structural rearrangements that decrease the affinity towards eIF2α. Additionally, recent kinetic experiments revealed that both eIF2α and ATP followed the Michaelis-Menten model.[13] This study has also implied that heme inhibition is noncompetitive with eIF2α and HRI. In summary, although the key regulatory heme-binding site was localized in the kinase domain, it appears to lie at a sufficient distance from the active site.[13]

1.3.5 HRI as a dual target in cancer treatment strategies

Since the development of many cancers rely on the disruption of normal protein synthesis, any strategies for its restoration may in principle reverse malignant transformations.[10–12] In the case of HRI, such a strategy is provided by both activating and inhibiting its kinase activity (see below). However, the significance of HRI in cancer research extends beyond this direct role. Tumor cells with abnormally high/low HRI activity often exhibit decreased sensitivity to other therapeutic approaches, such as proteasomal inhibition. Therefore, combining these approaches with the modulation of HRI activity presents a promising avenue for cancer treatment.[10–12] This section reviews the studies investigating HRI in both contexts: as a direct anticancer agent and as a means to enhance the efficacy of other cancer therapies.

The levels of translation initiation factors (including eIF2) are generally higher in cancer cells, which presumably corresponds to their need for rapid and intense protein synthesis.[169,170] eIF2α signaling seems to have multiple implications in this process. On one hand, the eIF2α kinases act as tumor suppressors, since they activate the downstream apoptotic mechanisms, thereby preventing uncontrolled cell proliferation.[171] For instance, it was reported that the forced expression of non-phosphorylatable eIF2 mutant drove the malignant transformation of normal cells,[172] and that upregulation of the PKR/eIF2α pathway was a positive prognostic marker in early-stage lung cancer.[173]

In this view, it seems that triggering the pro-death mechanisms downstream of eIF2α phosphorylation could be helped by sustained pharmacological activation of HRI. On the other hand, the HRI/eIF2α pathway seems to contribute to the coordinated gradual changes in tumor cell signaling, which promote tumor growth, such as by the preferential expression of oncogenic factors.[12,174,175] From this viewpoint, inhibiting the activity of HRI may also serve as an anticancer strategy. However, it has been hypothesized that deactivation of eIF2α is more likely to be associated with target-dependent toxicities, such as pancreatic injuries or impairments in behavioral flexibility.[176,177]

Indeno[1,2-c]pyrazoles were the first synthetic inhibitors of HRI identified.[178] Later, molecular dynamic simulations suggested that these compounds interacted with the putative ATP-binding site.[179] However, their therapeutic potential is yet to be evaluated. As for HRI activators, *N,N′*-diarylureas were suggested based on a screening of more than 100000 compounds.[180] This study also confirmed that these agents were indeed able to directly activate HRI and that the downstream pathways were able to induce cancer regression *in vivo*. Furthermore, an important advantage of *N,N′*-diarylureas is the absence of reported organ toxicity at the administered doses.[180]

Subsequent research focused on optimizing the structures of *N,N′*-disubstituted ureas to develop highly potent and specific HRI activators. As a part of a study investigating the impact of substitutions on the *N*-aryl and *N′*-cyclohexylphenoxy groups, the CHOP protein was identified as an important effector induced by eIF2α phosphorylation.[181] Through further testing, 1-((1,4-*trans*)-4-aryloxycyclohexyl)-3-arylureas with optimized physicochemical properties emerged as the most promising candidates for drug development.[182] It is important to note that the efficacy of HRI activators relies on the levels of HRI expression in tumor cells.[180] Therefore, quantifying HRI in tissues will be essential in the clinical trials of HRI activators.[12]

Furthermore, the therapeutic potential of HRI activators and inhibitors extends to cases where resistance to anticancer treatment is linked to abnormal eIF2α phosphorylation. For instance, proteasomal inhibitors (such as bortezomib) were successfully used to promote apoptosis in multiple myeloma cells, with the participation of the CHOP protein induced by eIF2α phosphorylation.[183,184] Accordingly, cells with reduced levels of eIF2α–P were resistant to bortezomib treatment.[185] With the precise mechanism unknown, it seems that the resistant cells stimulate eIF2α–P dephosphorylation in order to avoid the proapoptotic CHOP-dependent response. Overcoming this resistance has been achieved through inhi-

bition of the GADD34-PP1 complex;[185] however, an alternative approach could involve activating the upstream HRI kinase.

This approach of enhancing anticancer therapies by a simultaneous activation HRI was successfully applied in dexamethasone-treated multiple myeloma cells. Although the mechanisms of dexamethasone resistance are complex, a study by Burwick et al. showed that the proapoptotic eIF2α–P/ATF4 pathway was only activated in dexamethasone-sensitive cells.[186] However, it was shown that pharmacological activation of HRI induced rapid eIF2α phosphorylation and induction of apoptosis in both sensitive and resistant cells.[186] This study also showed that synergizing effects on apoptosis may be reached by combining HRI activation with the inhibition of the mammalian target of rapamycin.

Moreover, the role of HRI extends to modulating the response of tumor cells to therapies that directly target the intrinsic apoptotic pathway.[187,188] The key participants in this pathway are the proteins belonging to the B-cell lymphoma 2 (Bcl2) family, which possess the Bcl-2 homology (BH) domains. Briefly, the BH3-only subgroup of these proteins initiates apoptosis by activating the Bcl2-proapoptotic proteins. Once activated, these proteins undergo oligomerization and form pores to permeabilize the outer mitochondrial membrane. Normally, the activity of the Bcl2-proapoptotic proteins is suppressed by Bcl2-prosurvival proteins. In the context of cancer therapies, these pathways are specifically targeted using BH3 mimetics, which 'mimic' the function of the BH3-only proteins and consequently trigger apoptosis in cancer cells.[189–191]

However, tumor cells often exhibit overexpression of Bcl2-prosurvival proteins, leading to potential resistance against BH3 mimetics.[190] For instance, the induced myeloid leukemia cell differentiation (MCL-1) protein often causes resistance to approved BH3-mimetics, thereby necessitating the development of inhibitors for this protein, such as dihydroartemisinin (DHA). Studies have demonstrated that DHA can suppress the expression of MCL-1 through the HRI/eIF2α pathway in leukemic cells.[187] Therefore, the sensitivity of leukemic cells to DHA treatment depends on the activity of HRI. Accordingly, a synergistic effect was observed when DHA treatment was combined with an HRI activator.[187]

Furthermore, recent research has unveiled the involvement of HRI in the acquisition of cancer cell *persistence* to BH3-mimetics.[188] It has been demonstrated that cells that survive BH3-mimetic treatment acquire a new translational program, resulting in their insensitivity to repeated treatments, and therefore, increased metastatic potential. The translational reprogramming relies on the HRI/ATF4 pathway, which, in this case, helps the cells to evade apoptosis.[188] Specifically,

BH3-mimetics induce an incomplete permeabilization of the outer mitochondrial membrane, leading to the release of cytochrome *c* into the cytosol. Cytochrome *c* then activates HRI, triggering the synthesis of ATF4, which in turn activates pro-survival mechanisms. The direct activation of HRI by cytochrome *c* has been supported by kinase assays and immunoprecipitation experiments.[188]

2 Aims

- First, it was first necessary to overexpress and purify the wild-type HRI enzyme.
- For the purpose of subsequent experiments, it was also needed to verify the purity of the purchased NTPs (ATP, GTP, UTP, and CTP).
- The primary objective of this master thesis was to determine the apparent kinetic parameters of HRI–catalyzed eIF2α phosphorylation, with respect to different NTPs (ATP, GTP, UTP, and CTP) serving as the phosphate donors in the reaction.
- Another goal was to study the effect of heme on the HRI–catalyzed eIF2α phosphorylation with different NTPs (ATP, GTP, UTP, and CTP) serving as the phosphate donors in the reaction.
- An additional objective was to examine the impact of cytochrome *c* on the kinase activity of HRI under various conditions.
- Finally, the thesis aimed to assess whether a direct protein—protein interaction between cytochrome *c* and the HRI holoform induces structural changes in the vicinity of the heme-binding sites.

3 Materials and methods

3.1 Chemicals

Abcam, Netherlands
InstantBlue™ Protein Stain

Bio-Rad, USA
ammonium persulfate (APS)
Precision Plus Protein™ Unstained Standards

Carl Roth, Germany
aprotinin
CTP disodium salt trihydrate (> 98%)
isopropyl β-D-1-thiogalactopyranoside (IPTG)
Luria-Bertani agar (LB agar)
Luria-Bertani Broth (LB Broth)
lysozyme
pepstatin A
UTP trisodium salt trihydrate (> 98%)

Fluka, Switzerland
2-mercaptoethanol
acrylamide
N,N′-methylenebisacrylamide
sodium dodecyl sulfate (SDS)
tris(hydroxymethyl)aminomethane hydrochloride (Tris-HCl)

GE Healthcare, USA
GTP trisodium salt hydrate (> 95%)
TALON® Metal Affinity Resin

Lach-Ner, Czechia
bromophenol blue
dipotassium phosphate

ethylenediaminetetraacetic acid (EDTA)
glycerol
imidazole
magnesium chloride
manganese(II) chloride
methanol
monopotassium phosphate
potassium chloride
sodium dithionite
sodium chloride

Merck, Germany
cytochrome *c*

Roche, Switzerland
ampicillin
phenylmethylsulfonyl fluoride (PMSF)

SERVA Electrophoresis, Germany
ATP disodium salt hydrate (> 98%)

Sigma-Aldrich, USA
dimethyl sulfoxide (DMSO)
glycine hydrochloride
hemin
leupeptin
N,N,N′,N′-tetramethylethylenediamine (TEMED)
tetrabutylammonium hydrogensulfate

Stratagen, USA
BL-21(DE3) *E. coli* cells

Thermo Fisher Scientific, USA
Bacto Tryptone
Bacto Yeast Extract

Wako Pure Chemical Industries, Japan
Phos-tag (1,3-bis[bis(pyridin-2-ylmethyl)amino]propan-2-olato manganese(II) complex)

All chemicals, unless specified, were acquired in the highest available purity; the specific value is provided in the list above only for the NTPs.

eIF2α and HRI wild-type proteins
Sufficient amounts of the eIF2α substrate were obtained by recombinant expression as a part of my bachelor thesis.[192] The HRI enzyme was prepared by introducing the pET-21c(+)/HRI plasmid (see below) into the BL-21(DE3) *E. coli* cells (for details, see Section 3.3.1 on p. 42).

pET-21c(+)/HRI plasmid
The pET-21c(+) vector (5441 pairs of bases) was kindly provided by a collaborating laboratory (prof. Toru Shimizu, Sendai, Japan). The key elements of the sequence include (see the plasmid map in Fig. 3.1 on p. 39): T7 promotor (specific to T7 RNA polymerase), the ampicillin resistance gene, *lac* operator, and the genes for the *N*-terminal T7 tag and the *C*-terminal $(His)_6$ tag. The sequence for the human HRI was inserted into the multiple cloning site downstream of the T7 promoter during previous experiments in our laboratory.[193,194]

3.2 Instruments

Analytical balance
HM-200-EC, A&D Instruments

Autoclave
MLS-37812, Panasonic

Centrifuge
Avanti JXN-26, Beckman Coulter
Allegra X-30R, Beckman Coulter

Dry bath
MINIB-100 Mini Dry Bath, Hangzhou Miu Instruments

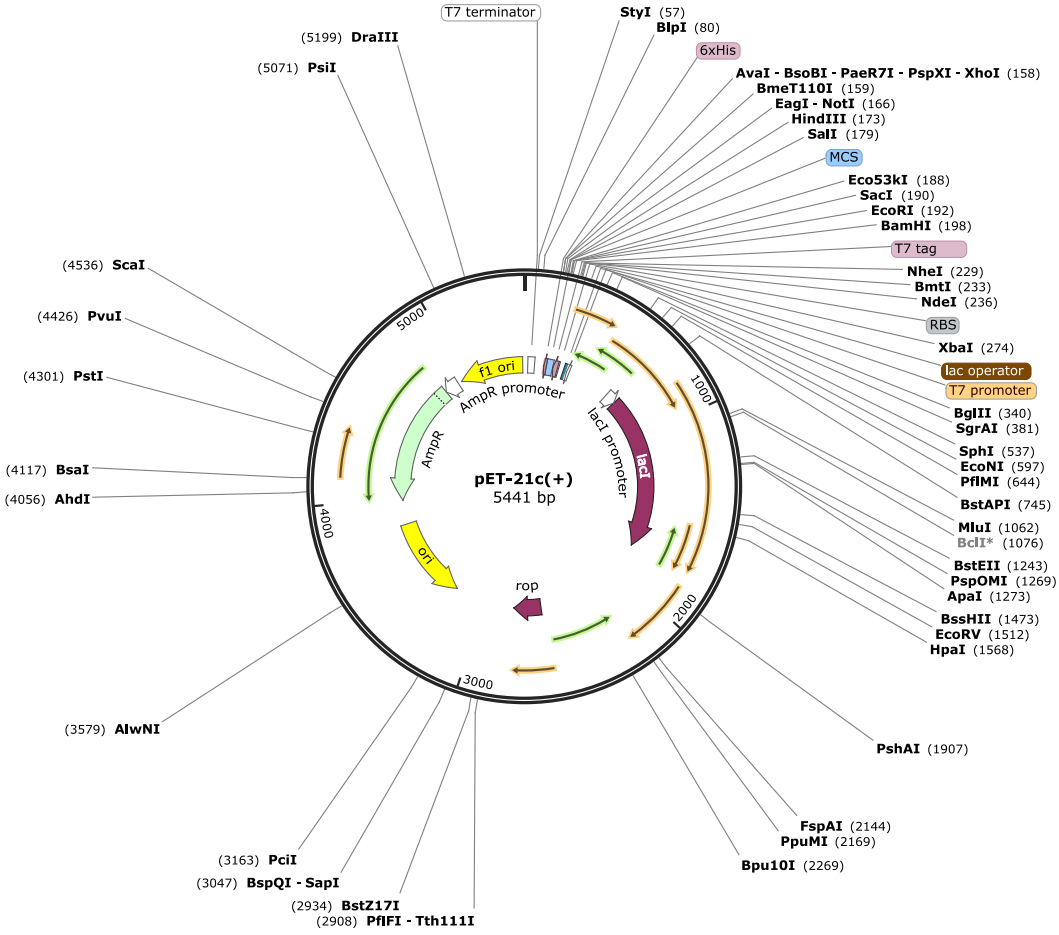

Figure 3.1: Map of the pET-21c(+) plasmid (adapted from Ref.[195]). The key elements include the T7 promoter (orange frame), the multiple cloning site (MCS, blue frame), the *lac* operator (brown frame), the ampicillin resistance gene (*AmpR*, green arrow), the genes for the T7 tag (pink frame), and $(His)_6$ tag (pink frame).

Electrophoresis power supply

PowerPac Basic Power Supply, Bio-Rad

Electrophoresis system

Mini-PROTEAN® Tetra Cell, Bio-Rad

Gas burner

Gasprofi2 SCS, WLD-TEC

Gel permeation chromatography (GPC) system

ÄKTAprime plus™, GE Healthcare

High-performance liquid chromatography (HPLC) system
1200 Series Gradient HPLC System, Agilent

Incubator
IB-01E-120 Bench Top Incubator, Jeio Tech

Laboratory rotator
LR-03, Chemos Group

Laminar flow cabinet
BIO 126, Labox

Magnetic stirrer
C-MAG MS 7, IKA

Orbital shaker
Vývojové dílny ČSAV

Orbital shaker–incubator
ES-60 Incubator Shaker, Hangzhou Miu Instruments
Multitron Pro, INFORS HT
Multitron Standard, INFORS HT

pH meter
pHenomenal® pH 1100 L, VWR®

Scanner
Epson Perfection V500 Scanner

Spectrophotometer
Cary 60 UV-Vis, Agilent
DS-11+ Spectrophotometer, DeNovix

Top loading balance
440-35N, KERN

Ultracentrifuge
Optima™ LE-80K, Beckman Coulter

Ultrasonic homogenizer
Sonopuls HD 3100, Bandelin

Vortex mixer
MS1 S1 Vortex Shaker, IKA

3.3 Methods

3.3.1 Overexpression of the HRI enzyme

The procedure of the HRI enzyme overexpression was analogous to protocols described in the literature.[134,137] First, two LB agar plates with 100 µg/ml ampicillin were prepared as follows. Agar [2.5% (w/v) LB agar, previously sterilized at 120 °C for 4 hours] was melted by a microwave treatment and then cooled to room temperature. The melted agar was placed in a laminar flow cabinet (BIO 126, Labox), where the subsequent steps were also performed. A stock solution of ampicillin (100 mg/ml, sterilized using a filter with a pore size of 0.22 µm) was added to the melted agar in a sterile tube (Falcon). The resulting mixture (20 ml, 100 µg/ml ampicillin) was stirred and poured into two Petri dishes. Both dishes were then stored in the laminar flow cabinet for 30 minutes.

During the solidification of the agar plates, the competent cells were transformed by the recombinant plasmid. The *E. coli* BL-21(DE3) cells were first thawed on wet ice and then placed in a laminar flow cabinet (BIO 126, Labox), where the subsequent steps were also performed. Two cell suspension aliquots (25 µl) were pipetted into microcentrifuge tubes (Eppendorf). After the addition of the pET-21c(+)/ HRI plasmid (0.5 µl) into one of the tubes, both tubes were incubated on wet ice for 10 minutes (the second tube was used as a negative control). Next, LB medium [175 µl of 4% (w/v) LB Broth, previously sterilized at 120 °C for 4 hours] was added into each tube and the resulting mixtures were transferred onto the agar plates prepared previously (see above). The mixtures were spread on the plates using a sterile spreader. The agar plates were sealed with parafilm and incubated for 16 hours at 37 °C (IB-01E-120 Bench Top Incubator, Jeio Tech). Finally, the plates were stored in a refrigerator.

Next, two average-sized single colonies grown on the first agar plate were selected. In the laminar flow cabinet, a sample of each colony was collected using a sterile wooden toothpick and transferred to two sterile tubes (Falcon) containing 5 ml of LB medium (prepared as described above) with 100 µg/ml ampicillin. Both sterile tubes were then incubated at an orbital shaker set to 37 °C and 200 RPM (ES-60 Incubator Shaker, Hangzhou Miu Instruments). After 16 hours of incubation, aliquots (0.5 ml) of the cell cultures were transferred to 16 Erlenmayer flasks, each of them containing 0.5 l of TB medium [1.2% (w/v) Bacto Tryptone, 2.4% (w/v) Bacto Yeast Extract, 0.2% (w/v) K_2HPO_4, 1.3% (w/v) KH_2PO_4, 0.4% (w/v) glycerol, previously sterilized at 120 °C for 4 hours] with

100 µg/ml ampicillin. The flasks were then incubated at 37 °C and 150 RPM at two orbital shakers (Multitron Pro, INFORS HT; and Multitron Standard, INFORS HT).

After 3.5 hours of incubation at the two orbital shakers, a cell suspension sample's optical density at 600 nm (OD_{600}) was measured (DS-11+ Spectrophotometer, DeNovix, "OD_{600} method"). Then, the cell suspensions were incubated at 15 °C and 150 RPM for 30 minutes (Multitron Pro, INFORS HT; and Multitron Standard, INFORS HT). After adding 100 µM IPTG aseptically, the cell suspensions were incubated at 15 °C and 120 RPM for 16 hours at the same orbital shakers (the IPTG stock solution was previously sterilized using a filter with a pore size of 0.22 µm). Finally, the suspensions were centrifuged at 4 °C and 3000 RPM for 45 minutes (Avanti JXN-26, Beckman Coulter, JLA-9.1000 rotor). The cells were weighed (440-35N, KERN) and stored in sterile test tubes (Falcon) at −80 °C.

The procedure of the protein overexpression was repeated with another two single colonies grown on the same agar plate as previously.

3.3.2 Isolation and purification of the HRI enzyme

The procedure of the HRI enzyme isolation and purification was analogous to protocols described in the literature.[134,137] First, the cells containing the HRI enzyme were preincubated at room temperature for 20 minutes and resuspended in a buffer containing protease inhibitors (50 mM Tris-HCl, pH 8.0, 100 mM NaCl, 1 mM EDTA, 1 mM PMSF, 0.2 mg/ml lysozyme, 1 µg/ml aprotinin, 1 µg/ml pepstatin A, 1 µg/ml leupeptin). The crude extract (ca 400 ml) was sonified on wet ice (KE 76 tip, Sonopuls HD 3100, Bandelin) under magnetic stirring (C-MAG MS 7, IKA). A one-minute sonication was repeated six times at 55% amplitude, with a one-minute pause after each sonication. The resulting cell lysates were then centrifuged at 5 °C and 40000 RPM for 60 minutes (Optima™ LE-80 K, Beckman Coulter, 45Ti rotor).

The HRI enzyme was next purified by affinity chromatography. The affinity resin (TALON® Metal Affinity Resin) was centrifuged at 4 °C and 200 RPM for 5 minutes (Allegra X-30R, Beckman Coulter, F0685 rotor). The pelleted resin was then mixed with the equilibration buffer (50 mM Tris-HCl, pH 8.0, 100 mM NaCl) and centrifuged at the same conditions. The addition of equilibration buffer and centrifugation was then repeated twice. After the last centrifugation, the resin was mixed with the supernatant to yield a homogenous solution. The equilibrated

resin was then incubated with the supernatant obtained by cell lysate ultracentrifugation (see above) at 4 °C under slow stirring for 60 minutes (LR-03, Chemos Group). The mixture was then applied to the affinity column (pre-washed with deionized water). After the whole mixture passed through, the column was washed with 50 ml of the equilibration buffer and 15 ml of the elution buffer (50 mM Tris-HCl, pH 8.0, 100 mM NaCl, 200 mM imidazole). The eluate was concentrated using centrifugal ultrafiltration units with a 30 kDa cut-off (Amicon® Ultra Centrifugal Filters). The centrifugations (4 °C, 3500 RPM, 15 min, Allegra X-30R, Beckman Coulter, F0685 rotor) were repeated until the volume of the eluate was reduced to 300 µl.

Next, the HRI enzyme was further purified using GPC. The concentrated eluate obtained from the previous step (300 µl) was applied to the Superdex 200 10/300 GL column (10 × 300 mm, Merck), previously equilibrated with the mobile phase (20 mM Tris-HCl, pH 8.0, 150 mM NaCl). The flow rate was set to 0.8 ml/min and the desired fractions were selected by monitoring the absorbance at 280 nm (ÄKTAprime™ plus, GE Healthcare). The collected fractions were concentrated using the centrifugal ultrafiltration units with a 30 kDa cut-off (4 °C, 3500 RPM, 3 min, Allegra X-30R, Beckman Coulter, F0685 rotor). The centrifugations were repeated until the volume of the eluate was reduced to 280 µl.

The concentration of the final product was determined by measuring the absorbance at 280 nm (DS-11+ Spectrophotometer, DeNovix, "A280 method"). The molar absorption coefficient at 280 nm (ε_{280} = 46465 l mol^{-1} cm^{-1}), as well as the theoretical molecular weight of the HRI enzyme (M = 71000 g mol^{-1}) were estimated from the primary sequence of the HRI enzyme (obtained from the UniProt Database)[196] using the ProtParam tool.[197] Finally, aliquots (à 20 µl) of the product were rapidly frozen in liquid nitrogen and stored at −80 °C.

3.3.3 Assessment of HRI preparation steps by SDS–PAGE

Samples collected during the overexpression, isolation, and purification of the HRI enzyme were analyzed by the SDS–PAGE,[198] using the Mini-PROTEAN® Tetra Cell apparatus (Bio-Rad). Table 3.1 on p. 45 lists the samples selected for analysis.

First, the 10% (w/v) resolving gel solution was prepared by mixing 3.35 ml of buffer A [0.375 M Tris-HCl, pH 8.8, 0.1% (w/v) SDS], 1.65 ml of polymerization solution A [30% (w/v) acrylamide, 0.8 % (w/v) *N,N′*-methylenebisacrylamide in buffer A], 10 µl of TEMED and 100 µl of APS stock solution (100 mg/ml). The

resulting mixture was poured between glass plates (with a space of 1 mm) and covered with deionized water. After 30 minutes of polymerization, the water was discarded and the surface of the solid resolving gel was dried with filter paper. The 4% stacking gel solution was prepared by mixing the reagents as follows: 1.3 ml of buffer B [0.125 M Tris-HCl, pH 8.8, 0.1% (w/v) SDS], 400 µl of polymerization solution B [30% (w/v) acrylamide, 0.8% (w/v) *N,N′*-methylenebisacrylamide in buffer B], 3 µl of TEMED and 60 µl of APS stock solution (100 mg/ml). The solid resolving gel was covered with the 4% stacking gel solution and the sample comb was inserted in the cassette (10 wells with a width of 1 mm). After 25 minutes of polymerization, the electrophoresis cell was assembled and the inner and outer chambers were filled with running buffer [25 mM Tris-HCl, pH 8.3, 0.192 M glycine, 0.1% (w/v) SDS].

The samples for analysis were mixed with the 4× stock sample buffer [0.25 M Tris-HCl, pH 6.8, 8% (w/v) SDS, 50% (v/v) glycerol, 22% (w/v) 2-mercaptoethanol, 0.004% (w/v) bromophenol blue] and deionized water in microcentrifuge tubes (Eppendorf). The volumes of the components are summarized in Table 3.1. The resulting mixtures were incubated in a dry bath at 100 °C for 5 minutes (MINIB-100 Mini Dry Bath, Hangzhou Miu Instruments) and vortexed.

Table 3.1: Analysis of the individual steps of the overexpression, isolation, and purification of the HRI enzyme: preparation of samples for the 10% SDS–PAGE. The sample loaded on the gel was prepared by mixing a given volume of the original sample, deionized water, and 4× stock sample buffer.

	original sample (µl)	deionized water (µl)	sample buffer (µl)	loaded on gel (µl)
cell suspension before IPTG induction	15	0	5	20
cell suspension after IPTG induction	15	0	5	20
supernatant from the ultracentrifugation of the cell lysate	10	20	10	15
flow-through sample from the affinity chromatography	10	20	10	15
eluate from the affinity chromatography	30	0	10	15
final product	5	10	5	10
fraction 12 from the GPC	30	0	10	20
fraction 15 from the GPC	30	0	10	20
fraction 17 from the GPC	30	0	10	20

After the sample comb was removed, each well was filled with a particular volume of a sample (see Tab. 3.1 on p. 45) or with 10 µl of the molecular weight marker (Precision Plus Protein™ Standards). The cell was connected to the power supply (PowerPac Basic Power Supply, Bio-Rad) and the separation was launched for 70 minutes at constant voltage (200 V). After the electrophoresis was complete, the gel was stained with InstantBlue® Coomassie Protein Stain. After a one-hour incubation and shaking (Vývojové dílny ČSAV), the gel was transferred to deionized water for 16 hours. The stained gel was finally imaged using Epson Perfection V500 Scanner.

3.3.4 Assessment of the purity of NTPs

The crystalline NTPs were purchased from three different companies at the highest purity possible (see Section 3.1 on p. 36). The purity of the NTPs was verified using the ion-pair reversed-phase HPLC with the detection of absorbance at 254 nm as the main signal.[199] For each NTP (ATP, GTP, UTP, and CTP, respectively), 10 µl of a 100 mM solution was injected into a monolithic C18 column (Chromolith RP-18e, 10 × 4.6 mm, Merck) at 35 °C. Mobile phase A contained 8 mM tetrabutylammonium hydrogensulfate in 50 mM potassium phosphate buffer (pH 6.0, pHenomenal® pH 1100 L, VWR®), mobile phase B was pure methanol. At a constant flow rate (1.6 ml/min), the following gradient of mobile phase B was applied (1200 Series Gradient HPLC System, Agilent): 0% B for 25 minutes, 30% B for 3 minutes, and 70% B for 3 minutes. Full absorption spectra (200–600 nm) of fractions at selected elution volumes were recorded and analyzed. In the case of ATP, a diluted solution was separately analyzed under the same conditions (10 µl of a 100 mM solution was injected into the column).

3.3.5 Kinetic analysis of the HRI kinase reaction in the presence of different NTPs

3.3.5.1 Time course of the HRI kinase reaction

The time course of the HRI–catalyzed eIF2α phosphorylation in the presence of various NTPs (ATP, GTP, UTP, and CTP, respectively) was assayed at 20 °C by a procedure adapted from previous reports.[134,137] Each reaction mixture had a volume of 20 µl and contained 5.4 µM eIF2α and 0.35 µM HRI in 20 mM Tris-HCl, 2 mM $MgCl_2$, and 60 mM KCl (pH 8.0, pHenomenal® pH 1100 L, VWR®). After preincubation for 5 minutes, 1000 µM of ATP (or GTP, UTP, and CTP,

respectively) was added to the mixture to initiate the reaction. In each mixture, the reaction was stopped at a given time after initiation (0 min, 0.5 min, 1 min, 2 min, 3 min, 5 min, 7 min, 10 min, 15 min, 30 min, 45 min, 60 min), by adding 20 µl of 2× stock sample buffer [0.25 M Tris-HCl, pH 6.8, 8% (w/v) SDS, 50% (v/v) glycerol, 22% (w/v) 2-mercaptoethanol, 0.004% (w/v) bromophenol blue] and incubating the mixture at 95 °C for 5 minutes (MINIB-100 Mini Dry Bath, Hangzhou Miu Instruments).

The reaction mixtures were analyzed with Phos-tag SDS–PAGE,[87,137] using the Mini-PROTEAN© Tetra Cell apparatus (Bio-Rad). The procedure was analogous to the analysis of protein samples described in Section 3.3.3 (p. 44), only the composition of the resolving gel was different. For each NTP, a single 10% resolving gel was prepared as follows: 3.3 ml of buffer A [0.375 M Tris-HCl, pH 8.8, 0.1% (w/v) SDS], 1.65 ml of polymerization solution A [30% (w/v) acrylamide, 0.8 % (w/v) *N,N′*-methylenebisacrylamide in buffer A], 10 µl of $MnCl_2$ stock solution (100 mM), 37.5 µl of 10 mM Phos-tag, 5 µl of TEMED, 50 µl of APS stock solution (100 mg/ml). The 4% stacking gel was prepared as described in Section 3.3.3 (p. 44). Each reaction mixture (see above) was vortexed and a sample of the mixture (5 µl) was loaded on the gel. After 70 minutes of separation at constant voltage (200 V), the gel was stained with InstantBlue® Coomassie Protein Stain for an hour (Vývojové dílny ČSAV) and then washed with deionized water for 16 hours. The stained gel was imaged using Epson Perfection V500 Scanner.

Amounts of the phosphorylated and unphosphorylated eIF2α were determined by quantifying the scanned gels using the ImageJ software. To calculate the concentration of eIF2α–P in a sample, the total concentration of eIF2α in the sample (5.4 µM) was multiplied by the relative intensity of the eIF2α–P band in the lane which was used for the analysis of the sample.

3.3.5.2 Kinetic parameters of the HRI kinase reaction

The kinetic parameters of the HRI–catalyzed eIF2α phosphorylation in the presence of various NTPs (ATP, GTP, UTP, and CTP, respectively) were studied at 20 °C by a procedure adapted from previous reports.[134,137] Each reaction mixture had a volume of 20 µl and contained 5.4 µM eIF2α and 0.35 µM HRI in 20 mM Tris-HCl, 2 mM $MgCl_2$, and 60 mM KCl (pH 8.0, pHenomenal® pH 1100 L, VWR®). After preincubation for 5 minutes, the reaction was initiated by adding ATP (or GTP, UTP, CTP, respectively) at different concentrations: 0 µM, 5 µM, 10 µM, 20 µM, 30 µM, 50 µM, 100 µM, 250 µM, 500 µM, 750 µM, 900 µM. In each mixture, the reaction was stopped after 1 minute (UTP, CTP), or after 3 minutes

(CTP, UTP), by adding 20 µl of 2× stock sample buffer [0.25 M Tris-HCl, pH 6.8, 8% (w/v) SDS, 50% (v/v) glycerol, 22% (w/v) 2-mercaptoethanol, 0.004% (w/v) bromophenol blue] and incubating the mixture at 95 °C for 5 minutes (MINIB-100 Mini Dry Bath, Hangzhou Miu Instruments).

For UTP and CTP, an analogous separate experiment was next performed with i) a longer incubation time (6 minutes) and the same range of concentrations as above (0–900 µM), ii) a longer incubation time (6 minutes) and a broader range of NTP concentrations: 0 µM, 750 µM, 1000 µM, 1250 µM, 2000 µM, 2500 µM, 3000 µM.

The procedure of the Phos-tag SDS–PAGE analysis of the assays (including the determination of the eIF2α–P concentration in each sample) was identical to the one described in Section 3.3.5.1 (p. 46). The initial velocity v_0 for a given concentration of NTP ([NTP]) was calculated as the ratio of the product concentration [eIF2α–P] and the reaction time Δt:

$$v_0 = \frac{[\text{eIF2}\alpha\text{–P}]}{\Delta t}. \tag{3.1}$$

The v_0 vs. [NTP] data were fitted with kinetic equations for bisubstrate reactions by non-linear regression, either with the Michaelis–Menten equation (Eq. 3.2):

$$v_0 = \frac{v_{\text{lim}}^{\text{NTP}}[\text{NTP}]}{K_{\text{M}}^{\text{NTP}} + [\text{NTP}]}, \tag{3.2}$$

or with the Hill equation (Eq. 3.3):

$$v_0 = \frac{v_{\text{lim}}^{\text{NTP}}[\text{NTP}]^{h^{\text{NTP}}}}{(K_{0.5}^{\text{NTP}})^{h^{\text{NTP}}} + [\text{NTP}]^{h^{\text{NTP}}}}, \tag{3.3}$$

where $v_{\text{lim}}^{\text{NTP}}$ is the limiting reaction rate, $K_{\text{M}}^{\text{NTP}}$ is the apparent Michaelis–Menten constant, $K_{0.5}^{\text{NTP}}$ is the apparent half-saturation constant, and h^{NTP} is the Hill coefficient.

Furthermore, the catalytic constant $k_{\text{cat}}^{\text{NTP}}$ was expressed as:

$$k_{\text{cat}}^{\text{NTP}} = \frac{v_{\text{lim}}^{\text{NTP}}}{[\text{E}]_0}, \tag{3.4}$$

where $[\text{E}]_0$ is the total concentration of the HRI enzyme in the reaction mixture.

Finally, the catalytic efficiency η^{NTP} was calculated using Eq. 3.5:

$$\eta^{\text{NTP}} = \frac{k_{\text{cat}}^{\text{NTP}}}{K^{\text{NTP}}}, \tag{3.5}$$

where K^{NTP} is either $K_{\text{M}}^{\text{NTP}}$ (if Eq. 3.2 was used for fitting the data) or $K_{0.5}^{\text{NTP}}$ (if Eq. 3.3 was used for fitting the data).

3.3.5.3 Heme inhibition of the HRI kinase reaction

The heme inhibition of the HRI–catalyzed eIF2α phosphorylation in the presence of various NTPs (ATP, GTP, UTP, and CTP, respectively) was assayed at 20 °C by a procedure adapted from previous reports.[134,137] Each reaction mixture had a volume of 20 µl and contained 5.4 µM eIF2α and 0.35 µM HRI in 20 mM Tris-HCl, 2 mM $MgCl_2$, and 60 mM KCl (pH 8.0, pHenomenal® pH 1100 L, VWR®). After preincubation for 5 minutes, different concentrations of hemin (solution in DMSO) were added to the mixtures: 0 µM, 0.1 µM, 0.2 µM, 0.5 µM, 0.75 µM, 1 µM, 1.5 µM, 5 µM, 10 µM, 30 µM, 50 µM, 100 µM. The control mixtures without heme contained either water or DMSO. In each mixture, the reaction was initiated by adding 900 µM ATP (or GTP, UTP, or CTP, respectively). The reaction was stopped after 10 minutes by adding 20 µl of 2× stock sample buffer [0.25 M Tris-HCl, pH 6.8, 8% (w/v) SDS, 50% (v/v) glycerol, 22% (w/v) 2-mercaptoethanol, 0.004% (w/v) bromophenol blue] and incubating the mixture at 95 °C for 5 minutes (MINIB-100 Mini Dry Bath, Hangzhou Miu Instruments).

The procedure of the Phos-tag SDS–PAGE analysis (including the determination of the eIF2α–P concentration in each sample) of the assays was identical to the one described in Section 3.3.5.1 (p. 46). The concentrations of the product [eIF2α–P] were converted into relative kinase activities a_{rel} for each concentration of heme:

$$a_{\mathrm{rel}} = \frac{[\text{eIF2}\alpha\text{–P}]}{[\text{eIF2}\alpha\text{–P}]_0}, \tag{3.6}$$

where the expression of the maximal kinase activity $[\text{eIF2}\alpha\text{–P}]_0$ will be specified below.

The half-maximal inhibitory concentrations for each NTP ($\mathrm{IC}_{50}^{\mathrm{NTP}}$) were evaluated by fitting the a_{rel} vs. [heme] data using non-linear regression, either with a sigmoidal curve (Eq. 3.7):

$$a_{\mathrm{rel}} = \frac{1}{1 + \left(\frac{[\mathrm{heme}]}{\mathrm{IC}_{50}^{\mathrm{NTP}}}\right)^{n^{\mathrm{NTP}}}}, \tag{3.7}$$

or with a hyperbolic curve (Eq. 3.8):

$$a_{\mathrm{rel}} = \frac{1}{2 + n^{\mathrm{NTP}}([\mathrm{heme}] - \mathrm{IC}_{50}^{\mathrm{NTP}})}, \tag{3.8}$$

where n^{NTP} is the second parameter in each model.

For the sigmoidal model (Eq. 3.7), the maximal kinase activity $[\text{eIF2}\alpha\text{–P}]_0$ was expressed as the average [eIF2α–P] obtained from several initial points. On the other hand, for the hyperbolic model (Eq. 3.8), $[\text{eIF2}\alpha\text{–P}]_0$ was the value of [eIF2α–P] in a mixture containing DMSO instead of heme.

3.3.6 Effect of cytochrome *c* on the kinase activity of HRI

The HRI–catalyzed eIF2α phosphorylation in the presence of cytochrome *c* and/or heme was studied with a Phos-tag SDS–PAGE assay analogous to the experiments described in Section 3.3.5 (p. 46). Each reaction mixture had a volume of 20 µl and contained 5.4 µM eIF2α and 0.35 µM HRI in 20 mM Tris-HCl, 2 mM $MgCl_2$, and 60 mM KCl (pH 8.0, pHenomenal® pH 1100 L, VWR®). After preincubation for 5 minutes, different combinations of the following reagents were added into each mixture: 9 µM hemin (solution in DMSO), 0.35 µM cytochrome *c* (solution in 20 mM Tris-HCl, pH 8.0, 2 mM $MgCl_2$, 60 mM KCl), 500 µM $Na_2S_2O_4$ (solution in water). The composition of the 8 mixtures prepared in total is indicated in the Table 3.2 (the addition of each component was always followed by a 5-minute preincubation).

Table 3.2: Study of the interaction of HRI with cytochrome *c*: preparation of samples for the 10% SDS–PAGE with 75 µM Phos-tag and 200 µM $MnCl_2$. The sign indicates whether a given component (9 µM heme, 0.35 µM cytochrome *c*, 500 µM $Na_2S_2O_4$) was added into a pre-incubated mixture of 5.4 µM eIF2α and 0.35 µM HRI in 20 mM Tris-HCl, 2 mM $MgCl_2$, 60 mM KCl (pH 8.0).

mixture	heme	cytochrome *c*	$Na_2S_2O_4$
1	−	−	−
2	+	−	−
3	−	+	−
4	+	+	−
5	−	−	+
6	+	−	+
7	−	+	+
8	+	+	+

In each mixture, the reaction was initiated by adding 900 µM ATP. The reaction was stopped after 10 minutes by adding 20 µl of 2× stock sample buffer [0.25 M Tris-HCl, pH 6.8, 8% (*w*/*v*) SDS, 50% (*v*/*v*) glycerol, 22% (*w*/*v*) 2-mercaptoethanol, 0.004% (*w*/*v*) bromophenol blue] and incubating the mixture at 95 °C for 5 minutes (MINIB-100 Mini Dry Bath, Hangzhou Miu Instruments). The procedure of the Phos-tag SDS–PAGE analysis of the assays (including the determination of the eIF2α–P concentration in each sample) was identical to the one described in Section 3.3.5.1 (p. 46).

3.3.7 Effect of cytochrome *c* on the absorption spectra of HRI

The interaction of HRI with heme and/or cytochrome c in different redox states was further studied using ultraviolet–visible spectroscopy. All absorption spectra were measured in a quartz cuvette (with a path length of 1 cm) in the 200–700 nm wavelength range (Cary 60 UV-Vis, Agilent). Both HRI and cytochrome c were first diluted in 20 mM Tris-HCl, 150 mM NaCl (pH 8.0). The same buffer was also used as a blank sample (1 ml). First, the spectrum of pure cytochrome c (500 µl, 5 µM) was measured before and after a 5-minute incubation with a small amount of crystalline $Na_2S_2O_4$ added into the cuvette. Next, the spectrum of pure HRI (500 µl, 5 µM) was recorded. After the addition of 2.5 µl hemin stock solution (1 mM) into the cuvette containing the HRI solution, the mixture was incubated for 10 minutes and the spectrum was then recorded. Another spectrum was measured after adding a small amount of crystalline $Na_2S_2O_4$ into the HRI–heme mixture and a short incubation. Finally, the spectrum of a protein mixture (1 ml, 2.5 µM cytochrome c, 2.5 µM HRI, 2.5 µM heme) was measured before and after a 5-minute incubation with a small amount of crystalline $Na_2S_2O_4$ added into the cuvette.

Additionally, a hypothetical spectrum of the equimolar mixture of cytochrome c and the HRI holoform was modeled under the assumption that no change in the absorption properties in either component occurs as a result of their interaction. Under this assumption, the absorbance A of the mixture at a given wavelength λ is given by a sum of absorbances of the pure components (A_1, A_2) at the same wavelength. Since the mixture was equimolar $(c_1 = c_2)$, the theoretical absorbance A could be estimated simply as an arithmetic mean of the absorbances A_1, A_2 measured for the pure components as described above (A_1 was the absorbance of the 5 µM cytochrome c, A_2 was the absorbance of the 5 µM HRI holoform).

$$A = \frac{1}{2}(A_1 + A_2). \tag{3.9}$$

Using Eq. 3.9, hypothetical spectra of the equimolar mixture of cytochrome c and the HRI holoform were obtained for both non-reducing and reducing conditions.

4 Results

4.1 Overexpression, isolation, and purification of the HRI enzyme

After two weeks of incubation on an ampicillin agar plate, 25 colonies of the *E. coli* BL-21(DE3) cells transformed with the pET-21c(+)/HRI plasmid have grown. No colonies were formed on the ampicillin agar plate with cells lacking the plasmid (negative control).

Two single colonies of the transformed cells were selected for the first round of HRI overexpression as described in Section 3.3.1 (p. 42). After 3.5 hours of incubation in the TB medium, the OD_{600} value was 0.80. After the addition of IPTG and further incubation, 37.2 g of cells were harvested and stored at −80 °C. For the second round of HRI overexpression, another two single colonies from the same ampicillin agar plate were used. This time, the OD_{600} value reached 0.70 after 3.5 hours of incubation in the TB medium, and 33.7 g of cells were harvested and stored at −80 °C. In total, 4.4 g cells/l TB media were obtained and the HRI enzyme was then isolated as described in Section 3.3.2 (p. 43).

Samples collected at individual steps of the overexpression, isolation, and purification of the HRI enzyme were analyzed using 10% SDS–PAGE (see Fig. 4.1 on p. 53). The molecular weight marker was loaded into the first lane (the weights of the standards are indicated on the left; the theoretical molecular weight of the HRI enzyme is ca. 71000 g mol^{-1}).[196,197] The cell suspensions before (lane 2) and after (lane 3) IPTG induction contained a rich mixture of proteins, as indicated by the presence of numerous bands in both lanes. However, the band intensities are generally higher in lane 3. The supernatant from the ultracentrifugation of the cell lysate (lane 4) still contained a high concentration of various proteins, as was also the case of the flow-through sample from the affinity chromatography (lane 5). On the contrary, a lower number of bands were stained in lane 6, where a sample of the eluate from the affinity chromatography was loaded. There are two close bands corresponding to molecular weights slightly below 75000 g mol^{-1}. Apart from that, several bands corresponding to lower molecular weights were stained in this lane.

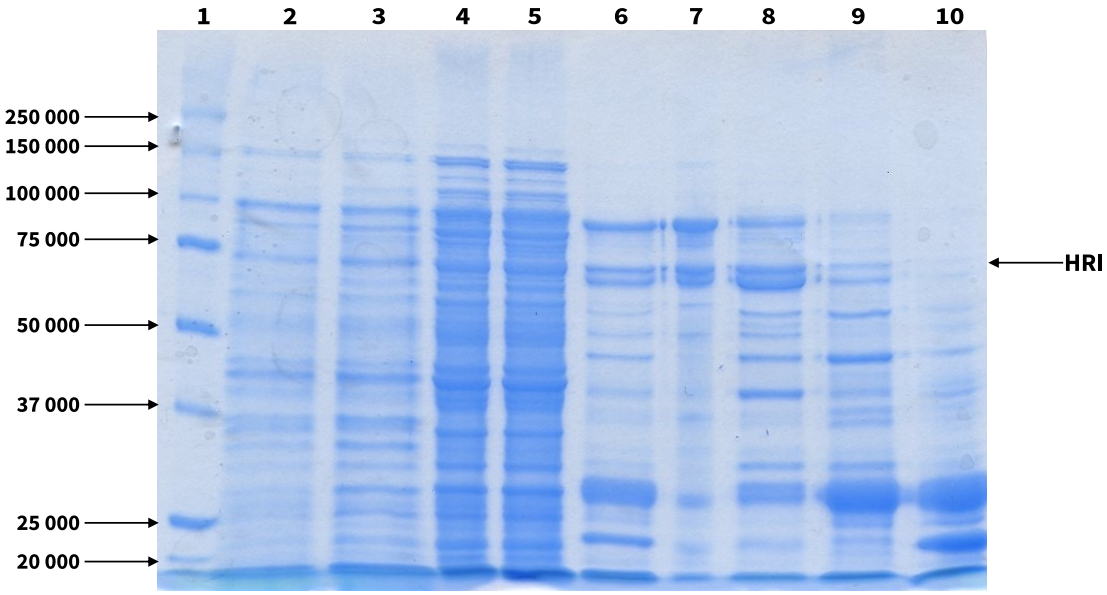

Figure 4.1: Analysis of samples collected during the overexpression, isolation, and purification of the HRI enzyme, using 10% SDS–PAGE: **1** – molecular weight marker (Precision Plus Protein™ Standards); **2** – suspension of the *E. coli* BL-21(DE3) cells before IPTG induction; **3** – suspension of the *E. coli* BL-21(DE3) cells after IPTG induction; **4** – supernatant from the ultracentrifugation of the cell lysate; **5** – flow-through sample from the affinity chromatography; **6** – eluate from the affinity chromatography; **7** – final product; **8** – fraction 12 from the GPC; **9** – fraction 15 from the GPC; **10** – fraction 17 from the GPC. The gel was stained with InstantBlue® Coomassie Protein stain.

The final step of the HRI enzyme purification was the GPC with the detection of absorbance at 280 nm (see Fig. 4.2 on p. 54). Samples of fractions 12, 15, and 17, were loaded into lanes 8, 9, and 10, respectively, of the gel in Fig. 4.1. The pattern of bands in all three lanes is somewhat similar to that in lane 6 (eluate from the affinity chromatography). In lane 8 (sample of fraction 12 from the GPC), the intensity of the two bands corresponding to molecular weights slightly below 75000 g mol^{-1} is fairly high. However, the intensity of these bands is relatively lower in lane 9 (sample of fraction 15 from the GPC) and almost negligible in lane 10 (sample of fraction 17 from the GPC).

The final HRI enzyme product was obtained by combining fractions 13–16 from the GPC and reducing the volume of the mixture to 280 µl. The sample of the final product was loaded into lane 7 of the gel in Fig. 4.1. The total concentration of protein in the product was 78.3 µM, as determined by measuring its absorbance at 280 nm. The yield of the HRI enzyme obtained by recombinant expression in *E. coli* cells was 22.3 µg/g of cells, i.e. 98.9 µg/l TB medium.

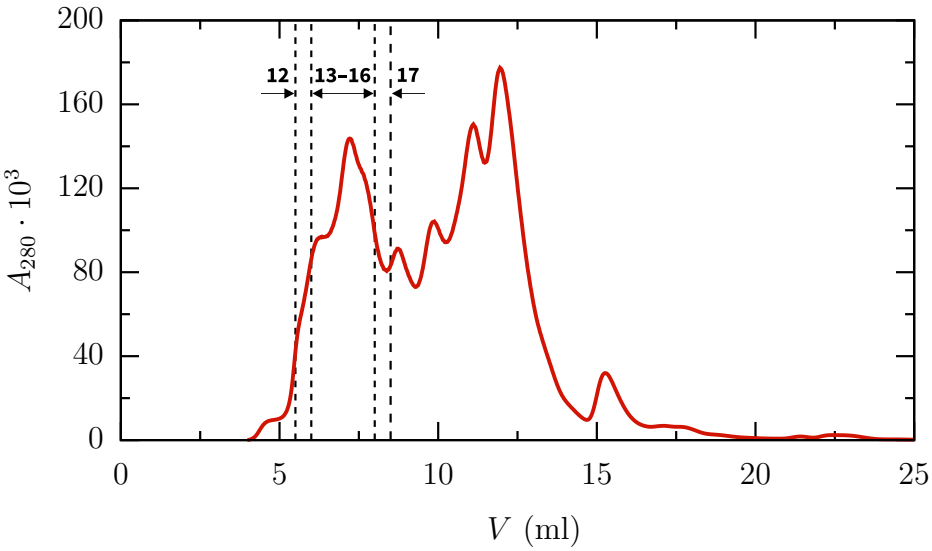

Figure 4.2: Purification of the HRI enzyme by the GPC with the detection of absorbance at 280 nm. The sample was injected (300 µl) into the Superdex 200 10/300 GL column (10 × 300 mm). The mobile phase contained 20 mM Tris-HCl and 150 mM NaCl (pH 8.0). A constant flow rate (0.8 ml/min) was used. Fractions 13–16 (elution volume 6–8 ml) were selected for further processing to obtain the final HRI enzyme product. Apart from the final product, samples of fractions 12, 15, and 17 were analyzed by SDS–PAGE (see Fig. 4.1 on p. 53).

4.2 Assessment of the purity of NTPs

Ion-pair reversed-phase HPLC with the detection of absorbance at 254 nm was used to verify the purity of NTPs. Figure 4.3 on p. 55 shows chromatograms of 100 mM solutions of each NTP (ATP, GTP, UTP, and CTP, respectively). Normalized areas of the largest peaks in each chromatogram are summarized in Table 4.1.

Table 4.1: Normalized areas (A_N) of the largest peaks in chromatograms of each 100 mM NTP solution (ATP, GTP, UTP, and CTP, respectively). The peaks are labeled according to the elution volume V at which the absorbance at 254 nm reached its maximum. The experimental setup is described in the caption to Fig. 4.3 on p. 55.

	V (ml)	A_N (%)
ATP	20.25	97.36
GTP	14.54	91.44
UTP	13.14	97.02
CTP	9.58	96.52

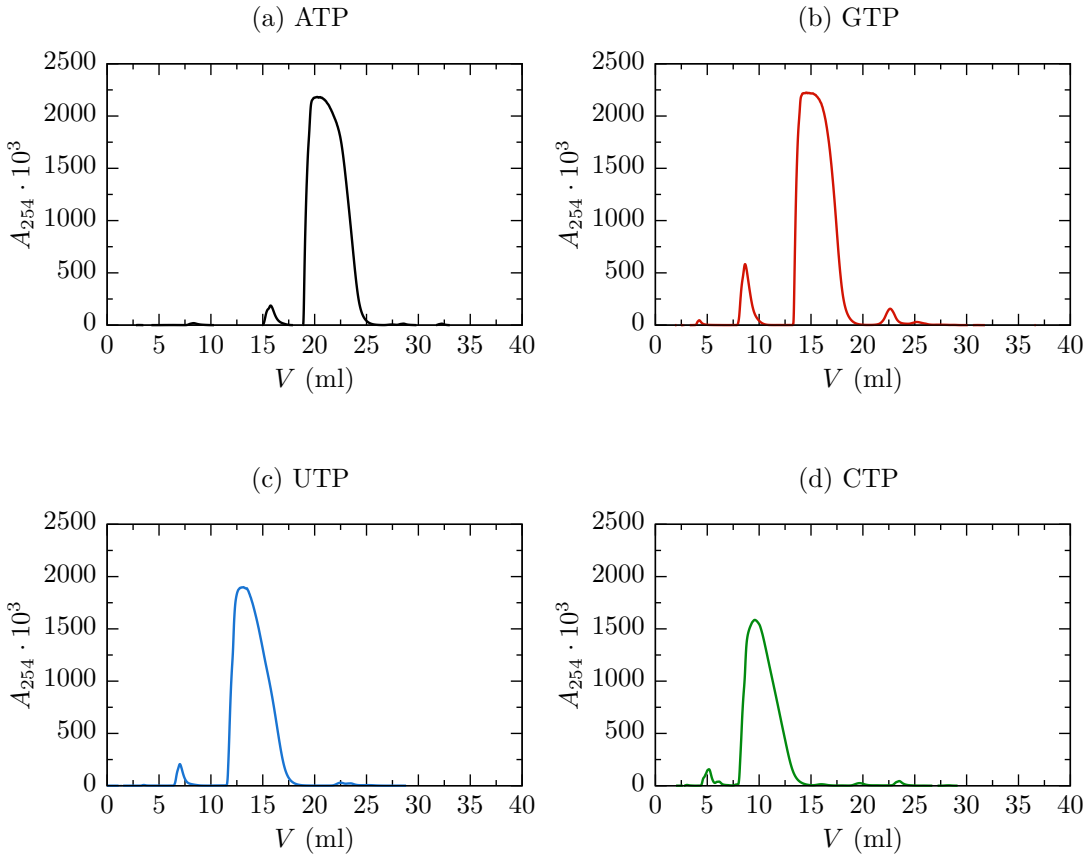

Figure 4.3: Analysis of 100 mM NTP solutions by ion-pair reversed-phase HPLC with the detection of absorbance at 254 nm: a) ATP, b) GTP, c) UTP, d) CTP. Samples of the solutions were injected (10 µl) into the Chromolith RP-18e column (10 × 4.6 mm) at 35 °C. Mobile phase A contained 8 mM tetrabutylammonium hydrogensulfate in 50 mM potassium phosphate buffer (pH 6.0), and mobile phase B was pure methanol. At a constant flow rate (1.6 ml/min), a 0–70% B gradient was applied.

In the case of ATP, the analysis was performed for a more diluted solution as well (100 µM). Using the same conditions of the separation as above, a single peak was recorded at $V = 23.44$ ml (see Fig. 4.4 on p. 56).

For further analysis, full absorption spectra (200–600 nm) of selected peaks were examined. In Fig. 4.5 on p. 56, a spectrum measured for the smaller peak in the chromatogram of the 100 mM ATP solution ($V = 15.71$ ml) is contrasted to the spectrum of the largest peak in the chromatogram of the 100 mM GTP solution ($V = 22.59$ ml).

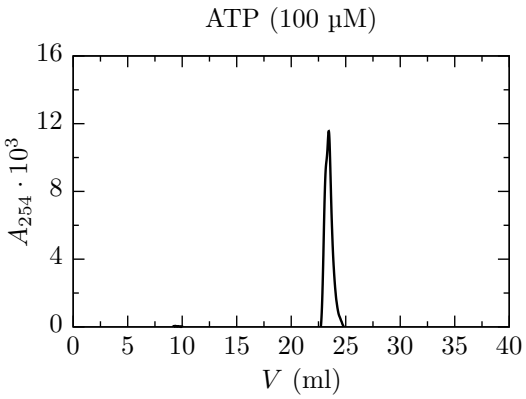

Figure 4.4: Analysis of a 100 µM ATP solution by ion-pair reversed-phase HPLC with the detection of absorbance at 254 nm. The experimental setup was identical to the one described in the caption to Fig. 4.3 on p. 55.

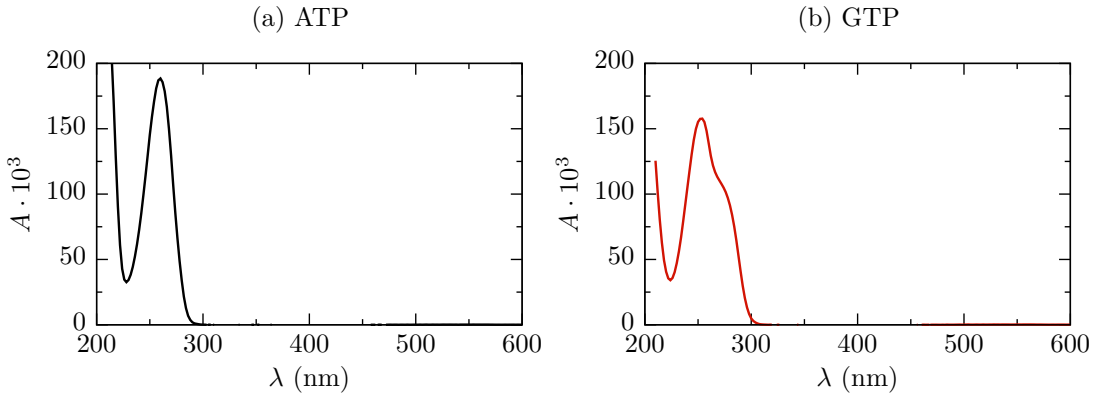

Figure 4.5: Absorption spectra of selected fractions from the ion-pair reversed-phase HPLC analysis of 100 mM NTP solutions: a) ATP solution at $V = 15.71$ ml, b) GTP solution at $V = 22.59$ ml. The experimental setup is described in the caption to Fig. 4.3 on p. 55.

4.3 Kinetic analysis of the HRI kinase reaction in the presence of different NTPs

4.3.1 Time course of the HRI kinase reaction

The HRI–catalyzed eIF2α phosphorylation in the presence of various NTPs (ATP, GTP, UTP, and CTP, respectively) was terminated at different reaction times and the reaction mixtures were analyzed by Phos-tag SDS–PAGE. Figure 4.6 on p. 57 shows the gels imaged after staining with InstantBlue® Coomassie Protein Stain. Three bands are observed in each lane: the phosphorylated and unphosphorylated

forms of eIF2α (labeled as eIF2α–P and eIF2α), and the HRI enzyme. No eIF2α–P band was observed in the lane with the negative control sample (this mixture contained eIF2α, HRI, and the buffer only).

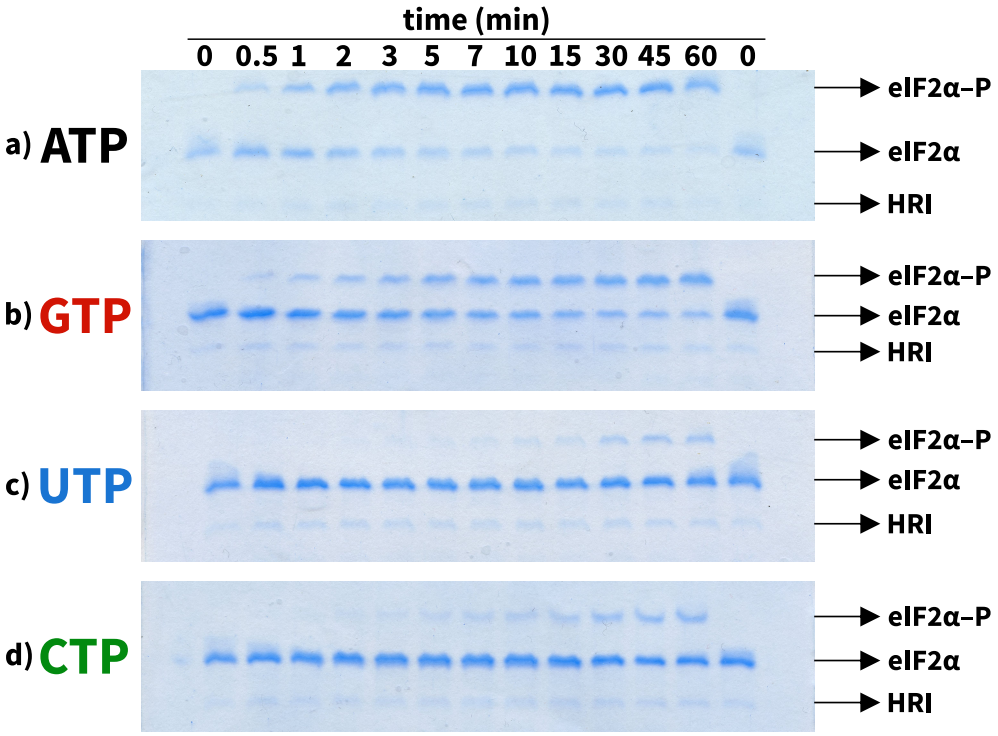

Figure 4.6: Time course analysis of the HRI–catalyzed eIF2α phosphorylation in the presence of various NTPs: a) ATP, b) GTP, c) UTP, d) CTP. The reaction mixtures were analyzed using 10% SDS–PAGE with 75 µM Phos-tag and 200 µM $MnCl_2$. The gels were stained with InstantBlue® Coomassie Protein Stain. Each mixture contained 5.4 µM eIF2α, 0.35 µM HRI, 20 mM Tris-HCl, 2 mM $MgCl_2$, and 60 mM KCl (pH 8.0). The reactions were initiated by adding 1000 µM NTP, and terminated at a selected time by adding the 2× stock sample buffer and incubating at 95 °C for 5 minutes. In all cases, the negative control (lanes labeled as '0') contained eIF2α, HRI, and the buffer only.

The concentrations of eIF2α–P in samples injected into each lane were determined using ImageJ. The results for each NTP are reported in Fig. 4.7 on p. 58. In each plot, a line was fitted to the first several points. For ATP and GTP, the last point in the linear region is at 3 minutes, while for UTP and CTP, it is at 7 minutes.

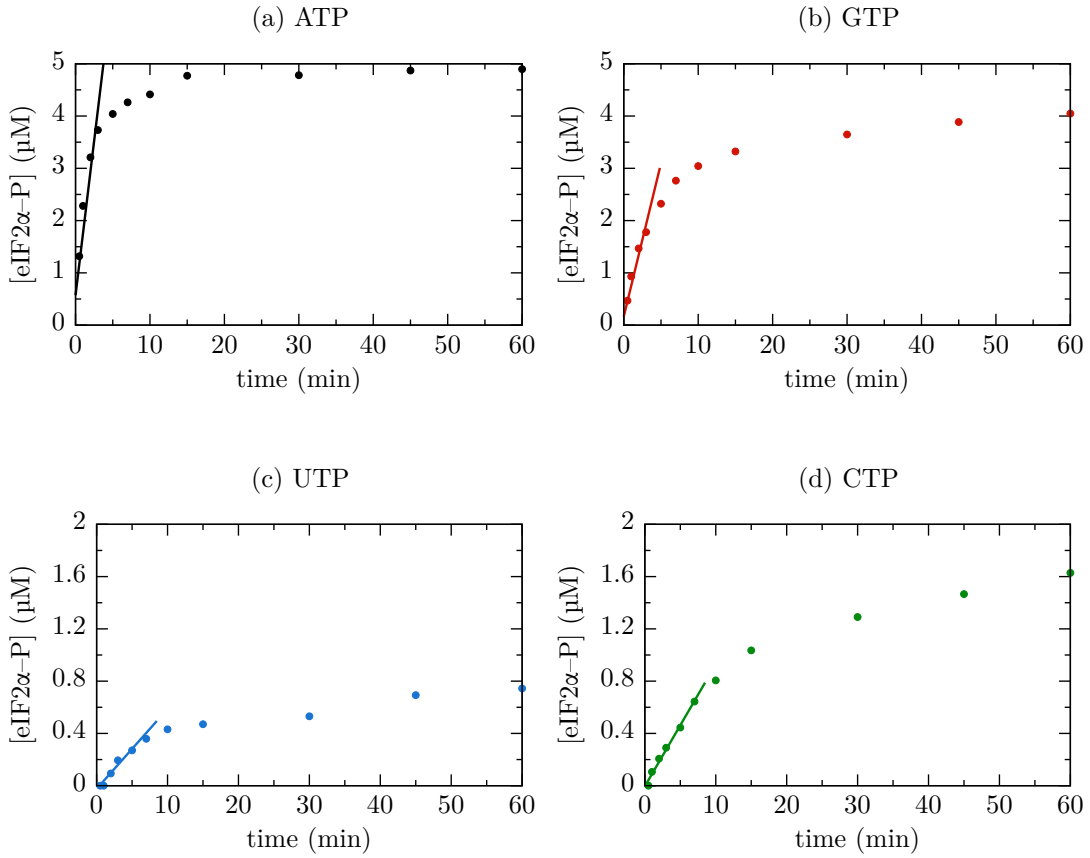

Figure 4.7: Concentrations of eIF2α–P at different reaction times of the HRI–catalyzed eIF2α phosphorylation in the presence of various NTPs: a) ATP, b) GTP, c) UTP, d) CTP. The concentrations were determined by quantifying the gels in Fig. 4.6 on p. 57 using ImageJ. The lines in each plot indicate the regions of the initial velocity conditions.

4.3.2 Kinetic parameters of the HRI kinase reaction

The HRI–catalyzed eIF2α phosphorylation in the presence of various NTPs (ATP, GTP, UTP, and CTP, respectively) was performed with varying concentrations of NTP while keeping the concentration of eIF2α constant, at conditions when initial velocity conditions were assured. The reaction mixtures were analyzed by Phos-tag SDS–PAGE. Figure 4.8 on p. 59 shows the gels imaged after staining with InstantBlue® Coomassie Protein Stain. Three bands are observed in each lane: the phosphorylated and unphosphorylated forms of eIF2α (labeled as eIF2α–P and eIF2α), and the HRI enzyme. No eIF2α–P band was observed in the lane with the negative control sample (this mixture contained eIF2α, HRI, and the buffer only).

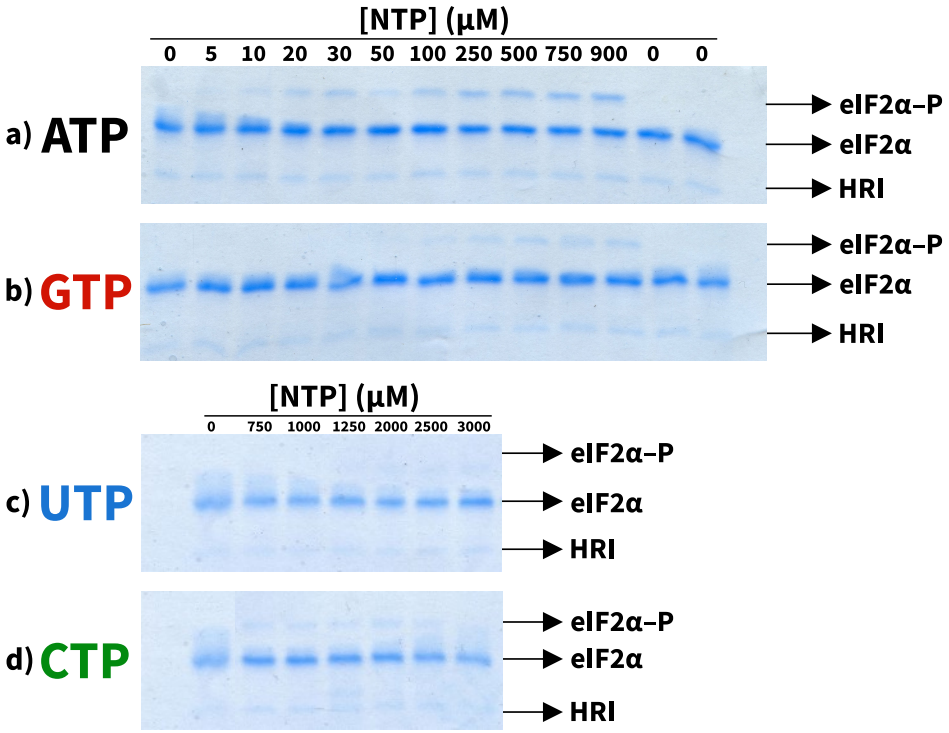

Figure 4.8: Determination of kinetic parameters of the HRI–catalyzed eIF2α phosphorylation in the presence of various NTPs: a) ATP, b) GTP, c) UTP, d) CTP. The reaction mixtures were analyzed using 10% SDS–PAGE with 75 μM Phos-tag and 200 μM $MnCl_2$. The gels were stained with InstantBlue® Coomassie Protein Stain. Each mixture contained 5.4 μM eIF2α, 0.35 μM HRI, 20 mM Tris-HCl, 2 mM $MgCl_2$, and 60 mM KCl (pH 8.0). The reactions were initiated by adding 0–900 μM NTP (ATP, GTP) or 0–3000 μM NTP (UTP, CTP), and terminated at a selected time (1 minute – ATP, GTP; or 6 minutes – UTP, CTP) by adding the 2× stock sample buffer and incubating at 95 °C for 5 minutes. In all cases, the negative control (lanes labeled as '0') contained eIF2α, HRI, and the buffer only.

The concentrations of eIF2α–P in samples injected into each lane were determined using ImageJ. These values were used to calculate the initial velocities v_0 according to Eq. 3.1 on p. 48, where $\Delta t = 1$ min for ATP and GTP, while $\Delta t = 6$ min for UTP and CTP. These data (v_0 vs. [NTP]) are plotted in Fig. 4.9 on p. 60, along with the curves obtained by fitting these data either with the Michaelis–Menten equation (Eq. 3.2 on p. 48, ATP and GTP), or the Hill equation (Eq. 3.3 on p. 48, UTP and CTP). Note that several initial points (5–50 μM) in the GTP series were excluded from the regression analysis.

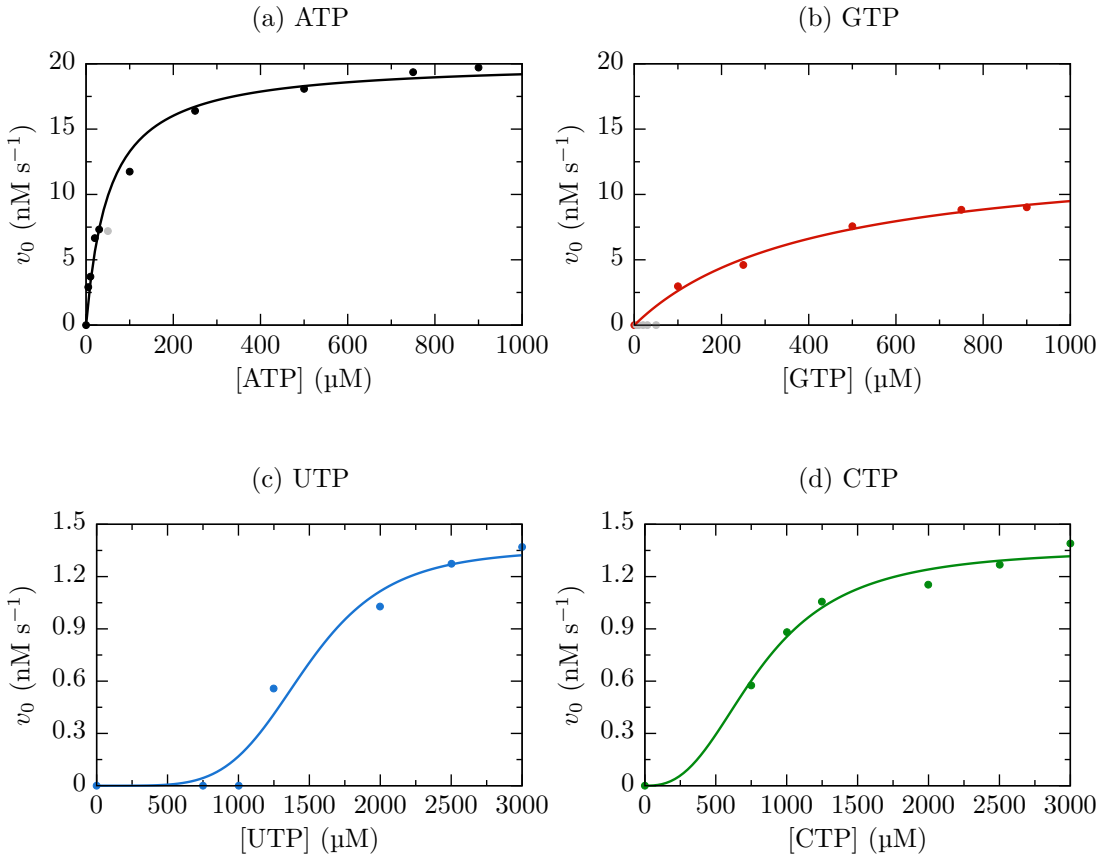

Figure 4.9: Initial velocities of the HRI–catalyzed eIF2α phosphorylation in the presence of a) ATP, b) GTP, c) UTP, d) CTP, as functions of [NTP]. The initial velocities were determined by quantifying the gels in Fig. 4.8 on p. 59 using ImageJ and Eq. 3.1 on p. 48. The curves in each plot were obtained by fitting the data to the Michaelis–Menten equation (ATP, GTP), or to the Hill equation (UTP, CTP). The kinetic parameters obtained from these equations are summarized in Tab. 4.2 on p. 61. Note that the initial data points (5–50 µM, grey) in the GTP series (b) were excluded from the regression analysis.

Table 4.2 on p. 61 summarizes the kinetic parameters obtained from the equations of the fitted curves (the total concentration of the HRI enzyme was $[E]_0 = 0.35$ µM). For ATP, the experiment was repeated twice (data not shown). The deviations of [eIF2α–P] at each ATP concentration were consistently below 5%.

Table 4.2: Kinetic parameters of the HRI–catalyzed eIF2α phosphorylation in the presence of various NTPs (ATP, GTP, UTP, and CTP, respectively) as the phosphate donors. The parameters were obtained from equations fitted to the data in Fig. 4.9 on p. 60, either the Michaelis–Menten equation (ATP, GTP), or the Hill equation (UTP, CTP). The parameters were introduced in Section 3.3.5.2 (p. 47): $v_{\mathrm{lim}}^{\mathrm{NTP}}$ is the limiting velocity, $K_{\mathrm{M}}^{\mathrm{NTP}}$ is the apparent Michaelis–Menten constant, $K_{0.5}^{\mathrm{NTP}}$ is the apparent half-saturation constant, h^{NTP} is the Hill coefficient, $k_{\mathrm{cat}}^{\mathrm{NTP}}$ is the catalytic constant, and η^{NTP} is the catalytic efficiency.

(a)

	ATP	GTP
$v_{\mathrm{lim}}^{\mathrm{NTP}}$ (nM s^{-1})	20	13
$K_{\mathrm{M}}^{\mathrm{NTP}}$ (µM)	52	410
$k_{\mathrm{cat}}^{\mathrm{NTP}}$ (min^{-1})	3.43	2.23
η^{NTP} (mM^{-1} min^{-1})	65.93	5.44

(b)

	UTP	CTP
$v_{\mathrm{lim}}^{\mathrm{NTP}}$ (nM s^{-1})	1	1
$K_{0.5}^{\mathrm{NTP}}$ (µM)	1477	819
h^{NTP}	5.0	2.6
$k_{\mathrm{cat}}^{\mathrm{NTP}}$ (min^{-1})	0.17	0.17
η^{NTP} (mM^{-1} min^{-1})	0.12	0.21

4.3.3 Heme inhibition of the HRI kinase reaction

The HRI–catalyzed eIF2α phosphorylation in the presence of various NTPs (ATP, GTP, UTP, and CTP, respectively) was performed with different concentrations of heme while keeping the concentration of all reaction components (eIF2α, HRI, NTP) constant. The reaction mixtures were analyzed by Phos-tag SDS–PAGE. Figure 4.10 on p. 62 shows the gels imaged after staining with InstantBlue® Coomassie Protein Stain. Three bands are observed in each lane: the phosphorylated and unphosphorylated forms of eIF2α (labeled as eIF2α–P and eIF2α), and the HRI enzyme. Note that two types of negative control were used: eIF2α and HRI were mixed with either the reaction buffer or DMSO. The former type of negative control was injected into the first lane in each gel in Fig. 4.10 on p. 62, and the latter type was injected into the last lane in each gel.

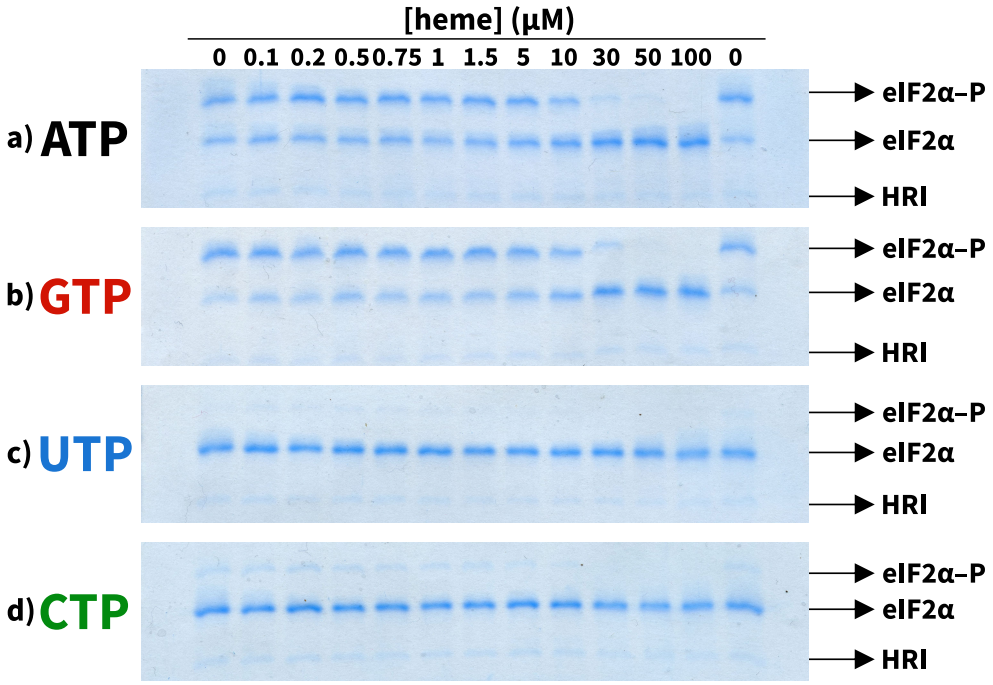

Figure 4.10: Heme inhibition study of the HRI–catalyzed eIF2α phosphorylation in the presence of a) ATP, b) GTP, c) UTP, d) CTP. The reaction mixtures were analyzed using 10% SDS–PAGE with 75 µM Phos-tag and 200 µM $MnCl_2$. The gels were stained with InstantBlue® Coomassie Protein Stain. Each mixture contained 5.4 µM eIF2α, 0.35 µM HRI, 20 mM Tris-HCl, 2 mM $MgCl_2$, 60 mM KCl (pH 8.0), and 0–100 µM heme (solution in DMSO). The reactions were initiated by adding 900 µM NTP and terminated after 10 minutes by adding the 2× stock sample buffer and incubating at 95 °C for 5 minutes. The negative control in the first (last, respectively) lane was prepared by replacing the heme solution with the reaction buffer (or DMSO, respectively).

The concentrations of eIF2α–P in samples injected into each lane were determined using ImageJ. These values were used to calculate the relative kinase activities a_{rel} according to Eq. 3.6 on p. 49. For ATP and GTP, the points were fitted with a sigmoidal model (Eq. 3.7 on p. 49). The maximal kinase activity $[\mathrm{eIF2\alpha–P}]_0$ was obtained by averaging [eIF2α–P] over the 0–1.5 µM heme concentration range. However, the data for UTP and CTP were better described by a hyperbolic model (Eq. 3.8 on p. 49). In this case, the $[\mathrm{eIF2\alpha–P}]_0$ was given by the [eIF2α–P] in the mixture containing DMSO instead of heme. The inhibition curves are shown in Fig. 4.11 on p. 63, along with the values of $\mathrm{IC}_{50}^{\mathrm{NTP}}$ values obtained for each NTP.

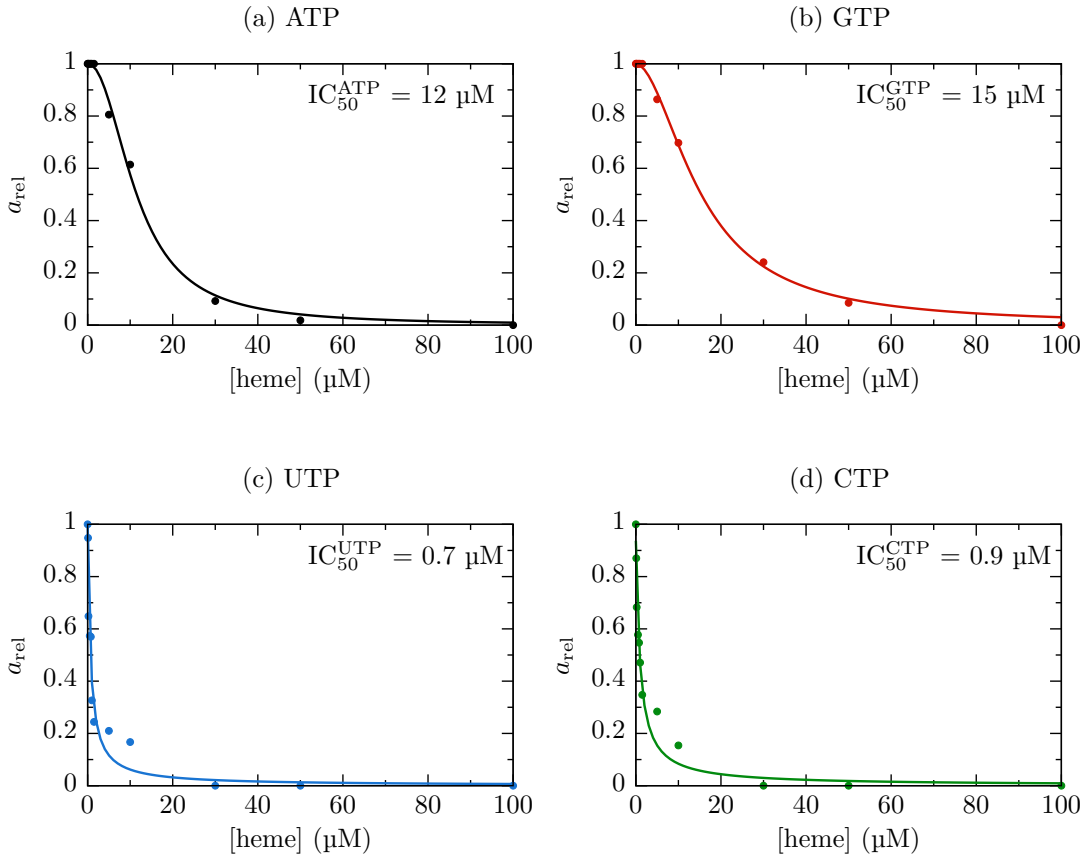

Figure 4.11: Relative kinase activity a_{rel} in the heme-inhibited HRI–catalyzed eIF2α phosphorylation by different NTPs, for different concentrations of heme: a) ATP, b) GTP, c) UTP, d) CTP. The a_{rel} values were determined by quantifying the gels in Fig. 4.10 on p. 62 using ImageJ and Eq. 3.6 on p. 49. The maximal kinase activity for each NTP $[eIF2\alpha–P]_0$ was determined by quantifying the last lane in the respective gel in Fig. 4.10 on p. 62. The curves in each plot were obtained by fitting the data with either a sigmoidal curve (ATP, GTP) or a hyperbolic curve (UTP, CTP).

4.4 Effect of cytochrome *c* on the kinase activity of HRI

The effect of cytochrome *c* and/or heme on the HRI–catalyzed eIF2α phosphorylation in the presence of ATP was studied using a Phos-tag SDS–PAGE assay. Figure 4.12 on p. 64 shows the gel imaged after staining with InstantBlue® Coomassie Protein Stain, with the indication of reagents ($Na_2S_2O_4$, heme, cytochrome *c*) added into a preincubated mixture of eIF2α and HRI. The concentrations of eIF2α–P in samples injected into each lane were determined using ImageJ. These values are indicated by the bars below the corresponding lanes of

the gel in Fig. 4.12.

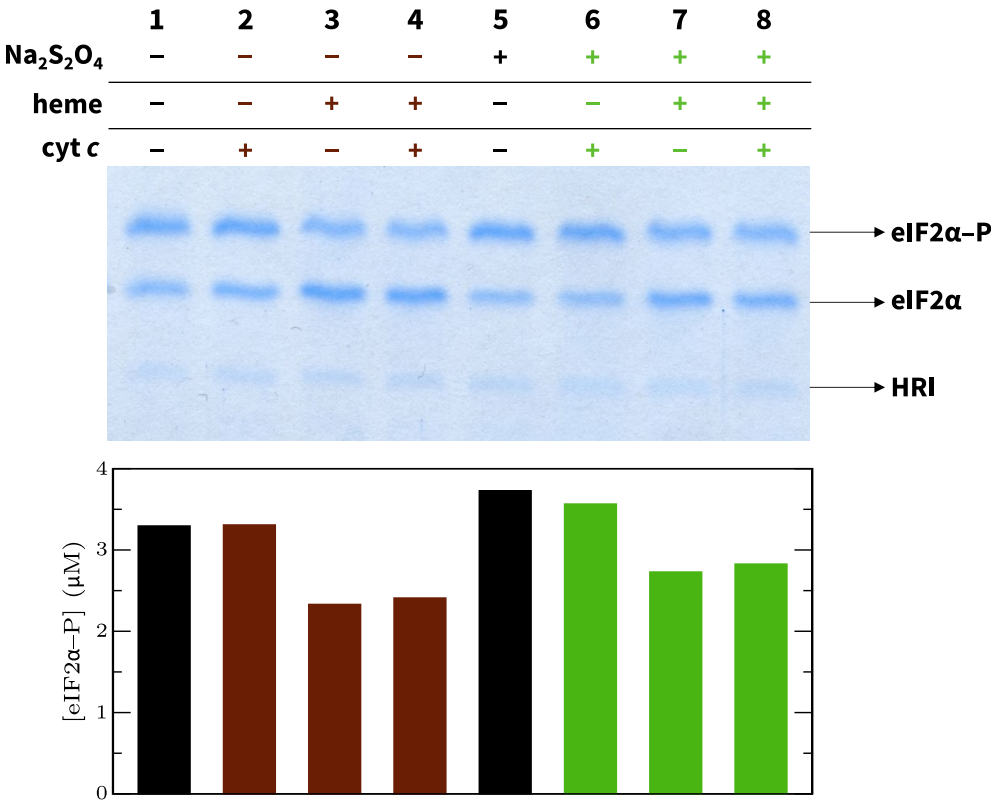

Figure 4.12: Study of the HRI–catalyzed eIF2α phosphorylation by ATP in the presence of cytochrome c and/or heme in different redox states. The reaction mixtures were analyzed using 10% SDS–PAGE with 75 µM Phos-tag and 200 µM $MnCl_2$. The gels were stained with InstantBlue® Coomassie Protein Stain. Each mixture contained 5.4 µM eIF2α and 0.35 µM HRI in 20 mM Tris-HCl, 2 mM $MgCl_2$, and 60 mM KCl (pH 8.0). Additional components (9 µM heme, 0.35 µM cytochrome c, 500 µM $Na_2S_2O_4$) were added into the mixtures if indicated by the '+' sign. The reactions were initiated by adding 900 µM ATP and terminated after 10 minutes by adding the 2× stock sample buffer and incubating at 95 °C for 5 minutes. The concentration of eIF2α–P in each sample is indicated by the bar below the corresponding lane. These values were obtained by quantifying the gel using ImageJ.

Comparing the respective pairs of lanes, the presence of heme generally decreases the resulting concentrations of eIF2α–P, while the opposite is true for $Na_2S_2O_4$. On the contrary, the effect of the presence of cytochrome c is virtually negligible. A small increase in [eIF2α–P] ($< 5\%$) was observed in lane 2 (compared to lane 1), lane 4 (compared to lane 3), and lane 8 (compared to lane 7). However, a slight decrease ($< 5\%$) in [eIF2α–P] occurred in lane 6 (compared to lane 5).

4.5 Effect of cytochrome *c* on the absorption spectra of HRI

The interaction of HRI with cytochrome *c* and/or heme in different redox states was further examined with the aid of ultraviolet–visible spectroscopy. The absorption spectra are presented below, indicating the positions of the Soret peaks along with the Q bands (shown in the insets of the figures).

Figure 4.13 shows absorption spectra of pure cytochrome *c* (brown) and of cytochrome *c* after adding a small amount of crystalline $Na_2S_2O_4$ into the solution (i.e, under reducing conditions, green). The Soret peak of pure cytochrome *c* (409 nm) is shifted to lower energy (414 nm) and higher absorbance after adding $Na_2S_2O_4$ into the solution. Moreover, while two clear maxima of the Q bands emerge in the spectrum of cytochrome *c* after adding $Na_2S_2O_4$ (520 nm, 549 nm), a single peak at 529 nm only is present in the spectrum of pure cytochrome *c*.

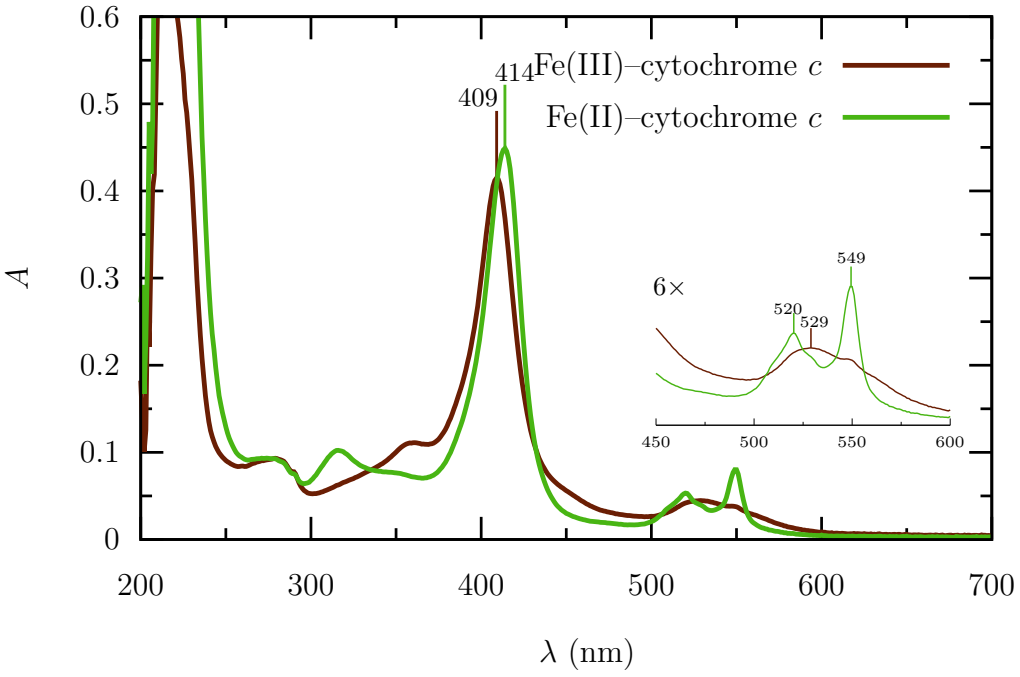

Figure 4.13: Absorption spectra of cytochrome *c* in 20 mM Tris-HCl, 150 mM NaCl, pH 8.0: **brown** – 5 µM cytochrome *c*; **green** – 5 µM cytochrome *c* and a small amount of crystalline $Na_2S_2O_4$. The buffer was used as the blank sample. The spectra were measured using a quartz cuvette (with a path length of 1 cm).

Figure 4.14 on p. 66 shows absorption spectra of three different forms of the HRI enzyme: pure HRI (i.e., apoform, grey), HRI after adding heme solution (i.e., holoform under non-reducing conditions, brown), and HRI after adding heme and

a small amount of crystalline $Na_2S_2O_4$ (i.e., holoform under reducing conditions, green). While the Soret peak of the HRI apoform (410 nm) is insignificant, a clear maximum at 405 nm was observed for the HRI holoform under non-reducing conditions, with an intensity ratio 0.065 compared to the apoform. The reduction by adding $Na_2S_2O_4$ led to a slight redshift of the Soret peak (408 nm), but the structure of the Q bands was not altered. In this region of the spectra, only a single maximum was observed for the HRI holoform both under non-reducing (529 nm) and reducing (520 nm) conditions.

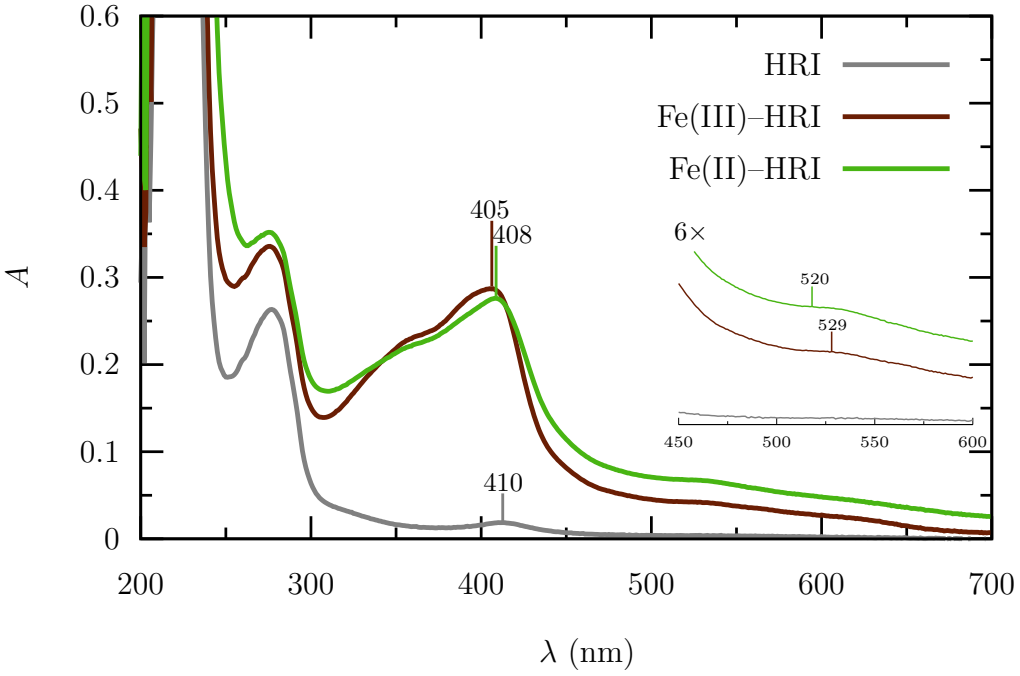

Figure 4.14: Absorption spectra of different forms of the HRI enzyme in 20 mM Tris-HCl, 150 mM NaCl, pH 8.0: **grey** – 5 µM HRI apoform; **brown** – 5 µM HRI holoform under non-reducing conditions; **green** – 5 µM HRI holoform under reducing conditions (induced by a small amount of crystalline $Na_2S_2O_4$). The buffer was used as the blank sample. The spectra were measured using a quartz cuvette (with a path length of 1 cm).

Finally, Figure 4.15 on p. 67 shows absorption spectra of an equimolar mixture of cytochrome *c* and HRI (Fig. 4.15a on p. 67), and of the same mixture after adding a small amount of crystalline $Na_2S_2O_4$ (Fig. 4.15b on p. 67). In both subfigures, the dashed lines represent hypothetical spectra obtained by averaging the spectra of the pure components using Eq. 3.9 on p. 51. While the spectrum measured under non-reducing conditions aligns well with the calculated one, deviations from the calculation are observed under reducing conditions.

(a) Fe(III)–HRI + Fe(III)–cytochrome *c*

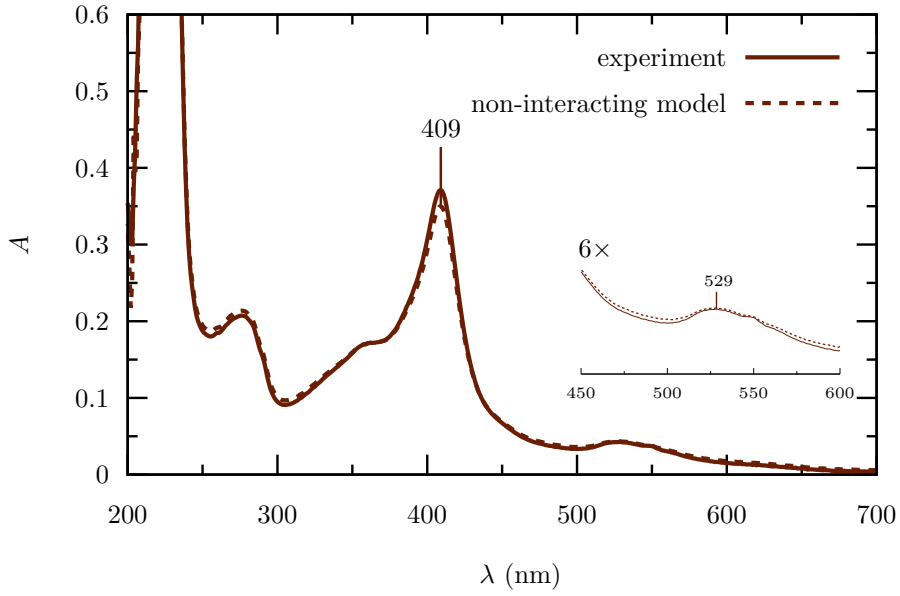

(b) Fe(II)–HRI + Fe(II)–cytochrome *c*

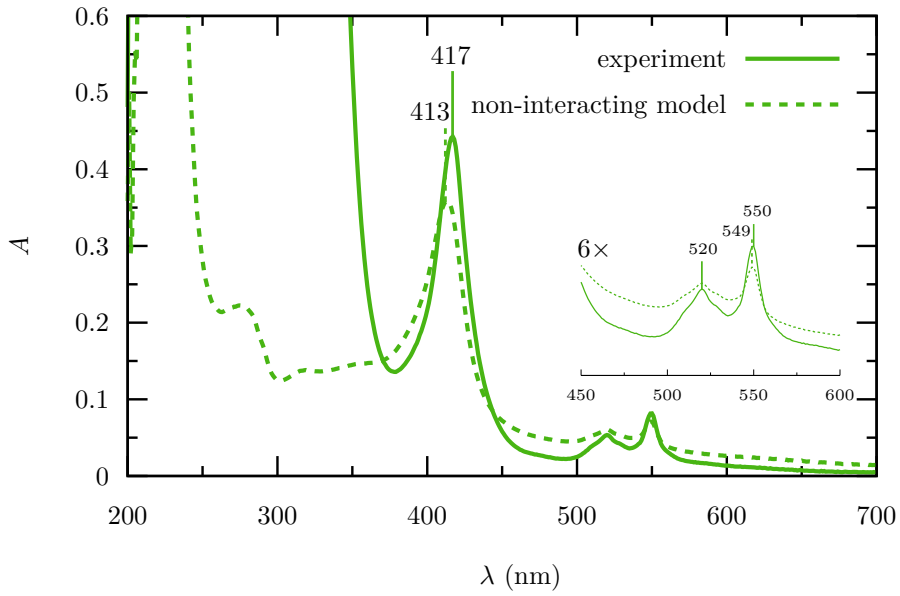

Figure 4.15: Absorption spectra of an equimolar mixture of HRI holoform and cytochrome *c* in 20 mM Tris-HCl, 150 mM NaCl, pH 8.0: a) 2.5 µM HRI holoform with 2.5 µM cytochrome *c* under non-reducing conditions, b) 2.5 µM HRI holoform with 2.5 µM cytochrome *c* under reducing conditions (induced by adding a small amount of crystalline $Na_2S_2O_4$ into the solution). In both subfigures, the dashed lines indicate the hypothetical spectra obtained by averaging the spectra of pure components using Eq. 3.9 on p. 51. The buffer was used as the blank sample. The spectra were measured using a quartz cuvette (with a path length of 1 cm).

In particular, in the spectrum measured under non-reducing conditions (Fig. 4.15a on p. 67), the Soret peak is observed at 409 nm, and a single maximum is found in the Q band region at 529 nm, both of which are in agreement with the calculated results. However, in the spectrum measured under reducing conditions, a relatively strong absorption is seen at 417 nm, whereas the calculated Soret peak appears at 413 nm and its intensity is comparatively lower. Although the structure of the Q bands remains fairly consistent between the measured and calculated spectra, some differences in intensities are present.

5 Discussion

While initially recognized for its essential role in regulating hemoglobin synthesis, further research has unveiled the broader impact of the HRI enzyme in governing the cell's translational program. These discoveries suggest a critical regulatory function of HRI across diverse cellular pathways, including those implicated in cancer development. Despite the significance of HRI, many details of its function remain to be clarified at the molecular level. This knowledge gap mainly arises from the limited availability of structural information on HRI, caused by challenges in obtaining samples for conventional protein structure elucidation techniques, such as X-ray crystallography. To gain insights into the structure-function relationships in HRI, indirect approaches such as kinetic and spectroscopic studies can be employed.[1–6,108]

This thesis aimed to contribute to the understanding of the HRI functions within two biologically relevant contexts. The first objective was to conduct a comparative kinetic analysis of the HRI–catalyzed eIF2α phosphorylation in the presence of different phosphate sources (ATP, GTP, UTP, and CTP). While the kinetic parameters for the canonical ATP substrate have been previously reported,[13,134] there are no reports on the utilization of the other NTPs (GTP, UTP, CTP) as the phosphate donors for this reaction. The second objective focused on studying the effect of cytochrome *c* on the kinase activity and absorption spectra of HRI, since the activation of HRI by cytochrome *c* has recently been implicated in translational reprogramming in persistent lung cancer cells.[188]

5.1 Overexpression, isolation, and purification of the HRI enzyme

For the purpose of the subsequent experiments, it was first necessary to overexpress and purify the wild-type HRI enzyme. The eIF2α substrate was available from previous experiments.[192] The pET-21c(+) plasmid encoding the $(His)_6$-tagged human HRI was introduced into the *E. coli* BL-21(DE3) cells. At the outset, it is important to address two key aspects of the methodology employed.

First, the choice of a prokaryotic expression system (*E. coli*) to produce a eukaryotic protein (human HRI) raises concerns about the potential absence of

posttranslational modifications and proper folding. Nevertheless, the conducted experiments unequivocally demonstrated that the enzyme acquired its kinase activity, which would not have been possible without correct autophosphorylation and folding. The validity of this methodology has been further supported by previous studies.[131,134]

Second, the $(His)_6$ tag was not cleaved after the HRI enzyme was purified, to eliminate the risk of non-specific proteolysis. This strategy was supported by several investigations that reported no discernible differences in behavior between the free and $(His)_6$-tagged HRI enzymes.[130,131,134]

Let us now discuss the individual steps in the process of overexpression, isolation, and purification of the HRI enzyme. The transformation of the *E. coli* cells was presumably successful, as evidenced by the absence of colonies on the control ampicillin agar plate. The next key step was the induction of overexpression by the addition of IPTG. This induction stimulated the synthesis of numerous proteins, as indicated by the comparison of lanes 2 and 3 in Fig. 4.1 on p. 53 (samples of cell suspensions before and after IPTG induction). Although the amount of the HRI enzyme increased after this step, the magnitude of the increase was not as significant as would probably be observed if a prokaryotic protein was being produced.[194,200]

The sonication of cell suspensions and subsequent ultracentrifugation of the cell lysates effectively disintegrated the cells, resulting in the release of cytosolic contents. This is documented by the noticeable global increase in band intensities observed in lane 4 compared to lane 3 in Fig. 4.1 on p. 53. It is plausible that a certain proportion of the proteins might have formed inclusion bodies, a common occurrence when utilizing a prokaryotic expression system for the production of a eukaryotic protein.[201] This hypothesis could be verified by analyzing a sample of the pellet obtained from the ultracentrifugation of the cell lysate. However, additional processing of the pellet was unnecessary as the yield of the HRI enzyme from the supernatant proved to be sufficient.

The subsequent affinity chromatography step was a critical part of the purification process. A sample of the eluate was injected into lane 6 of the gel shown in Fig. 4.1 on p. 53. The noticeable decrease in the number of bands with significant intensities confirmed that the affinity resin predominantly interacted with the $(His)_6$-tagged HRI enzyme. Conversely, most of the remaining proteins passed through the column (especially those with higher molecular weights), as indicated by the analysis of a flow-through sample (lane 5 in Fig. 4.1 on p. 53). However, it was observed that a certain proportion of the $(His)_6$-tagged HRI enzyme was still

present in the flow-through sample (lane 5), suggesting that the resin's capacity might not have been sufficient. It is possible that the resin's capacity was partially occupied by co-expressed His-rich cytosolic proteins, which might also exhibit a strong affinity for the resin. The presence of such proteins or the products of their proteolytic cleavage is indicated by the appearance of low molecular weight bands in lane 6 of Fig. 4.1 on p. 53.

Further purification of the HRI enzyme was achieved by concentrating the eluate at centrifugal ultrafiltration units with a 30 kDa cut-off and finally, by GPC. Fractions 13–16 from the GPC were collected as the final product (elution volume 6–8 ml), based on previous reports from our laboratory.[193,202] Additionally, fractions 12 and 17 from the GPC were individually analyzed (lanes 8 and 10 in Fig. 4.1 on p. 53). Most importantly, fraction 17 (lane 10) exhibited an enrichment of proteins with lower molecular weights, while containing a relatively low amount of the HRI enzyme. In contrast, a certain fraction of the HRI enzyme was lost in fraction 12 (lane 8). Considering the abundance of proteins with lower molecular weights, however, using this fraction would introduce a higher level of contamination to the final product.

The concentration of the HRI enzyme in the final product was determined by measuring the absorbance at 280 nm. Previous reports from our laboratory have confirmed the reliability of this method for analyzing HRI, as it aligns with results obtained from a bicinchoninic acid assay.[193,202] Although the yield of the HRI enzyme was sufficient for the purpose of the subsequent experiments (22.3 µg/g of cells, i.e. 98.9 µg/l TB medium), it could potentially be increased by co-expressing the enzyme with its cofactor. To achieve this, the addition of a heme precursor (such as δ-aminolevulinic acid) into the cultivation medium would be needed. However, this strategy would yield the holoform of the HRI enzyme, which could not be used in the subsequent kinetic experiments.

5.2 Assessment of the purity of NTPs

Prior to conducting kinetic experiments with the HRI enzyme, it was crucial to ensure the absence of contaminations by ATP in the other purchased NTPs (GTP, UTP, and CTP). For instance, the presence of even a small amount of ATP in the GTP solutions would compromise the reliability of the experiments performed with GTP, as ATP would likely serve as the phosphate source for HRI instead. To address this, solutions of the NTPs were analyzed using ion-pair reversed-phase HPLC with absorbance detection at 254 nm as the primary signal.

The methodology employed was adapted from a previous study conducted in our laboratory.[199]

As expected, each NTP solution exhibited a single dominant peak in the chromatogram (see Fig. 4.3 on p. 55). In the ion-pair reversed-phase HPLC, the elution volume of a species is influenced by its interaction with the ion-pairing reagent (in this study, tetrabutylammonium hydrogensulfate). It was anticipated that the more hydrophilic purine NTPs would have stronger binding affinity for the ion-pairing reagent, resulting in their elution at higher volumes. Consistent with this expectation, CTP was eluted first (at 9.58 ml), while ATP eluted last (at 20.25 ml).

The presence of small peaks in the chromatograms raised concerns about potential contaminations in the NTP solutions. For this reason, the full absorption spectra of selected fractions obtained during the analysis of each NTP solution were analyzed. This was especially important in the case of the GTP solution (Fig. 4.3b on p. 55), where a slight peak emerged at $V = 22.59$ ml, a volume akin to the ATP's elution ($V = 20.25$ ml). Nonetheless, the absorption spectrum recorded for the GTP solution at $V = 22.59$ ml (see Fig. 4.5b on p. 56) clearly corresponds to a guanosine derivative, with regard to the presence of a characteristic shoulder around 280 nm.[203]

Similarly, the minor peak at $V = 15.71$ ml sighted in the ATP solution's chromatogram (Fig. 4.3a on p. 55) might have hinted at GTP contamination, given that GTP eluted at a comparable volume ($V = 14.54$ ml). However, the spectrum of the fraction of the ATP solution eluted at $V = 15.71$ ml clearly corresponds to an adenosine derivative, based on a comparison with the literature (see Fig. 4.5a on p. 56).[203] In the chromatograms of UTP and CTP (Figs. 4.3c and 4.3d on p. 55) solutions, minor peaks emerged at rather low elution volumes, making the possibility of ATP contamination highly implausible. This possibility was again ruled out by spectral analysis of these fractions (data not shown). No minor peaks were observed in the chromatogram of the more diluted ATP solution (100 µM, see Fig. 4.4 on p. 56).

5.3 Kinetic analysis of the HRI kinase reaction in the presence of different NTPs

Previous studies have examined the steady-state kinetics of the HRI–catalyzed phosphorylation of eIF2α in the presence of ATP as the phosphate donor.[13,134,137] However, there are no reports on the potential utilization of other NTPs (GTP,

UTP, CTP) as potential phosphate sources for this reaction. This possibility arises in cancer cells, where the relative concentrations of NTPs can deviate from those found in normal cells.[58] Consequently, the primary objective of this thesis was to investigate the kinase activity of HRI in the presence of these alternative NTPs, and to study the inhibition of these reactions by heme.

The methodology of the kinetic experiments was adapted from the reports cited above. These studies employed diverse techniques to detect the eIF2α–P product, including immunoblotting and radioactive labeling.[13,134] In this thesis, the Phos-tag SDS–PAGE assay was applied, as was the case in the study by Igarashi et al.[137] This method has recently been optimized in our laboratory for the research of other heme-regulated kinases as well.[87]

The reaction conditions of the HRI–catalyzed eIF2α phosphorylation, including temperature and pH, were optimized previously.[13,134,137] It is worth noting that the previous reports have shown that room temperature (20 °C) is optimal due to the enzyme's stability.[13,134,137] Therefore, the experiments in this thesis were also carried out at 20 °C, even though the enzyme typically functions at around 37 °C under physiological conditions. To investigate the steady-state kinetics of phosphorylation by each NTP, it was necessary to further optimize the reaction time to ensure initial velocity conditions. By measuring the initial velocity as a function of NTP concentration, the kinetic parameters were determined. The results obtained for each NTP are discussed below.

In the case of ATP being utilized as the phosphate donor for the HRI–catalyzed eIF2α phosphorylation, the concentration of eIF2α–P increased linearly with time until 3 minutes, as shown in Fig. 4.7a on p. 58. However, when comparing the gel image of this particular experiment (Fig. 4.6a on p. 57) with the gels from the other assays (Figs. 4.6b-d on p. 57, and Figs. 4.8 on p. 59, 4.10 on p. 62), slight differences in band distances can be observed. This is probably caused by the fact that the time-course experiment with ATP was performed separately from the remaining assays. The solutions used to prepare the gel were different and may have undergone nonspecific compositional changes, which is why the more recent gels were not reproduced in terms of band distances. Nevertheless, this discrepancy is highly unlikely to compromise the reliability of any of the experiments, as it solely impacts the resolution of the two protein forms and not the quantity of protein in each fraction.

The initial velocities of the HRI–catalyzed eIF2α phosphorylation for various concentrations of ATP were measured using a reaction time of 1 minute, ensuring compliance with the initial velocity conditions. Consistent with previous

studies, the results demonstrated that the reaction follows Michaelis-Menten kinetics with respect to ATP (Fig. 4.9a on p. 4.9a).[13,134,137] However, the catalytic constant ($k_{\text{cat}}^{\text{ATP}} = 3.43\ \text{min}^{-1}$) was somewhat higher than in the most recent report ($k_{\text{cat}}^{\text{ATP}} = 1.17\ \text{min}^{-1}$),[13] which may be attributed to slight differences in methodology, including the utilization of a short segment of the eIF2α substrate in the cited report, compared to the use of a full-length eIF2α in this thesis. Otherwise, the apparent kinetic parameters with respect to ATP are consistent with previous reports (see Tab. 5.1).[13,134,137] For ATP, the determination of kinetic parameters was repeated three times, and the statistical errors in determining eIF2α–P concentration consistently remained below 5%. It should be noted that for the remaining NTPs, data acquisition was limited to single experiments due to the enzyme's high consumption. Nevertheless, it is reasonable to anticipate a similar magnitude of statistical error in these experiments as well, given that they were carried out using identical procedures.

Table 5.1: Apparent kinetic parameters of the HRI–catalyzed eIF2α phosphorylation in the presence of ATP, reported in the literature for the wild-type HRI enzyme. Unreported values are labeled as 'NA'.

	$k_{\text{cat}}^{\text{ATP}}(\text{min}^{-1})$	$K_{\text{M}}^{\text{ATP}}(\mu\text{M})$
this study	3.43	52
(Miksanova et al., 2006)[134]	NA	31
(Igarashi et al., 2008)[137]	11.0	9.3
(Rickets et al., 2022)[13]	1.17	71.9

The time course of the phosphorylation by GTP exhibited a similar trend to ATP (Fig. 4.7b on p. 58). For this reason, the reaction time for the determination of kinetic parameters was again chosen as 1 minute. The results undeniably demonstrate GTP's potential as an alternative substrate for HRI. Analogously to ATP, the reaction follows the Michaelis–Menten kinetics with respect to GTP. However, the catalytic constant in comparison to ATP is nearly two-fold lower ($k_{\text{cat}}^{\text{GTP}} = 1.89\ \text{min}^{-1}$, $k_{\text{cat}}^{\text{ATP}} = 3.43\ \text{min}^{-1}$). It is important to note that the initial data points (5–50 µM) were excluded from the regression analysis since the corresponding eIF2α–P band intensities were too low (Fig. 4.8b on p. 59). Although it is highly likely that eIF2α phosphorylation occurred even at these low GTP concentrations, the amount of eIF2α–P was too low to be detected in the assay. It would be advisable to try injecting a larger volume of the sample into each lane, since in the current experiment, the injection volume was selected according to the optimization performed for ATP (5 µl). Nevertheless, the inclusion of the low-concentration points would probably introduce a significant error in the

regression analysis of the current results.

The analysis of phosphorylation by pyrimidine NTPs (UTP, CTP) presented several challenges. Time-course experiments indicated that these NTPs could also serve as phosphate sources, although likely less efficiently (Figs. 4.7c and 4.7d on p. 58). The concentration of the product increased linearly over time until 6 minutes, with the NTP concentration set at 1000 µM. To determine the kinetic parameters, a reaction time of 3 minutes was initially employed with an NTP concentration range of 0–900 µM. However, no eIF2α–P was detected in these assays (data not shown). Subsequently, the reaction time was extended to 6 minutes, but no improvement was observed. Therefore, it became necessary to explore a broader range of NTP concentrations (0–3000 µM) with the extended reaction time (6 minutes). This way, sufficient data points were obtained to determine the kinetic parameters. With regard to the low kinase activity observed at the low concentrations, the data were fitted to a sigmoidal curve (Figs. 4.9c and 4.9d on p. 60). The obtained values should be interpreted with caution, considering that the reaction time (6 minutes) was not optimized for the larger concentration range. Nevertheless, the results confirm the potential of pyrimidine NTPs as alternative phosphate sources for HRI, particularly when ATP and GTP levels are limited due to their excessive consumption by other reactions.

Additionally, the kinase reaction was conducted with each NTP while varying heme concentrations to determine the IC_{50} values. Interestingly, when purine NTPs (ATP, GTP) were utilized, a basal level of kinase activity persisted at low heme concentrations. However, in the case of pyrimidine NTPs (UTP, CTP), the phosphorylation process was inhibited, even at extremely low heme concentrations. Consequently, the data points obtained for ATP and GTP were fitted to a sigmoidal curve, while the data points for UTP and CTP conformed to a hyperbolic curve (see Fig. 4.11 on p. 63). These findings highlight that the heme-sensory function of HRI remains intact when ATP and GTP are used as phosphate sources, while a heme-deficient environment is required to facilitate the utilization of UTP and CTP in the kinase reaction.

Recently, our laboratory reported the kinetic parameters and heme IC_{50} values for the reaction in the presence of various NTPs, and these findings revealed consistently higher catalytic efficiencies than those reported in this thesis.[204] However, the experiments in the published report were conducted using a separately prepared HRI enzyme. The increased activity observed in the report may be due to a higher degree of HRI autophosphorylation during the overexpression process. Consequently, the elevated enzyme activity led to a more pronounced signal of

eIF2α–P even at lower concentrations of UTP and CTP. To analyze the kinetic data for UTP and CTP, a Michaelis–Menten model was employed in the report, in contrast to the sigmoidal model applied in this thesis. Therefore, further explorations will be necessary to assess the allosteric effects associated with pyrimidine NTPs. This can be achieved through the application of alternative methodologies, such as isothermal titration calorimetry.

In summary, the experiments have confirmed the expected finding that ATP is the most efficient phosphate source for HRI. However, the determination of half-saturation constants (K_{M} or $K_{0.5}$) suggests that the other NTPs may serve as alternative phosphate sources in physiologically relevant scenarios, such as transient developmental phases of the cell or tumor growth. From the structural viewpoint, these results are remarkably surprising, given that the highly conserved catalytic core of eukaryotic protein kinases appears to exhibit specific affinity towards the adenine ring of ATP only. However, a modified binding model was proposed for CK2, which explained its capability to utilize GTP as efficiently as ATP.[68–71] The key aspect of this model is the assistance of water molecules in mimicking the hydrogen bond pattern of the adenine ring (see Section 1.1.2, p. 12).[71] The results of this thesis indicate that this atypical substrate binding may also be applicable to HRI. It may be hypothesized that the pyrimidine NTPs (UTP, CTP) partially mimic the hydrogen bonding pattern of ATP with the aid of water molecules as well, albeit substantially less efficiently than GTP.

To further explore the preferential utilization of various NTPs in the HRI–catalyzed eIF2α phosphorylation, it would be intriguing to conduct a competition study, comparing the enzyme's consumption of different NTPs when all are available simultaneously. However, undertaking such a study would require the implementation of a novel detection method capable of distinguishing and quantifying the utilization of different NTPs as phosphate donors. This is currently unattainable with the Phos-tag SDS–PAGE method utilized in the present research.

5.4 Effect of cytochrome *c* on the kinase activity and absorption spectra of HRI

A recent study demonstrated the significance of the HRI/ATF4 pathway in the formation of persister phenotype in lung cancer cells, where the activation of HRI by cytochrome *c* plays a crucial role.[188] This study suggested the existence of a direct interaction between cytochrome *c* and HRI, as supported by an antibody

kinase assay and immunoprecipitation experiment. In this thesis, we investigated this interaction at a molecular level using a Phos-tag SDS–PAGE kinase assay and ultraviolet–visible spectroscopy.

Surprisingly, our results showed no significant effect of cytochrome *c* on the kinase activity of HRI, regardless of the presence or absence of heme, or even its redox state (see Fig. 4.12 on p. 64). Under the various conditions assayed, the changes in the eIF2α–P product amounts were below 5%, falling within the expected range of experimental error. These findings contradict the outcomes of the previous study, where cytochrome *c* was found to induce a marked increase in HRI kinase activity, both in the absence and presence of heme.[188] However, it should be noted that the previous study employed a 4-fold higher concentration of cytochrome *c* compared to HRI. In our experiment, equimolar concentrations of cytochrome *c* and HRI were utilized. These results suggest that the HRI dimer requires multiple cytochrome *c* molecules to enhance its kinase activity. Further investigations could explore the HRI kinase activity at varying concentrations of cytochrome *c*, providing additional insights into this interaction.

Moreover, an additional noteworthy finding emerged from the kinase experiments, albeit unrelated to the impact of cytochrome *c*. In all assays conducted, an increase in kinase activity was observed when Fe(III) heme was reduced to Fe(II). This observation holds significance as conflicting reports on this issue have been documented (see Section 1.3, p. 23).[134,136] The results obtained in this study align with the findings of Igarashi et al., indicating that the activity of the HRI–heme complex is enhanced following the reduction of heme iron to Fe(II).[136]

Let us now discuss the spectroscopic experiments conducted to explore the heme coordination in the HRI holoform, cytochrome *c*, and their mixture. The absorption spectra of cytochrome *c* (Fig. 4.13 on p. 65) are consistent with previous literature reports.[205] This strongly supports the expectation that Fe(III) heme was present in the native solution of cytochrome *c* and that reduction to Fe(II) heme occurred upon the addition of $Na_2S_2O_4$. The change in the heme redox state is prominently reflected in the Q band region of the spectra. In our experiment, we observed a broader peak at 529 nm for the native solution, while two narrower peaks at 520 nm and 549 nm emerged after the addition of $Na_2S_2O_4$. These findings align perfectly with the previous study, which reported a single peak for the Fe(III) state (at 530 nm) and two peaks for the Fe(II) state (at 521 nm and 550 nm).[205]

As anticipated, only a low Soret peak (410 nm) was observed in the absorption spectrum of the purified HRI enzyme (Fig. 4.14 on p. 66), as it was produced as

an apoform. Upon the addition of equimolar heme, the peak shifted to 405 nm with a significant increase in intensity, indicating the formation of a holoform. By comparing the intensities of the Soret peak before and after heme addition, it can be inferred that the purified HRI enzyme contained approximately 6% heme. The Soret peak of a pure heme solution is typically observed at 398 nm.[136,140] Although the shift to 405 nm indicates partial heme binding by HRI, previous studies have reported even larger shifts (see Tab. 5.2 on p. 78).[131,134,136,137,140] These findings suggest that the incubation period of HRI with heme was insufficient to establish the equilibrium ratio between free and bound heme. This also explains why the expected emergence of two peaks in the Q band region did not occur after adding Na_2SO_4 to the solution, as reported in the literature.[136,137]

Table 5.2: Absorption maxima positions reported in the literature for the wild-type HRI enzyme (apoform) and its holoforms in the Fe(III) and Fe(II) states. Unreported values are labeled as 'NA'.

	HRI	Fe(III)–HRI	Fe(II)–HRI
this study	410 nm	405 nm, 529 nm	408 nm, 520 nm
(Fagard & London, 1981)[140]	400 nm	418 nm	NA
(Bauer et al., 2001)[131]	NA	422 nm, 550 nm	NA
(Igarashi et al., 2004)[136]	418 nm	418 nm, 538 nm	426 nm, 531 nm, 560 nm
(Miksanova et al., 2006)[134]	NA	422 nm	NA
(Igarashi et al., 2008)[137]	NA	423 nm, 539 nm	427 nm, 530 nm, 560 nm

Furthermore, the absorption spectrum of an equimolar mixture of cytochrome *c* and the HRI holoform was analyzed (Fig. 4.15 on p. 67). Under non-reducing conditions, the positions and shapes of the peaks were identical to those of pure cytochrome *c* (409 nm, 529 nm). Upon the addition of $Na_2S_2O_4$, the Soret peak shifted to 417 nm, slightly higher than the position of the peak observed for Fe(II) cytochrome *c* (414 nm). For further investigations, the experimental data were compared to hypothetical absorption spectra, which were calculated by averaging the absorbances of pure components (Eq. 3.9 on p. 51). This model corresponds to a situation where no structural alterations in the vicinity of the heme-binding sites in either protein are induced by the interaction of the two proteins. While the experimental spectrum measured under non-reducing conditions aligns with this hypothetical model (Fig. 4.15a on p. 67), a distinct deviation from the model was observed in the spectrum recorded under reducing conditions (Fig. 4.15b on p. 67).

The implications drawn from these findings suggest a potential direct protein–protein interaction between cytochrome *c* and the HRI holoform, inducing

a conformational change in proximity to the heme-binding site within either or both proteins. However, drawing more specific conclusions from the current results is challenging. The interaction might plausibly involve an electron transfer between the heme molecules coordinated within these proteins. In the absence of reducing conditions, both heme molecules were observed to be in the Fe(III) state. Yet, upon exposure to $Na_2S_2O_4$, it is conceivable that a combination of various redox states emerged in both proteins. This could provide a suitable environment for the electron transfer to take place. Nonetheless, further experiments with the control of the redox state of both proteins will be necessary to provide additional clues for the detailed model of the interaction.

In summary, this master thesis has shown that while ATP is the most efficient phosphate donor for the HRI–catalyzed eIF2α phosphorylation, non-canonical NTPs (GTP, UTP, CTP) may serve as alternative phosphate sources for this reaction as well, with GTP being even able to maintain the heme-sensing function of HRI. These findings hold implications for cellular dynamics during developmental phases and abnormal states like tumor growth, as such conditions are associated with deviations from the normal cellular NTPs concentrations. Although cytochrome *c* did not have any pronounced effect on the HRI's kinase activity, spectral experiments suggest a potential direct protein-protein interaction influencing the surroundings of the heme-binding sites in either or both proteins. These results prompt further research in this area.

Conclusions

This master thesis focused on the phosphorylation of eIF2α by HRI, with the use of different NTPs (ATP, GTP, UTP, CTP) serving as the phosphate donors for this reaction. Apart from that, the effect of cytochrome *c* on HRI kinase activity and absorption spectra was studied. The objectives of the thesis were successfully accomplished, leading to the following results:

- The wild-type HRI enzyme was overexpressed in *E. coli* BL-21(DE3) cells, and subsequently purified. The final product contained 78.3 µM of the HRI enzyme, with a resulting yield of 22.3 µg/g of cells, equivalent to 98.9 µg/l TB medium.

- High purity of the purchased NTPs (ATP, GTP, UTP, and CTP) was confirmed by the ion-pair reversed-phase HPLC. Contaminations by ATP in the solutions of GTP, UTP, and CTP were excluded by spectral analysis of the minor peaks present in the chromatograms.

- Steady-state kinetic analysis unequivocally confirmed the potential of both purine (ATP, GTP) and pyrimidine (UTP, CTP) NTPs to serve as phosphate donors for the HRI–catalyzed phosphorylation of eIF2α. Phosphorylation by ATP and GTP followed classical Michaelis-Menten kinetics, while UTP and CTP utilization displayed a sigmoidal dependence and considerably lower catalytic efficiency.

- The phosphorylation of eIF2α by HRI was inhibited by heme, regardless of the NTP serving as the phosphate donor in the reaction. While the response to heme was sigmoidal with purine NTPs (ATP, GTP), hyperbolic curves were obtained for pyrimidine NTPs (UTP, CTP). Furthermore, the kinase activity was inhibited by much lower concentrations of heme if UTP and CTP served as the phosphate donors, compared to the case of ATP and GTP.

- No significant effect of cytochrome *c* on the kinase activity of HRI was observed in assays employing a 1:1 ratio of HRI and cytochrome *c*, regardless of the presence of heme and/or reducing conditions.

- As a side result, it was demonstrated that the reduction of the heme iron in the HRI holoform increased its kinase activity, resolving an inconsistency in previous literature.

- Finally, spectroscopical measurements provided insight into the heme iron coordination and redox states in solutions of cytochrome *c*, HRI holoform, and their equimolar mixtures. The findings imply that a direct protein–protein interaction between cytochrome *c* and the HRI holoform cannot be excluded, although further investigation is warranted.

Bibliography

(1) Wang, X.; Proud, C. G. *Biochemical Journal* **2022**, *479*, 1059–1082.

(2) Costa-Mattioli, M.; Walter, P. *Science* **2020**, *368*, DOI: 10.1126/science.aat5314.

(3) Wek, R. C. *Cold Spring Harbor Perspectives in Biology* **2018**, *10*, a032870.

(4) Pakos-Zebrucka, K.; Koryga, I.; Mnich, K.; Ljujic, M.; Samali, A.; Gorman, A. M. *EMBO reports* **2016**, *17*, 1374–1395.

(5) Taniuchi, S.; Miyake, M.; Tsugawa, K.; Oyadomari, M.; Oyadomari, S. *Scientific Reports* **2016**, *6*, DOI: 10.1038/srep32886.

(6) Donnelly, N.; Gorman, A. M.; Gupta, S.; Samali, A. *Cellular and Molecular Life Sciences* **2013**, *70*, 3493–3511.

(7) Maxwell, C.; Rabinovitz, M. *Biochemical and Biophysical Research Communications* **1969**, *35*, 79–85.

(8) Mellor, H.; Flowers, K. M.; Kimball, S. R.; Jefferson, L. S. *Journal of Biological Chemistry* **1994**, *269*, 10201–10204.

(9) Berlanga, J. J.; Herrero, S.; de Haro, C. *Journal of Biological Chemistry* **1998**, *273*, 32340–32346.

(10) Yerlikaya, A. *Medical Oncology* **2022**, *39*, DOI: 10.1007/s12032-022-01668-1.

(11) Tian, X.; Zhang, S.; Zhou, L.; Seyhan, A. A.; Borrero, L. H.; Zhang, Y.; El-Deiry, W. S. *Frontiers in Pharmacology* **2021**, *12*, DOI: 10.3389/fphar.2021.747837.

(12) Burwick, N.; Aktas, B. H. *Expert Opinion on Therapeutic Targets* **2017**, *21*, 1171–1177.

(13) Ricketts, M. D.; Emptage, R. P.; Blobel, G. A.; Marmorstein, R. *Journal of Biological Chemistry* **2022**, *298*, 102451.

(14) Fischer, E. H.; Krebs, E. G. *Journal of Biological Chemistry* **1955**, *216*, 121–132.

(15) Miranda, R. R.; Zhang, C. *RSC Medicinal Chemistry* **2022**, *13*, 783–797.

(16) Roskoski, R. *Pharmacological Research* **2015**, *100*, 1–23.

(17) Fabbro, D.; Cowan-Jacob, S. W.; Moebitz, H. *British Journal of Pharmacology* **2015**, *172*, 2675–2700.

(18) Fischer, E. H. *Angewandte Chemie International Edition in English* **1993**, *32*, 1130–1137.

(19) Krebs, E. G. *Angewandte Chemie International Edition in English* **1993**, *32*, 1122–1129.

(20) Jacobsen, D. M.; Bao, Z.-Q.; O'Brien, P.; Brooks, C. L.; Young, M. A. *Journal of the American Chemical Society* **2012**, *134*, 15357–15370.

(21) Shugar, D. *Acta Biochimica Polonica* **1996**, *43*, 9–23.

(22) Manning, G.; Whyte, D. B.; Martinez, R.; Hunter, T.; Sudarsanam, S. *Science* **2002**, *298*, 1912–1934.

(23) Lindberg, R. A.; Quinn, A. M.; Hunter, T. *Trends in Biochemical Sciences* **1992**, *17*, 114–119.

(24) Cieśla, J.; Frączyk, T.; Rode, W. *Acta Biochimica Polonica* **2011**, *58*, DOI: 10.18388/abp.2011_2258.

(25) Klumpp, S.; Krieglstein, J. *European Journal of Biochemistry* **2002**, *269*, 1067–1071.

(26) Hunter, T. *Molecular Cell* **2022**, *82*, 2190–2200.

(27) Nelson, D. L.; Cox, M. M., *Lehninger Principles of Biochemistry (Fifth Edition)*; W. H. Freeman: New York, 2008.

(28) Schwartz, P. A.; Murray, B. W. *Bioorganic Chemistry* **2011**, *39*, 192–210.

(29) Wang, Z.; Cole, P. A. In *Methods in Enzymology*; Elsevier: 2014, pp 1–21.

(30) Ferreira-Cerca, S.; Sagar, V.; Schäfer, T.; Diop, M.; Wesseling, A.-M.; Lu, H.; Chai, E.; Hurt, E.; LaRonde-LeBlanc, N. *Nature Structural & Molecular Biology* **2012**, *19*, 1316–1323.

(31) Ho, M.; Bramson, H. N.; Hansen, D. E.; Knowles, J. R.; Kaiser, E. T. *Journal of the American Chemical Society* **1988**, *110*, 2680–2681.

(32) Hubbard, S. R.; Cole, P. A.; Parang, K.; Till, J. H.; Ablooglu, A. J.; Kohanski, R. A. *Nature Structural Biology* **2001**, *8*, 37–41.

(33) Endicott, J. A.; Noble, M. E.; Johnson, L. N. *Annual Review of Biochemistry* **2012**, *81*, 587–613.

(34) Taylor, S. S.; Kornev, A. P. *Trends in Biochemical Sciences* **2011**, *36*, 65–77.

(35) Knighton, D. R.; Zheng, J.; Eyck, L. F. T.; Ashford, V. A.; Xuong, N.-H.; Taylor, S. S.; Sowadski, J. M. *Science* **1991**, *253*, 407–414.

(36) Knighton, D. R.; Zheng, J.; Eyck, L. F. T.; Xuong, N.-h.; Taylor, S. S.; Sowadski, J. M. *Science* **1991**, *253*, 414–420.

(37) Meharena, H. S.; Chang, P.; Keshwani, M. M.; Oruganty, K.; Nene, A. K.; Kannan, N.; Taylor, S. S.; Kornev, A. P. *PLoS Biology* **2013**, *11*, ed. by Petsko, G. A., e1001680.

(38) Taylor, S. S.; Keshwani, M. M.; Steichen, J. M.; Kornev, A. P. *Philosophical Transactions of the Royal Society B: Biological Sciences* **2012**, *367*, 2517–2528.

(39) Li, M.; Rehman, A. U.; Liu, Y.; Chen, K.; Lu, S. In *Advances in Protein Chemistry and Structural Biology*; Elsevier: 2021, pp 87–119.

(40) Vulpetti, A.; Bosotti, R. *Il Farmaco* **2004**, *59*, 759–765.

(41) Goldsmith, E. J.; Akella, R.; Min, X.; Zhou, T.; Humphreys, J. M. *Chemical Reviews* **2007**, *107*, 5065–5081.

(42) Biondi, R. M.; Nebreda, A. R. *Biochemical Journal* **2003**, *372*, 1–13.

(43) Johnson, L. N.; Lowe, E. D.; Noble, M. E.; Owen, D. J. *FEBS Letters* **1998**, *430*, 1–11.

(44) Foulkes, J. G.; Chow, M.; Gorka, C.; Frackelton, A. R.; Baltimore, D. *Journal of Biological Chemistry* **1985**, *260*, 8070–8077.

(45) Taylor, S. S.; Radzio-Andzelm, E.; Hunter, T. *The FASEB Journal* **1995**, *9*, 1255–1266.

(46) Smith, C. M.; Radzio-Andzelm, E.; Madhusudan; Akamine, P.; Taylor, S. S. *Progress in Biophysics and Molecular Biology* **1999**, *71*, 313–341.

(47) Zhou, J.; Adams, J. A. *Biochemistry* **1997**, *36*, 15733–15738.

(48) Nolen, B.; Taylor, S.; Ghosh, G. *Molecular Cell* **2004**, *15*, 661–675.

(49) Adams, J. A. *Biochemistry* **2002**, *42*, 601–607.

(50) Kornev, A. P.; Haste, N. M.; Taylor, S. S.; Eyck, L. F. T. *Proceedings of the National Academy of Sciences* **2006**, *103*, 17783–17788.

(51) Kornev, A. P.; Taylor, S. S.; Eyck, L. F. T. *Proceedings of the National Academy of Sciences* **2008**, *105*, 14377–14382.

(52) Bastidas, A. C.; Deal, M. S.; Steichen, J. M.; Guo, Y.; Wu, J.; Taylor, S. S. *Journal of the American Chemical Society* **2013**, *135*, 4788–4798.

(53) Waas, W. F.; Dalby, K. N. *Biochemistry* **2003**, *42*, 2960–2970.

(54) Liu, M.; Girma, E.; Glicksman, M. A.; Stein, R. L. *Biochemistry* **2010**, *49*, 4921–4929.

(55) Adams, J. A.; Taylor, S. S. *Protein Science* **1993**, *2*, 2177–2186.

(56) Knape, M. J.; Ballez, M.; Burghardt, N. C.; Zimmermann, B.; Bertinetti, D.; Kornev, A. P.; Herberg, F. W. *Metallomics* **2017**, *9*, 1576–1584.

(57) Andreini, C.; Bertini, I.; Cavallaro, G.; Holliday, G. L.; Thornton, J. M. *JBIC Journal of Biological Inorganic Chemistry* **2008**, *13*, 1205–1218.

(58) Traut, T. W. *Molecular and Cellular Biochemistry* **1994**, *140*, 1–22.

(59) Allende, J. E.; Allende, C. C. *The FASEB Journal* **1995**, *9*, 313–323.

(60) Bostrom, S. L.; Dore, J.; Griffith, L. C. *Biochemical and Biophysical Research Communications* **2009**, *390*, 1154–1159.

(61) Yurimoto, S.; Fujimoto, T.; Magari, M.; Kanayama, N.; Kobayashi, R.; Tokumitsu, H. *BMC Biochemistry* **2012**, *13*, DOI: 10.1186/1471-2091-13-27.

(62) Schinkmann, K.; Blenis, J. *Journal of Biological Chemistry* **1997**, *272*, 28695–28703.

(63) Carpenter, G.; King, L.; Cohen, S. *Journal of Biological Chemistry* **1979**, *254*, 4884–4891.

(64) Gschwendt, M.; Kittstein, W.; Kielbassa, K.; Marks, F. *Biochemical and Biophysical Research Communications* **1995**, *206*, 614–620.

(65) Becher, I.; Savitski, M. M.; Savitski, M. F.; Hopf, C.; Bantscheff, M.; Drewes, G. *ACS Chemical Biology* **2013**, *8*, 599–607.

(66) Bossemeyer, D.; Engh, R.; Kinzel, V.; Ponstingl, H.; Huber, R. *The EMBO Journal* **1993**, *12*, 849–859.

(67) Nobeli, I.; Laskowski, R.; Valdar, W.; Thornton, J. *Nucleic acids research* **2001**, *29*, 4294–4309.

(68) Jakobi, R.; Traugh, J. A. *European Journal of Biochemistry* **2008**, *230*, 1111–1117.

(69) Srinivasan, N.; Antonelli, M.; Jacob, G.; Korn, I.; Romero, F.; Jedlicki, A.; Dhanaraj, V.; Sayed, M. F.-R.; Blundell, T. L.; Allende, C. C.; Allende, J. E. *Protein Engineering, Design, and Selection* **1999**, *12*, 119–127.

(70) Niefind, K. *The EMBO Journal* **1998**, *17*, 2451–2462.

(71) Niefind, K.; Pütter, M.; Guerra, B.; Issinger, O.-G.; Schomburg, D. *Nature Structural Biology* **1999**, *6*, 1100–1103.

(72) O'Donoghue, L.; Smolenski, A. *Journal of Proteomics* **2022**, *259*, 104558.

(73) Areces, L. B.; Matafora, V.; Bachi, A. *European Journal of Mass Spectrometry* **2004**, *10*, 383–392.

(74) Zhang, J.; Allen, M. D. *Molecular BioSystems* **2007**, *3*, 759.

(75) Hastie, C. J.; McLauchlan, H. J.; Cohen, P. *Nature Protocols* **2006**, *1*, 968–971.

(76) De Graauw, M.; Hensbergen, P.; van de Water, B. *Electrophoresis* **2006**, *27*, 2676–2686.

(77) Sefton, B. M.; Shenolikar, S. *Current Protocols in Molecular Biology* **1996**, *33*, DOI: 10.1002/0471142727.mb1801s33.

(78) Oberprieler, N. G.; Taskén, K. *Cellular Signalling* **2011**, *23*, 14–18.

(79) Mandell, J. W. *Histochemistry and Cell Biology* **2008**, *130*, 465–471.

(80) Tong, Q.-H.; Tao, T.; Xie, L.-Q.; Lu, H.-J. *Biosensors and Bioelectronics* **2016**, *80*, 385–391.

(81) Gafken, P. R.; Lampe, P. D. *Cell Communication & Adhesion* **2006**, *13*, 249–262.

(82) Kinoshita, E.; Takahashi, M.; Takeda, H.; Shiro, M.; Koike, T. *Dalton Transactions* **2004**, 1189.

(83) Kinoshita, E.; Kinoshita-Kikuta, E.; Matsubara, M.; Yamada, S.; Nakamura, H.; Shiro, Y.; Aoki, Y.; Okita, K.; Koike, T. *Proteomics* **2008**, *8*, 2994–3003.

(84) Kinoshita, E.; Kinoshita-Kikuta, E.; Koike, T. *Biochimica et Biophysica Acta (BBA) – Proteins and Proteomics* **2015**, *1854*, 601–608.

(85) Nagy, Z.; Comer, S.; Smolenski, A. *Current Protocols in Protein Science* **2018**, *93*, DOI: 10.1002/cpps.64.

(86) Örd, M.; Loog, M. In *Methods in Molecular Biology*; Springer US: 2020, pp 779–792.

(87) Vávra, J.; Sergunin, A.; Shimizu, T.; Martínková, M. In *Oxygen Sensing*; Springer US: 2023, pp 63–73.

(88) Hinnebusch, A. G.; Lorsch, J. R. *Cold Spring Harbor Perspectives in Biology* **2012**, *4*, a011544–a011544.

(89) Colthrust, D. R.; Campbell, D. G.; Proud, C. G. *European Journal of Biochemistry* **1987**, *166*, 357–363.

(90) Alone, P. V.; Dever, T. E. *Journal of Biological Chemistry* **2006**, *281*, 12636–12644.

(91) Erickson, F. L.; Hannig, E. M. *EMBO Journal* **1996**, *15*, 6311–6320.

(92) Rowlands, A. G.; Panniers, R.; Henshaw, E. C. *Journal of Biological Chemistry* **1988**, *263*, 5526–5533.

(93) Sudhakar, A.; Ramachandran, A.; Ghosh, S.; Hasnain, S. E.; Kaufman, R. J.; Ramaiah, K. V. A. *Biochemistry* **2000**, *39*, 12929–12938.

(94) Paulin, F. E.; Campbell, L. E.; O'Brien, K.; Loughlin, J.; Proud, C. G. *Current Biology* **2001**, *11*, 55–59.

(95) Boesen, T.; Mohammad, S. S.; Pavitt, G. D.; Andersen, G. R. *Journal of Biological Chemistry* **2004**, *279*, 10584–10592.

(96) Kashiwagi, K.; Yokoyama, T.; Nishimoto, M.; Takahashi, M.; Sakamoto, A.; Yonemochi, M.; Shirouzu, M.; Ito, T. *Science* **2019**, *364*, 495–499.

(97) Gordiyenko, Y.; Llácer, J. L.; Ramakrishnan, V. *Nature Communications* **2019**, *10*, DOI: 10.1038/s41467-019-10606-1.

(98) Zhang, H.; Wang, Y.; Lu, J. *Trends in Biochemical Sciences* **2019**, *44*, 782–794.

(99) Barbosa, C.; Peixeiro, I.; Romão, L. *PLoS Genetics* **2013**, *9*, ed. by Fisher, E. M. C., e1003529.

(100) Lu, P. D.; Harding, H. P.; Ron, D. *Journal of Cell Biology* **2004**, *167*, 27–33.

(101) Vattem, K. M.; Wek, R. C. *Proceedings of the National Academy of Sciences* **2004**, *101*, 11269–11274.

(102) Lee, Y.-Y.; Cevallos, R. C.; Jan, E. *Journal of Biological Chemistry* **2009**, *284*, 6661–6673.

(103) Jousse, C. *Nucleic Acids Research* **2001**, *29*, 4341–4351.

(104) Redpath, N. T.; Proud, C. G. *Biochemical Journal* **1990**, *272*, 175–180.

(105) Jousse, C.; Oyadomari, S.; Novoa, I.; Lu, P.; Zhang, Y.; Harding, H. P.; Ron, D. *Journal of Cell Biology* **2003**, *163*, 767–775.

(106) Novoa, I.; Zeng, H.; Harding, H. P.; Ron, D. *Journal of Cell Biology* **2001**, *153*, 1011–1022.

(107) Chen, J.-J. *Blood* **2006**, *109*, 2693–2699.

(108) Shimizu, T.; Lengálová, A.; Martínek, V.; Martínková, M. *Chemical Society Reviews* **2019**, *48*, 5624–5657.

(109) Lu, L.; Han, A.-P.; Chen, J.-J. *Molecular and Cellular Biology* **2001**, *21*, 7971–7980.

(110) Yerlikaya, A.; Kimball, S. R.; Stanley, B. A. *Biochemical Journal* **2008**, *412*, 579–588.

(111) Suragani, R. N. V. S.; Zachariah, R. S.; Velazquez, J. G.; Liu, S.; Sun, C.-W.; Townes, T. M.; Chen, J.-J. *Blood* **2012**, *119*, 5276–5284.

(112) Gal-Ben-Ari, S.; Barrera, I.; Ehrlich, M.; Rosenblum, K. *Frontiers in Molecular Neuroscience* **2019**, *11*, DOI: 10.3389/fnmol.2018.00480.

(113) Stern-Ginossar, N.; Thompson, S. R.; Mathews, M. B.; Mohr, I. *Cold Spring Harbor Perspectives in Biology* **2018**, *11*, a033001.

(114) Kim, Y.; Lee, J. H.; Park, J.-E.; Cho, J.; Yi, H.; Kim, V. N. *Genes & Development* **2014**, *28*, 1310–1322.

(115) Kim, Y.; Park, J.; Kim, S.; Kim, M.; Kang, M.-G.; Kwak, C.; Kang, M.; Kim, B.; Rhee, H.-W.; Kim, V. N. *Molecular Cell* **2018**, *71*, 1051–1063.e6.

(116) García, M. A.; Gil, J.; Ventoso, I.; Guerra, S.; Domingo, E.; Rivas, C.; Esteban, M. *Microbiology and Molecular Biology Reviews* **2006**, *70*, 1032–1060.

(117) Hovanessian, A. G.; Galabru, J. *European Journal of Biochemistry* **1987**, *167*, 467–473.

(118) Castilho, B. A.; Shanmugam, R.; Silva, R. C.; Ramesh, R.; Himme, B. M.; Sattlegger, E. *Biochimica et Biophysica Acta (BBA) – Molecular Cell Research* **2014**, *1843*, 1948–1968.

(119) Ye, J.; Kumanova, M.; Hart, L. S.; Sloane, K.; Zhang, H.; Panis, D. N. D.; Bobrovnikova-Marjon, E.; Diehl, J. A.; Ron, D.; Koumenis, C. *The EMBO Journal* **2010**, *29*, 2082–2096.

(120) Deng, J.; Harding, H. P.; Raught, B.; Gingras, A.-C.; Berlanga, J. J.; Scheuner, D.; Kaufman, R. J.; Ron, D.; Sonenberg, N. *Current Biology* **2002**, *12*, 1279–1286.

(121) Berlanga, J. J.; Ventoso, I.; Harding, H. P.; Deng, J.; Ron, D.; Sonenberg, N.; Carrasco, L.; de Haro, C. *The EMBO Journal* **2006**, *25*, 1730–1740.

(122) Harding, H. P.; Zhang, Y.; Ron, D. *Nature* **1999**, *397*, 271–274.

(123) Korennykh, A.; Walter, P. *Annual Review of Cell and Developmental Biology* **2012**, *28*, 251–277.

(124) Liang, S.-H.; Zhang, W.; Mcgrath, B. C.; Zhang, P.; Cavener, D. R. *Biochemical Journal* **2005**, *393*, 201–209.

(125) De la Cadena, S. G.; Hernández-Fonseca, K.; Camacho-Arroyo, I.; Massieu, L. *Apoptosis* **2013**, *19*, 414–427.

(126) Moore, C. E.; Omikorede, O.; Gomez, E.; Willars, G. B.; Herbert, T. P. *Molecular Endocrinology* **2011**, *25*, 315–326.

(127) Lu, Y.-N.; Kavianpour, S.; Zhang, T.; Zhang, X.; Nguyen, D.; Thombre, R.; He, L.; Wang, J. *PLOS Biology* **2021**, *19*, ed. by Gilbert, W. V., e3001096.

(128) Suzuki, A.; Hirata, M.; Kamimura, K.; Maniwa, R.; Yamanaka, T.; Mizuno, K.; Kishikawa, M.; Hirose, H.; Amano, Y.; Izumi, N.; Miwa, Y.; Ohno, S. *Current Biology* **2004**, *14*, 1425–1435.

(129) Chefalo, P. J.; Oh, J.; Rafie-Kolpin, M.; Kan, B.; Chen, J.-J. *European Journal of Biochemistry* **1998**, *258*, 820–830.

(130) Rafie-Kolpin, M.; Chefalo, P. J.; Hussain, Z.; Hahn, J.; Uma, S.; Matts, R. L.; Chen, J.-J. *Journal of Biological Chemistry* **2000**, *275*, 5171–5178.

(131) Bauer, B. N.; Rafie-Kolpin, M.; Lu, L.; Han, A.; Chen, J.-J. *Biochemistry* **2001**, *40*, 11543–11551.

(132) Uma, S.; Matts, R. L.; Guo, Y.; White, S.; Chen, J.-J. *European Journal of Biochemistry* **2000**, *267*, 498–506.

(133) Inuzuka, T.; Yun, B.-G.; Ishikawa, H.; Takahashi, S.; Hori, H.; Matts, R. L.; Ishimori, K.; Morishima, I. *Journal of Biological Chemistry* **2004**, *279*, 6778–6782.

(134) Mikšanová, M.; Igarashi, J.; Minami, M.; Sagami, I.; Yamauchi, S.; Kurokawa, H.; Shimizu, T. *Biochemistry* **2006**, *45*, 9894–9905.

(135) Hirai, K.; Martínková, M.; Igarashi, J.; Saiful, I.; Yamauchi, S.; El-Mashtoly, S.; Kitagawa, T.; Shimizu, T. *Journal of Inorganic Biochemistry* **2007**, *101*, 1172–1179.

(136) Igarashi, J.; Sato, A.; Kitagawa, T.; Yoshimura, T.; Yamauchi, S.; Sagami, I.; Shimizu, T. *Journal of Biological Chemistry* **2004**, *279*, 15752–15762.

(137) Igarashi, J.; Murase, M.; Iizuka, A.; Pichierri, F.; Martínková, M.; Shimizu, T. *Journal of Biological Chemistry* **2008**, *283*, 18782–18791.

(138) Shimizu, T. *Journal of Inorganic Biochemistry* **2012**, *108*, 171–177.

(139) Hargrove, M. S.; Barrick, D.; Olson, J. S. *Biochemistry* **1996**, *35*, 11293–11299.

(140) Fagard, R.; London, I. M. *Proceedings of the National Academy of Sciences* **1981**, *78*, 866–870.

(141) Rafie-Kolpin, M.; Han, A.-P.; Chen, J.-J. *Biochemistry* **2003**, *42*, 6536–6544.

(142) Igarashi, J.; Sasaki, T.; Kobayashi, N.; Yoshioka, S.; Matsushita, M.; Shimizu, T. *FEBS Journal* **2011**, *278*, 918–928.

(143) Yun, B.-G.; Matts, J. A.; Matts, R. L. *Biochimica et Biophysica Acta (BBA) – General Subjects* **2005**, *1725*, 174–181.

(144) Berwal, S. K.; Bhatia, V.; Bendre, A.; Suresh, C.; Chatterjee, S.; Pal, J. K. *International Journal of Biological Macromolecules* **2018**, *118*, 1604–1613.

(145) Sreejith, R. K.; Suresh, C. G.; Bhosale, S. H.; Bhavnani, V.; Kumar, A.; Gaikwad, S. M.; Pal, J. K. *Journal of Fluorescence* **2011**, *22*, 431–441.

(146) Bhavnani, V.; Kaviraj, S.; Panigrahi, P.; Suresh, C.; Yapara, S.; Pal, J. *Journal of Biomolecular Structure and Dynamics* **2017**, *36*, 2845–2861.

(147) Rose, D. W.; Wettenhall, R. E. H.; Kudlicki, W.; Kramer, G.; Hardesty, B. *Biochemistry* **1987**, *26*, 6583–6587.

(148) Méndez, R.; Moreno, A.; Haro, C. *Journal of Biological Chemistry* **1992**, *267*, 11500–11507.

(149) Matts, R. L.; Hurst, R. *Journal of Biological Chemistry* **1989**, *264*, 15542–15547.

(150) Uma, S.; Hartson, S. D.; Chen, J.-J.; Matts, R. L. *Journal of Biological Chemistry* **1997**, *272*, 11648–11656.

(151) Xu, Z.; Pal, J. K.; Thulasiraman, V.; Hahn, H. P.; Chen, J.-J.; Matts, R. L. *European Journal of Biochemistry* **1997**, *246*, 461–470.

(152) Pal, J. K. *Journal of Biosciences* **1998**, *23*, 353–360.

(153) Karnitz, L. M.; Felts, S. J. *Science's STKE* **2007**, *2007*, DOI: `10.1126/stke.3852007pe22`.

(154) Mukai, K.; Shimizu, T.; Igarashi, J. *Protein & Peptide Letters* **2011**, *18*, 1251–1257.

(155) Thulasiraman, V.; Xu, Z.; Uma, S.; Gu, Y.; Chen, J.-J.; Matts, R. L. *European Journal of Biochemistry* **1998**, *255*, 552–562.

(156) Uma, S.; Thulasiraman, V.; Matts, R. L. *Molecular and Cellular Biology* **1999**, *19*, 5861–5871.

(157) Gross, M.; Mendelewski, J. *Biochimica et Biophysica Acta (BBA) – Nucleic Acids and Protein Synthesis* **1978**, *520*, 650–663.

(158) Grankowski, N.; Kramer, G.; Hardesty, B. *Journal of Biological Chemistry* **1979**, *254*, 3145–3147.

(159) Olsen, J. V.; Blagoev, B.; Gnad, F.; Macek, B.; Kumar, C.; Mortensen, P.; Mann, M. *Cell* **2006**, *127*, 635–648.

(160) Méndez, R.; de Haro, C. *Journal of Biological Chemistry* **1994**, *269*, 6170–6176.

(161) Hurst, R.; Schatz, J. R.; Matts, R. L. *Journal of Biological Chemistry* **1987**, *262*, 15939–15945.

(162) Matts, R. L.; Schatz, J. R.; Hurst, R.; Kagen, R. *Journal of Biological Chemistry* **1991**, *266*, 12695–12702.

(163) Martínková, M.; Igarashi, J.; Shimizu, T. *FEBS Letters* **2007**, *581*, 4109–4114.

(164) McEwen, E.; Kedersha, N.; Song, B.; Scheuner, D.; Gilks, N.; Han, A.; Chen, J.-J.; Anderson, P.; Kaufman, R. J. *Journal of Biological Chemistry* **2005**, *280*, 16925–16933.

(165) Uma, S.; Yun, B.-G.; Matts, R. L. *Journal of Biological Chemistry* **2001**, *276*, 14875–14883.

(166) Igarashi, J.; Sato, A.; Kitagawa, T.; Sagami, I.; Shimizu, T. *Biochimica et Biophysica Acta (BBA) – Proteins and Proteomics* **2003**, *1650*, 99–104.

(167) Thomas, D. D.; Ridnour, L. A.; Isenberg, J. S.; Flores-Santana, W.; Switzer, C. H.; Donzelli, S.; Hussain, P.; Vecoli, C.; Paolocci, N.; Ambs, S.; Colton, C. A.; Harris, C. C.; Roberts, D. D.; Wink, D. A. *Free Radical Biology and Medicine* **2008**, *45*, 18–31.

(168) Heinemann, S. H.; Hoshi, T.; Westerhausen, M.; Schiller, A. *Chem. Commun.* **2014**, *50*, 3644–3660.

(169) Lobo, M. V.; Martín, M. E.; Pérez, M. I.; Alonso, F. J. M.; Redondo, C.; Álvarez, M. I.; Salinas, M. *Histochemical Journal* **2000**, *32*, 139–150.

(170) Rosenwald, I. B.; Wang, S.; Savas, L.; Woda, B.; Pullman, J. *Cancer* **2003**, *98*, 1080–1088.

(171) Aktas, B. H.; Qiao, Y.; Ozdelen, E.; Schubert, R.; Sevinc, S.; Harbinski, F.; Grubissich, L.; Singer, S.; Halperin, J. A. *Oncotarget* **2013**, *4*, 1606–1617.

(172) Donzé, O.; Jagus, R.; Koromilas, A. E.; Hershey, J. W.; Sonenberg, N. *The EMBO Journal* **1995**, *14*, 3828–3834.

(173) He, Y.; Correa, A. M.; Raso, M. G.; Hofstetter, W. L.; Fang, B.; Behrens, C.; Roth, J. A.; Zhou, Y.; Yu, L.; Wistuba, I. I.; Swisher, S. G.; Pataer, A. *PLoS ONE* **2011**, *6*, ed. by Minna, J. D., e24855.

(174) Staudt, L. M. *Cold Spring Harbor Perspectives in Biology* **2010**, *2*, a000109–a000109.

(175) Tornatore, L. et al. *Cancer Cell* **2014**, *26*, 495–508.

(176) Atkins, C.; Liu, Q.; Minthorn, E.; Zhang, S.-Y.; Figueroa, D. J.; Moss, K.; Stanley, T. B.; Sanders, B.; Goetz, A.; Gaul, N.; Choudhry, A. E.; Alsaid, H.; Jucker, B. M.; Axten, J. M.; Kumar, R. *Cancer Research* **2013**, *73*, 1993–2002.

(177) Trinh, M. A.; Kaphzan, H.; Wek, R. C.; Pierre, P.; Cavener, D. R.; Klann, E. *Cell Reports* **2012**, *1*, 676–688.

(178) Rosen, M. D.; Woods, C. R.; Goldberg, S. D.; Hack, M. D.; Bounds, A. D.; Yang, Y.; Wagaman, P. C.; Phuong, V. K.; Ameriks, A. P.; Barrett, T. D.; Kanelakis, K. C.; Chang, J.; Shankley, N. P.; Rabinowitz, M. H. *Bioorganic & Medicinal Chemistry Letters* **2009**, *19*, 6548–6551.

(179) Palrecha, S.; Lakade, D.; Kulkarni, A.; Pal, J. K.; Joshi, M. *Journal of Biomolecular Structure and Dynamics* **2018**, *37*, 1715–1723.

(180) Chen, T.; Ozel, D.; Qiao, Y.; Harbinski, F.; Chen, L.; Denoyelle, S.; He, X.; Zvereva, N.; Supko, J. G.; Chorev, M.; Halperin, J. A.; Aktas, B. H. *Nature Chemical Biology* **2011**, *7*, 610–616.

(181) Chen, T.; Takrouri, K.; Hee-Hwang, S.; Rana, S.; Yefidoff-Freedman, R.; Halperin, J.; Natarajan, A.; Morisseau, C.; Hammock, B.; Chorev, M.; Aktas, B. H. *Journal of Medicinal Chemistry* **2013**, *56*, 9457–9470.

(182) Yefidoff-Freedman, R. et al. *Journal of Medicinal Chemistry* **2017**, *60*, 5392–5406.

(183) Obeng, E. A.; Carlson, L. M.; Gutman, D. M.; Harrington, W. J.; Lee, K. P.; Boise, L. H. *Blood* **2006**, *107*, 4907–4916.

(184) Chauhan, D.; Tian, Z.; Zhou, B.; Kuhn, D.; Orlowski, R.; Raje, N.; Richardson, P.; Anderson, K. C. *Clinical Cancer Research* **2011**, *17*, 5311–5321.

(185) Schewe, D. M.; Aguirre-Ghiso, J. A. *Cancer Research* **2009**, *69*, 1545–1552.

(186) Burwick, N.; Zhang, M. Y.; de la Puente, P.; Azab, A. K.; Hyun, T. S.; Ruiz-Gutierrez, M.; Sanchez-Bonilla, M.; Nakamura, T.; Delrow, J. J.; MacKay, V. L.; Shimamura, A. *Leukemia Research* **2017**, *55*, 23–32.

(187) Smith, K. H.; Budhraja, A.; Lynch, J.; Roberts, K.; Panetta, J. C.; Connelly, J. P.; Turnis, M. E.; Pruett-Miller, S. M.; Schuetz, J. D.; Mullighan, C. G.; Opferman, J. T. *Molecular Cancer Research* **2020**, *19*, 636–650.

(188) Kalkavan, H.; Chen, M. J.; Crawford, J. C.; Quarato, G.; Fitzgerald, P.; Tait, S. W.; Goding, C. R.; Green, D. R. *Cell* **2022**, *185*, 3356–3374.e22.

(189) Singh, R.; Letai, A.; Sarosiek, K. *Nature Reviews Molecular Cell Biology* **2019**, *20*, 175–193.

(190) Merino, D.; Kelly, G. L.; Lessene, G.; Wei, A. H.; Roberts, A. W.; Strasser, A. *Cancer Cell* **2018**, *34*, 879–891.

(191) Kalkavan, H.; Green, D. R. *Cell Death & Differentiation* **2017**, *25*, 46–55.

(192) Ovad, T. Preparation and preliminary characterization of the eukaryotic initiation factor 2α and its heme regulated kinase, Bachelor Thesis, Prague: Charles University, Faculty of Science, Department of Biochemistry, 2021.

(193) Fojtík, L. Characterization of selected properties of model heme-containing sensor proteins, Bachelor Thesis, Prague: Charles University, Faculty of Science, Department of Biochemistry, 2018.

(194) Lengálová, A.; Fojtíková-Prošková, V.; Vávra, J.; Martínek, V.; Stráňava, M.; Shimizu, T.; Martínková, M. *Journal of Inorganic Biochemistry* **2019**, *201*, 110833.

(195) Novagen pET-21a-d(+) Vectors TB036 10/98.

(196) Bateman, A. et al. *Nucleic Acids Research* **2020**, *49*, D480–D489.

(197) Gasteiger, E.; Hoogland, C.; Gattiker, A.; Duvaud, S.; Wilkins, M. R.; Appel, R. D.; Bairoch, A. In *The Proteomics Protocols Handbook*, Walker, J. M., Ed.; Humana Press: 2005, pp 571–607.

(198) Gallagher, S. R. SDS-Polyacrylamide Gel Electrophoresis (SDS-PAGE), 2012.

(199) Kuipers, K.; Gallay, C.; Martínek, V.; Rohde, M.; Martínková, M.; van der Beek, S. L.; Jong, W. S. P.; Venselaar, H.; Zomer, A.; Bootsma, H.; Veening, J.-W.; de Jonge, M. I. *Molecular Microbiology* **2016**, *101*, 12–26.

(200) Fojtíková, V.; Stráňava, M.; Vos, M. H.; Liebl, U.; Hraníček, J.; Kitanishi, K.; Shimizu, T.; Martínková, M. *Biochemistry* **2015**, *54*, 5017–5029.

(201) Carrió, M.; Villaverde, A. *Journal of Biotechnology* **2002**, *96*, 3–12.

(202) Lengálová, A. Structure and function relationships of model hemoproteins, Dissertation thesis, Prague: Charles University, Faculty of Science, Department of Biochemistry, 2020.

(203) Voet, D.; Gratzer, W. B.; Cox, R. A.; Doty, P. *Biopolymers* **1963**, *1*, 193–208.

(204) Vávra, J.; Sergunin, A.; Farná, A.; Ovad, T.; Shimizu, T.; Martínková, M. *Catalysts* **2023**, *13*, 281.

(205) Butt, W. D.; Keilin, D. *Proceedings of the Royal Society of London. Series B. Biological Sciences* **1962**, *156*, 429–458.